

CONTRACTOR REPORT

SAND84-7212
(PNL-5306)
Unlimited Release
UC-70

Nevada Nuclear Waste Storage Investigations Project

Investigations of Sensitivity and Uncertainty in Some Hydrologic Models of Yucca Mountain and Vicinity

Elizabeth A. Jacobson, Mark D. Freshley, F. Harvey Dove
Pacific Northwest Laboratory
Richland, WA

Prepared by Sandia National Laboratories, Albuquerque, New Mexico 87185
and Livermore, California 94550 for the United States Department of Energy
under Contract DE-AC04-76DP00789

Printed October 1985

HYDROLOGY DOCUMENT NUMBER 145

SAND84-7212
(PNL-5306)
Unlimited Release
Printed October 1985

INVESTIGATIONS OF SENSITIVITY AND UNCERTAINTY IN SOME
HYDROLOGIC MODELS OF YUCCA MOUNTAIN AND VICINITY

by

Elizabeth A. Jacobson
Mark D. Freshley
F. Harvey Dove

Pacific Northwest Laboratory
Richland, Washington

for

Sandia National Laboratories
P. O. Box 5800
Albuquerque, New Mexico 87185

Under Sandia Contract: 47-5882

Sandia Contract Monitor
Martin S. Tierney
NNWSI Repository Performance
Assessments Division

ABSTRACT

The uncertainty in travel time for water through the unsaturated and saturated zones of Yucca Mountain and vicinity was determined by considering uncertainty associated with input parameters to the hydrologic models of these zones. A first-order analysis was used to investigate uncertainty in water travel time through the unsaturated zone at Yucca Mountain, based on an analytic solution for water flow. Results of the investigation of uncertainty for the unsaturated zone indicated that uncertainty in the percolation estimate contributed significantly more to uncertainty in travel time than uncertainty in estimates of hydraulic conductivity. Monte Carlo and first-order approaches were used to investigate uncertainty in ground-water travel time for different cases that varied in the treatment of the input parameters to the hydrologic model of the unsaturated zone. Comparison of the Monte Carlo and first-order estimates of mean ground-water travel time and travel time uncertainty in the saturated zone demonstrates that the first-order approach underestimated both the mean and variance of travel time for all cases considered. This underestimation suggests that the Monte Carlo approach should be used to estimate mean travel time and its variance as well as the probability density distribution of travel time. A sensitivity study of ground-water travel time in the saturated zone indicated that the zones with smaller transmissivity produced the largest influence in travel time for most cases.

ACKNOWLEDGMENTS

The authors wish to acknowledge the efforts of several individuals who contributed to this document. W. A. Rice contributed to the definition and modeling of the saturated flow system. G. W. Gee and R. W. Nelson from Pacific Northwest Laboratory (PNL) and M. S. Tierney and S. Sinnock from Sandia National Laboratories reviewed this document.

The authors also wish to acknowledge the editing services of D. R. Simpson and P. C. Hays, and the word processing support provided by D. A. Berg, M. V. Heid, D. J. Kennedy, and A. L. Seybold.

This work, performed by PNL, was supported under Contract 47-5882 with Sandia National Laboratories. Pacific Northwest Laboratory is operated by Battelle Memorial Institute for the U.S. Department of Energy.

CONTENTS

ACKNOWLEDGMENTS.....	ii
FOREWORD.....	x
INTRODUCTION.....	1
CONCEPTUAL HYDROLOGIC MODEL OF YUCCA MOUNTAIN.....	3
APPROACHES TO SENSITIVITY AND UNCERTAINTY.....	7
SENSITIVITY ANALYSIS.....	7
FIRST-ORDER ANALYSIS OF UNCERTAINTY.....	9
MONTE CARLO APPROACH TO UNCERTAINTY ANALYSIS.....	10
INVESTIGATION OF UNCERTAINTY IN THE UNSATURATED ZONE AT YUCCA MOUNTAIN.....	12
CALCULATION OF TRAVEL TIME THROUGH THE UNSATURATED ZONE.....	12
APPLICATION OF THE ANALYTIC SOLUTION TO YUCCA MOUNTAIN.....	14
SENSITIVITY FOR INVESTIGATION OF PERCOLATION THROUGH YUCCA MOUNTAIN.....	27
FIRST-ORDER UNCERTAINTY ANALYSIS FOR PERCOLATION.....	31
FIRST-ORDER UNCERTAINTY ANALYSIS FOR HYDRAULIC CONDUCTIVITY.....	33
COMPARISON OF THE UNCERTAINTY ANALYSES FOR PERCOLATION AND HYDRAULIC CONDUCTIVITY.....	36
UNCERTAINTY ANALYSIS OF GROUND-WATER TRAVEL TIME IN THE SATURATED ZONE.....	38
NUMERICAL CALCULATION OF GROUND-WATER TRAVEL TIME.....	39
ANALYSIS OF UNCERTAINTY IN GROUND-WATER TRAVEL TIME.....	40
Correlation Among Parameters.....	41
APPLICATION TO AQUIFER NEAR YUCCA MOUNTAIN.....	42
Seven Specific Cases for Uncertainty Analysis.....	44
Statistical Properties of Transmissivity.....	45

Generation of Realizations of Transmissivity.....	47
Statistical Properties of Effective Porosity.....	50
Generation of Realizations of Effective Porosity.....	52
UNCERTAINTY ANALYSIS FOR THREE CASES WITH UNIFORM EFFECTIVE POROSITY.....	54
Monte Carlo Analysis with Uniform Effective Porosity.....	54
Sensitivity Analysis with Uniform Effective Porosity.....	68
First-Order Analysis with Uniform Effective Porosity.....	69
Comparison of Monte Carlo and First-Order Results Using Uniform Effective Porosity.....	70
UNCERTAINTY ANALYSIS FOR FOUR CASES WITH SPATIALLY VARYING EFFECTIVE POROSITY.....	71
Monte Carlo Analysis with Spatially Varying Effective Porosity.....	72
Sensitivity Analysis with Spatially Varying Effective Porosity.....	78
First-Order Analysis with Spatially Varying Effective Porosity.....	84
Comparison of Monte Carlo and First-Order Results for Spatially Varying Effective Porosity.....	85
DISCUSSION AND CONCLUSIONS.....	86
REFERENCES.....	91
APPENDIX A - ONE-DIMENSIONAL ANALYTIC SOLUTION FOR PRESSURE HEAD IN THE UNSATURATED ZONE.....	A.1
APPENDIX B - DERIVATION OF EQUATIONS FOR THE FIRST-ORDER UNCERTAINTY ANALYSIS.....	B.1

FIGURES

1	Conceptual Diagram of the Saturated and Variably Saturated Flow Systems.....	4
2	Flow Paths for Travel-Time Calculations.....	6
3	Location of USW G-4 and Other Wells Within and Adjacent to the Conceptual Repository Boundary at Yucca Mountain.....	15
4	Geologic Profile for Well USW G-4.....	16
5	Simplified Stratigraphy for Modeling the One-Dimensional Profile Through Yucca Mountain.....	18
6	Moisture-Retention Characteristics Using Haverkamp's Formula for Core Samples Representing Stratigraphic Units in the One-Dimensional Yucca Mountain Profile.....	19
7	Unsaturated Hydraulic Conductivity for Core Sample G4-8 G4-12, and G4-13.....	20
8	Moisture Content from Numerical Evaluation of the Analytic Solution for the One-Dimensional Yucca Mountain Profile.....	23
9	Pressure Head from Numerical Evaluation of the Analytic Solution for the One-Dimensional Yucca Mountain Profile.....	24
10	Hydraulic Head from Numerical Evaluation of the Analytic Solution for the One-Dimensional Yucca Mountain Profile.....	25
11	Travel Time of Water Through the One-Dimensional Yucca Mountain Profile for the Baseline Case and Variations of the Recharge Estimate.....	26
12	Travel Time Versus Variation from the Baseline Percolation Flux of a 0.02 cm/yr.....	30
13	Sensitivity Versus Magnitude of Variation in the Percolation Flux....	31
14	Study Area for Saturated Flow.....	43
15	Transmissivity Zonation Pattern for the Study Area.....	45
16	Distribution of Gaussian Errors for Transmissivity Zones.....	49
17	Correlation Between Porosity and Hydraulic Conductivity for Small Cores USW GU-3 and USW G-4.....	51

18	Distribution of Gaussian Errors for Effective Porosity.....	53
19	Contours of Hydraulic Heads Obtained from the U.S. Geological Survey Interpretation.....	55
20	Histogram of Ground-Water Travel Time for Case 1.....	56
21	Cumulative Histogram of Ground-Water Travel Time for Case 1.....	57
22	Contours of Hydraulic Head Obtained from the Ground-Water Flow Simulation Using the Mean Transmissivity Values.....	58
23	Contours of Hydraulic Head Obtained from the Ground-Water Flow Simulation Using Transmissivity Realization Number 14.....	59
24	Contours of Hydraulic Head Obtained from the Ground-Water Flow Simulation Using Transmissivity Realization Number 88.....	60
25	Histogram of Ground-Water Travel Time for Case 2.....	61
26	Cumulative Histogram of Ground-Water Travel Time for Case 2.....	62
27	Histogram of Ground-Water Travel Time for Case 3.....	63
28	Cumulative Histogram of Ground-Water Travel Time for Case 3.....	64
29	Sample Mean and Sample Standard Deviation of Ground-Water Travel Time Versus Number of Realizations for Case 1.....	66
30	Sample Mean and Sample Standard Deviation of Ground-Water Travel Time Versus Number of Realizations for Case 2.....	66
31	Sample Mean and Sample Standard Deviation of Ground-Water Travel Time Versus Number of Realizations for Case 3.....	67
32	Histogram of Ground-Water Travel Time for Case 5.....	73
33	Cumulative Histogram of Ground-Water Travel Time for Case 5.....	74
34	Histogram of Ground-Water Travel Time for Case 6.....	75
35	Cumulative Histogram of Ground-Water Travel Time for Case 6.....	76
36	Histogram of Ground-Water Travel Time for Case 7.....	77
37	Cumulative Histogram of Ground-Water Travel Time for Case 7.....	79
38	Sample Mean and Sample Standard Deviation of Ground-Water Travel Time Versus Number of Realizations for Case 5.....	80

39	Sample Mean and Sample Standard Deviation of Ground-Water Travel Time Versus Number of Realizations for Case 6.....	81
40	Sample Mean and Sample Standard Deviation of Ground-Water Travel Time Versus Number of Realizations for Case 7.....	82

TABLES

1	Depths at Which Core Samples Were Taken from Well USW G-4.....	17
2	Summary of Saturated Hydraulic Characteristics for Core Samples Used to Represent the One-Dimensional Yucca Mountain Profile.....	18
3	Generalized Stratigraphy and Saturations for Yucca Mountain.....	21
4	Variations from the Baseline Percolation Flux of 0.02 cm/yr and the Corresponding Flux for the Sensitivity Analysis.....	28
5	Travel Times and Sensitivity Coefficients Corresponding to Variations from the Baseline Percolation Flux of 0.02 cm/yr.....	29
6	Range of Percolation Estimates for the First-Order Uncertainty Analysis.....	32
7	Variations of Saturated Hydraulic Conductivity of Sample G4-13 for Calculating the Sensitivity Coefficient for Travel Time with Respect to Hydraulic Conductivity.....	35
8	Travel Times and Sensitivity Coefficients Corresponding to Variations of the Saturated Hydraulic Conductivity of Sample G4-13.....	35
9	Range of Saturated Hydraulic Conductivities Used in the First-Order Uncertainty Analysis.....	36
10	Hydrologic Information Used in Each of the Seven Cases for Which Uncertainty in Ground-Water Travel Time was Calculated.....	46
11	Estimates of Mean and Standard Deviation of Log Transmissivity for Each Zone.....	48
12	Estimates of Mean and Standard Deviation of Effective Porosity for Each Zone.....	51
13	Zonal Transmissivity Values Corresponding to the Mean, Realization 14, and Realization 88.....	60
14	Sample Means, Sample Standard Deviations, Coefficient of Variations and Medians of Ground-Water Travel Time Obtained from Monte Carlo Analysis for Cases 1, 2, and 3.....	65
15	Travel Times, Sensitivity Coefficients, and Normalized Sensitivity Coefficients Corresponding to Variations of the Log Transmissivity in the Four Zones and Effective Porosity.....	68

16	Values of Mean, Standard Deviation, and Coefficient of Variation of Travel Time Obtained from Monte Carlo and First-Order Analysis for Cases 2 and 3 with Uniform Effective Porosity.....	71
17	Sample Means, Sample Standard Deviations, Coefficients of Variations, and Medians of Ground-Water Travel Time for Cases 4, 5, 6, and 7.....	80
18	Travel Times, Sensitivity Coefficients, and Normalized Sensitivity Coefficients Corresponding to Variations of the Log Transmissivity and Spatially Varying Effective Porosity in the Four Zones.....	83
19	Values of Mean, Standard Deviation, and Coefficient of Variation of Travel Time Obtained from Monte Carlo and First-Order Analysis for Cases 6 and 7 with Spatially Varying Effective Porosity.....	85

FOREWORD

The draft of this report was completed and submitted to Sandia National Laboratories in late 1984. Some data and parameters used as the basis for the work reported herein were selected earlier, based on the best information available at the time. Although some of the data and parameters have now been updated, the basic methods reported herein remain valid.

Martin S. Tierney
NNWSI Repository Performance
Assessments Division
Sandia National Laboratories
October 1985

INTRODUCTION

Pacific Northwest Laboratory (PNL) has been supporting Sandia National Laboratories during performance assessment activities for the Nevada Nuclear Waste Storage Investigations (NNWSI) project. Performance assessment contributions from PNL have included computer simulations of water flow and radionuclide transport at Yucca Mountain, which is located on and adjacent to the southwest corner of the Nevada Test Site. These simulations were designed to help supply technical insight into programmatic issues such as repository horizon selection, ground-water percolation, ground-water travel times, radionuclide migration projections, biosphere discharge points, repository stability, and suggested data-gathering programs.

One guideline prescribed by the Department of Energy (DOE) for repository siting is the 1000-year minimum ground-water travel time determined for the site prior to waste emplacement (DOE 1984). The time is to be evaluated for any potential path of likely radionuclide travel from the disturbed zone to the accessible environment. The accessible environment may be defined as 10 kilometers (10,000 meters) from the repository boundaries or possibly the nearest potable water supply. The DOE guidelines disqualify a site if the expected ground-water travel time along any path of likely and significant radionuclide travel from the disturbed zone to the accessible environment is less than 1000 years. Determination of uncertainty in travel time will be necessary to establish the credibility of the evaluation and to ultimately demonstrate compliance with regulatory standards.

Uncertainty analysis, as used in this report, is defined as a sensitivity analysis combined with parameter uncertainty. The goal of this study has been to demonstrate methods that relate uncertainty in hydrologic parameters to variations in ground-water travel time. (For purposes of clarity, an equally important issue, the amount of contaminant delivered to the accessible environment, will be neglected.) Parameters that directly relate to recharge and subsurface flow have been the focal point for analyses in the unsaturated and saturated hydrologic systems. Many analytical techniques are available to

quantify uncertainty. This study has been designed to use methods that preserve the basic understanding of the physical system.

At Yucca Mountain, Nevada, no direct measurements of recharge are currently available; however, interpretations from indirect measurements suggest that percolation at depth is less than 1 mm/yr. Because of the low flux, the longest travel time for moisture at Yucca Mountain will occur in the unsaturated system. Historically, the study of saturated flow systems has preceded the study of unsaturated flow systems in the field of hydrology. Consequently, the techniques used to quantify the effects of uncertainty in saturated flow systems are more advanced than those proposed for use in unsaturated flow systems. Further, the analysis of the unsaturated system is more complicated because of the nonlinear dependence of hydraulic properties on moisture content. Thus, another objective of this study has been to investigate techniques used to quantify uncertainty in the saturated system with a view toward future applications in the unsaturated system.

Although more is known about saturated flow systems, this report is organized along a typical hydrologic flow beginning with infiltration at the ground surface, percolation through the unsaturated zone, recharge to the regional water table, and finally flow through the saturated zone. A conceptual hydrologic model of Yucca Mountain is presented first to establish a framework for interconnection between the unsaturated and saturated flow systems. Uncertainty in the unsaturated system is then discussed followed by consideration of uncertainty in the saturated system. Suggestions for future directions in the development of uncertainty analyses for both unsaturated and saturated systems are made in the final section.

CONCEPTUAL HYDROLOGIC MODEL OF YUCCA MOUNTAIN

The saturated flow system surrounding Yucca Mountain has been included within the boundaries of two regional ground-water models (Rice 1984; Waddell 1982). In both cases, the unsaturated flow system was considered to be loosely coupled to a saturated regional system. The degree of coupling is related to the local infiltration passing through the mountain to recharge the water table. The term 'loosely coupled' is used because percolation of water through Yucca Mountain is not sufficient to produce a recharge mound in the water table. Although direct measurement of recharge at Yucca Mountain has not been obtained to date, flux within the mountain has been estimated to be very low--possibly less than 1 mm/yr (Sinnock et al. 1984). Such low rates are extremely difficult, if not impossible, to measure (Sammis et al. 1982). The conceptual hydrologic model of Yucca Mountain that has been used for purposes of uncertainty analysis is depicted schematically in Figure 1.

Yucca Mountain consists of layered Tertiary volcanic tuffs ranging from nonwelded to welded ash-flow or airflow materials (Winograd and Thordarson 1975). The layers dip to the east at an angle less than 8 degrees. The moisture content of the materials generally increases with depth in the unsaturated zone but can vary both within and between stratifications. Typical saturation, which is the ratio of moisture content to porosity of the tuff matrix, ranges from 34 to 96 percent, and the matrix porosity varies between 10 and 44 percent (Rush et al. 1983). The tuffs typically demonstrate low saturated matrix hydraulic conductivities ranging in order of magnitude from 10^{-10} cm/s to 10^{-3} cm/s (Peters et al. 1984).

For this study, water flow in the unsaturated zone is assumed to be occurring in the porous matrix even where the rock is highly fractured (e.g., the Topopah Spring Member of the Paintbrush Tuff Formation). This conceptualization of the flow considers the bulk properties of the rock as providing a porous flow equivalent or continuum approach to modeling. Peters and Gauthier

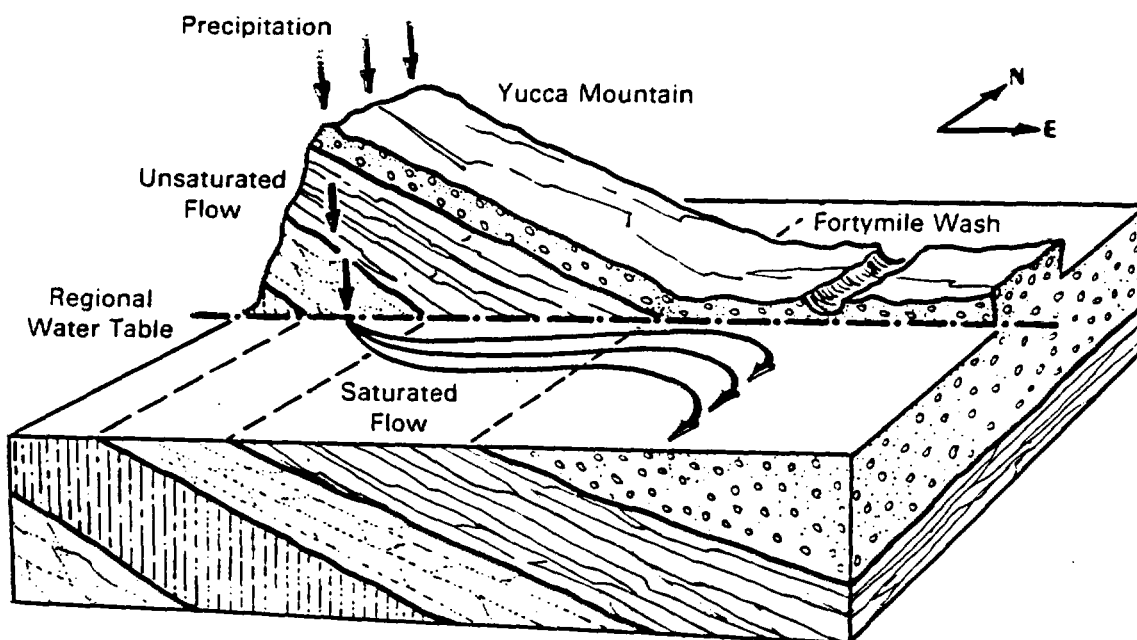


FIGURE 1. Conceptual Diagram of the Saturated and Variably Saturated Flow Systems

(1984)^(a) have proposed another representation that discriminates between fracture and matrix flow where the fractures are allowed to conduct excess matrix water. However, current interpretations of measured moisture content, suction head, and calculated recharge suggest an unsaturated flux that can be adequately described by porous flow concepts.

The saturated flow system consists of the Tertiary volcanic tuffs separated from a lower carbonate aquifer by a clastic confining layer (Winograd and Thordarson 1975). The regional flow system surrounding Yucca Mountain has been modeled as a single-layer aquifer (Rice 1984; Waddell 1982). This simplification is largely the result of available composite hydraulic head measurements, which do not allow correlation of potentiometric surfaces with specific hydrogeologic units. Recent observations from boreholes near Yucca Mountain

(a) R. R. Peters and J. H. Gauthier. 1984. Memorandum to F. W. Bingham entitled "Results of TOSPAC Hydrologic Calculations for Yucca Mountain," April 30, Sandia National Laboratories, Albuquerque, New Mexico, 51 pages.

suggest that an upward hydraulic gradient may exist between the lower confined carbonate aquifer, the clastic confining layer, and the unconfined aquifer below Yucca Mountain.

The Tertiary tuff layers in the saturated flow system also dip to the east at angles less than 8 degrees. The regional water table in the vicinity of Yucca Mountain is fairly flat and intersects the inclined volcanic tuffs. This intersection establishes a transmissive zone. A conceptual diagram illustrating the transmissive zone, inclined volcanic tuffs, and the regional water table in cross section is shown in Figure 2. For the investigation of uncertainty in travel time, only a local saturated system with a perimeter surrounding the repository portion of Yucca Mountain slightly in excess of 10,000 m (a subset of the regional flow system) was used.

Porous flow equivalence that combines the bulk effects of matrix and fractures is assumed for water flow in the saturated zone. Saturated portions of Topopah Spring welded tuff, which are downdip from the potential repository, demonstrate a high yield of ground water to wells with relatively low draw-down--in spite of low matrix porosity (Winograd and Thordarson 1975). This phenomenon suggests that flow through fractures dominates the bulk effects of the porous media equivalence in the saturated system. Lahoud et al. (1984) recently concluded that the flow in the saturated zone is dominated by fractures based on correlations between transmissivity and local rock structures.

Flow paths used to calculate travel time are vertically downward through the unsaturated zone and horizontal in the saturated zone. The location of Well J12 (shown in Fig. 2) is approximately 10,000 m from the perimeter of a potential repository. Preliminary calculations demonstrated that travel time through the unsaturated zone may exceed that of the saturated zone by at least a factor of 20 (Thompson et al. 1984). However, while the unsaturated zone can provide the longest travel times, it also has the greatest potential for uncertainty.

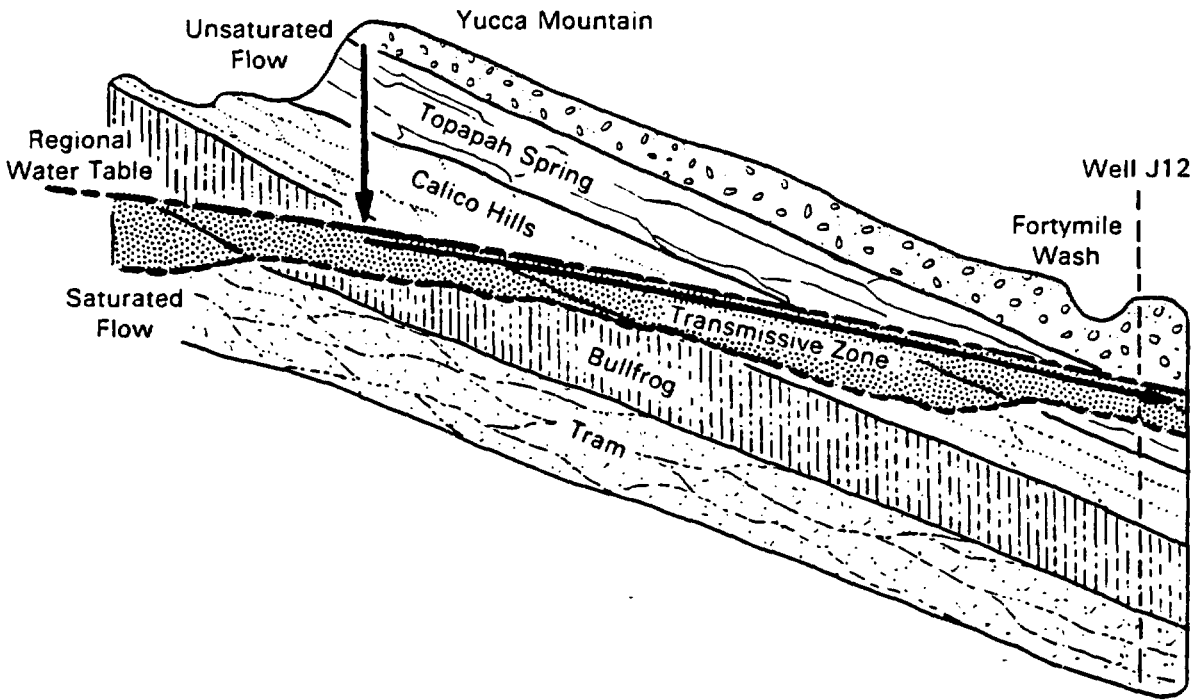


FIGURE 2. Flow Paths for Travel-Time Calculations

APPROACHES TO SENSITIVITY AND UNCERTAINTY

Uncertainty analyses quantify uncertainty in model output or model performance measures induced by uncertainties associated with input parameters. A number of different approaches can be used for uncertainty analyses; both first-order and Monte Carlo approaches were applied to our investigation of uncertainty in water flow through and adjacent to Yucca Mountain. Water travel time was selected as the model performance measure for investigation of uncertainty in the saturated and unsaturated zones at Yucca Mountain.

In first-order uncertainty analyses, sensitivity coefficients are combined with parameter uncertainty to propagate uncertainties in the input parameters to uncertainties in water travel time. Sensitivity coefficients are the output of sensitivity analyses that quantify the effect on a model performance measure produced by a change in a specific input parameter or input parameters. Parameter uncertainty is a measure of parameter error.

The Monte Carlo approach to uncertainty analyses is a simple and direct method for propagating uncertainty of input parameters to uncertainty in water travel time. The Monte Carlo approach involves generating a large number of 'realizations' of input parameters and their spatial distributions; calculating the corresponding values of water travel time; and determining the mean, variance, and probability density function of travel time.

The perturbation approach to determining sensitivity coefficients as well as the first-order and Monte Carlo approaches to uncertainty analyses are presented in the following sections. The strengths and weaknesses of the two approaches to uncertainty analyses are summarized. In addition, uses for the results of uncertainty analyses are briefly discussed.

SENSITIVITY ANALYSIS

For a model output function or model performance measure F , which depends on the parameters p_1, p_2, \dots, p_n , the general definition of a sensitivity coefficient is the derivative

$$S_i = \frac{\partial F}{\partial p_i} \quad (1)$$

where S_i is the sensitivity coefficient for the output function F with respect to parameter p_i . We used a finite difference approximation to Equation (1) as follows:

$$S_i = \frac{F_2 - F_1}{p_{i2} - p_{i1}} = \frac{\Delta F}{\Delta p_i} \quad (2)$$

where subscripts 1 and 2, respectively, correspond to the state of the system at positive and negative variations of p_i that are symmetric about the mean value.

Comparing the magnitude of the sensitivity coefficients indicates the parameters that have the most influence on the value of the function F . However, because differences in the magnitudes of the parameters will affect the value of S_i , comparison of the normalized sensitivity coefficients is a better indicator of the relative importance of the parameters contributing to F . The expression for the normalized sensitivity coefficients, Sn_i , is as follows:

$$Sn_i = \frac{\bar{p}_i}{F(\bar{p}_i)} \frac{\Delta F}{\Delta p_i} \quad (3)$$

where \bar{p}_i is the mean value of the i th parameter and $F(\bar{p}_i)$ is the value of the function when all parameters are equal to their mean values.

The perturbation approach to estimating sensitivity coefficients consists of repeated simulations with a model while varying the input parameters. Sensitivity coefficients are calculated with respect to positive and negative variations of the input parameters symmetric about their mean values.

FIRST-ORDER ANALYSIS OF UNCERTAINTY

The first-order approach to uncertainty analysis of water travel time is based on a Taylor series expansion for travel time about the mean values of the parameters (see Appendix B). This approach requires knowledge of the mean and variance of the parameters in addition to estimates of the derivatives of travel time with respect to the parameters. These derivatives, also called sensitivity coefficients [Equations (1) and (2)], are obtained from a sensitivity analysis.

The equations for the mean and variance of water travel time from first-order analysis are derived in Appendix B when F is a function of only one input parameter. These equations may be easily extended to include the case where F is a function of several parameters. Therefore, in analogy to Equation (B.8), the expression for the mean value of the travel time is

$$E(\text{Tr}) = \text{Tr}(\bar{p}_1, \bar{p}_2, \dots, \bar{p}_i) \quad (4)$$

where E denotes the expectation of travel time, Tr .

In a similar manner, Equation (B.12) for the variance of travel time may be written as follows:

$$\begin{aligned} \text{Var}(\text{Tr}) = & \sum_i \left(\frac{\partial \text{Tr}}{\partial p_i} \right)^2 \text{Var}(p_i) \\ & + \sum_i \sum_{\substack{j \\ i \neq j}} \text{Cov}(p_i, p_j) \left(\frac{\partial \text{Tr}}{\partial p_i} \right) \left(\frac{\partial \text{Tr}}{\partial p_j} \right) \end{aligned} \quad (5)$$

where Var denotes variance, which is a measure of uncertainty, and $\text{Cov}(p_i, p_j)$ is the covariance of p_i and p_j . If the parameters are independent, the covariance among the parameters is zero and Equation (5) reduces to the following expression:

$$\text{Var (Tr)} = \sum_i \left(\frac{\partial \text{Tr}}{\partial p_i} \right)^2 \text{Var (p}_i) \quad (6)$$

which is a first-order expression relating uncertainty in the input parameters p_i to uncertainty in Tr. Equation (6) is first-order because second order and higher derivatives of travel time with respect to p_i are not considered.

Because each term in Equation (6) is a function of only one parameter, the relative magnitudes of the terms can be compared to determine which of the parameters produces the most uncertainty in the water travel time. This information indicates which parameters should be more accurately determined so that travel-time uncertainty could be reduced. Thus, a first-order analysis of travel time not only allows estimation of travel-time uncertainty but also may be used to direct future data collection activities.

The estimate of travel-time uncertainty obtained from the first-order analysis may not be similar to those obtained from a Monte Carlo approach if the second order or higher derivatives are not negligible as has been assumed in the derivation in Appendix B. In addition, the validity of using a series expansion for estimating means and variances has not been successfully addressed to date. A Taylor series expansion of a function has been shown to be valid for very small variations of the parameters about a fixed value. However, when the series expansion is used to estimate the variance of the function, the corresponding variance of the input parameters may be quite large, which violates the condition of small variations in the parameters. Until this point has been resolved, the results from a first-order analysis must be considered as a rough estimate of the uncertainty in a function. In addition, the estimate of variance from a first-order analysis is not sufficient to obtain confidence interval estimates for travel time unless the probability density function of the travel time is known.

MONTE CARLO APPROACH TO UNCERTAINTY ANALYSIS

The model output of interest for application of the Monte Carlo approach to uncertainty in this study is water travel time. The Monte Carlo approach

involves generating a large number of 'realizations' of the hydrologic parameters and their spatial distributions, calculating the corresponding values of water travel time and determining the mean, variance, and probability density function of the travel time. A realization is generated by randomly selecting values from the assumed joint probability density function of the input parameters.

The major disadvantage of the Monte Carlo approach is that a large number of simulations of the flow system are needed in order to adequately estimate the mean, variance, and probability density function of water travel time. However, an advantage of this technique is that we can obtain an estimate of the probability density function of travel time, which in turn allows the calculation of reliability or confidence limits. Estimates of the mean and variance of travel time alone are not sufficient to calculate confidence on travel time, because determining confidence limits depends on knowledge of the probability density function.

INVESTIGATION OF UNCERTAINTY IN THE UNSATURATED ZONE
AT YUCCA MOUNTAIN

A one-dimensional, steady-state analytic solution for unsaturated flow was used to investigate the effect on water travel time of uncertainty in estimates of percolation through Yucca Mountain, Nevada. As used in this investigation, percolation is water flux at depth below the evaporative and root zones. The analytic solution was evaluated numerically by a computer code that determines the distribution of pressure head over a vertical profile of the mountain.

The analytic solution was derived by integrating Richards' (1931) extension of Darcy's law over a one-dimensional profile (see Appendix A). Gardner (1958) solved the integral using simple algebraic expressions for the material properties. Numerical evaluation of the integral allows more flexibility in the algebraic expressions used to describe material properties. Travel time for water was based on Darcy's law for unsaturated flow and definition of the seepage velocity using the distribution of head from the analytic solution.

The numerical code was applied to the unsaturated zone of Yucca Mountain to form a model covering a vertical profile from the prospective repository to the regional water table. A possible range of percolation through Yucca Mountain was used to perform an uncertainty analysis of travel time through the mountain. The mean value of recharge and resulting mean travel time were estimated by partial calibration of the model to field-measured saturations. An uncertainty analysis was used to quantify the uncertainty in travel time resulting from uncertainty in the estimates of percolation. We considered the percolation estimate as the parameter for uncertainty in travel time through the unsaturated zone.

CALCULATION OF TRAVEL TIME THROUGH THE UNSATURATED ZONE

For this study, water flow through the unsaturated zone of Yucca Mountain was treated as one dimensional and steady state. Steady-state water flow is defined as when the magnitude and direction of the flow velocity are constant with time at any point in a flow field (Freeze and Cherry 1979). An analytical solution for steady-state, one-dimensional downward flow of water through the

unsaturated zone was obtained by integrating Darcy's Law over a vertical profile (see Appendix A). The analytical solution over an incremental distance Δz_i is

$$\Delta z_i = \int_{\psi_{i-1}}^{\psi_i} \frac{d\psi}{q/K_i(\psi)-1} \quad (7)$$

where Δz_i is distance between the i and $i-1$ points, ψ_i is pressure head at the i^{th} point, q is the steady-state recharge rate, and $K_i(\psi)$ is unsaturated hydraulic conductivity over Δz_i . A harmonic mean hydraulic conductivity [Equation (A.12)] is used for $K_i(\psi)$. Solution of Equation (7) yields the distribution of pressure head over the profile.

Travel time over the increment Δz_i is obtained by the following equation:

$$\Delta t_i = \frac{(\Delta z_i)^2 \theta_i^*}{K_i^* \Delta h_i} \quad (8)$$

where Δt_i is the incremental travel time over Δz_i , θ_i^* is effective moisture content over Δz_i , K_i^* is a harmonic mean of the hydraulic conductivity over Δz_i , and Δh_i is the change in hydraulic head over Δz_i . Hydraulic head h is the sum of pressure head ψ and elevation head z . The effective moisture content is the product of saturation and effective porosity n_e ($\theta_i^* = S n_e$). Moisture content is an expression for the volume of water to volume of soil or rock, and saturation is the ratio of volume of water to volume of voids in the soil or rock. Effective porosity considers only those pore spaces through which flow can occur (Bear 1979).

Equations (4) and (8) are evaluated numerically by computer programs at discrete points over the vertical profile.

APPLICATION OF THE ANALYTIC SOLUTION TO YUCCA MOUNTAIN

A one-dimensional geologic profile was defined from the prospective repository horizon in Yucca Mountain to the water table. The profile is based on the geologic log of Well USW G-4, which is located within the conceptual repository boundary (Fig. 3).

The generalized geologic profile from USW G-4 is illustrated in Figure 4. The depths of core samples from USW G-4 covering the profile considered for this investigation are listed in Table 1. The stratigraphy used to model water flow from the repository horizon to the water table was simplified from the generalized stratigraphy in Figure 4 and is illustrated in Figure 5. Representative core samples based on lithology as well as hydraulic characteristics were used to represent the stratigraphic units in Figure 5.

The hydraulic characteristics of core samples from USW G-4 used to represent the simplified stratigraphic units in Figure 5 were reported by Peters et al. (1984). The saturated hydraulic characteristics for the core samples used are given in Table 2. Moisture-retention characteristics that describe the change in moisture content with change in pressure head for the core samples are illustrated in Figure 6. The moisture-retention characteristics, or characteristic curves, represent a statistical least squares fit of measured data with Haverkamp's formula (McKeon et al. 1983) for moisture retention, which is

$$\theta = \frac{\alpha(\theta_s - \theta_r)}{\alpha + |\psi|^\beta} + \theta_r \quad (9)$$

where θ is the volumetric moisture content at pressure head ψ , θ_s is the moisture content at saturation, θ_r is the residual moisture content, and α , β are empirical constants derived from fitting the data.

The unsaturated hydraulic conductivity $K(\psi)$ was generated from the shape of the moisture-retention characteristics using a method developed by Mualem (1976) (Fig. 7).

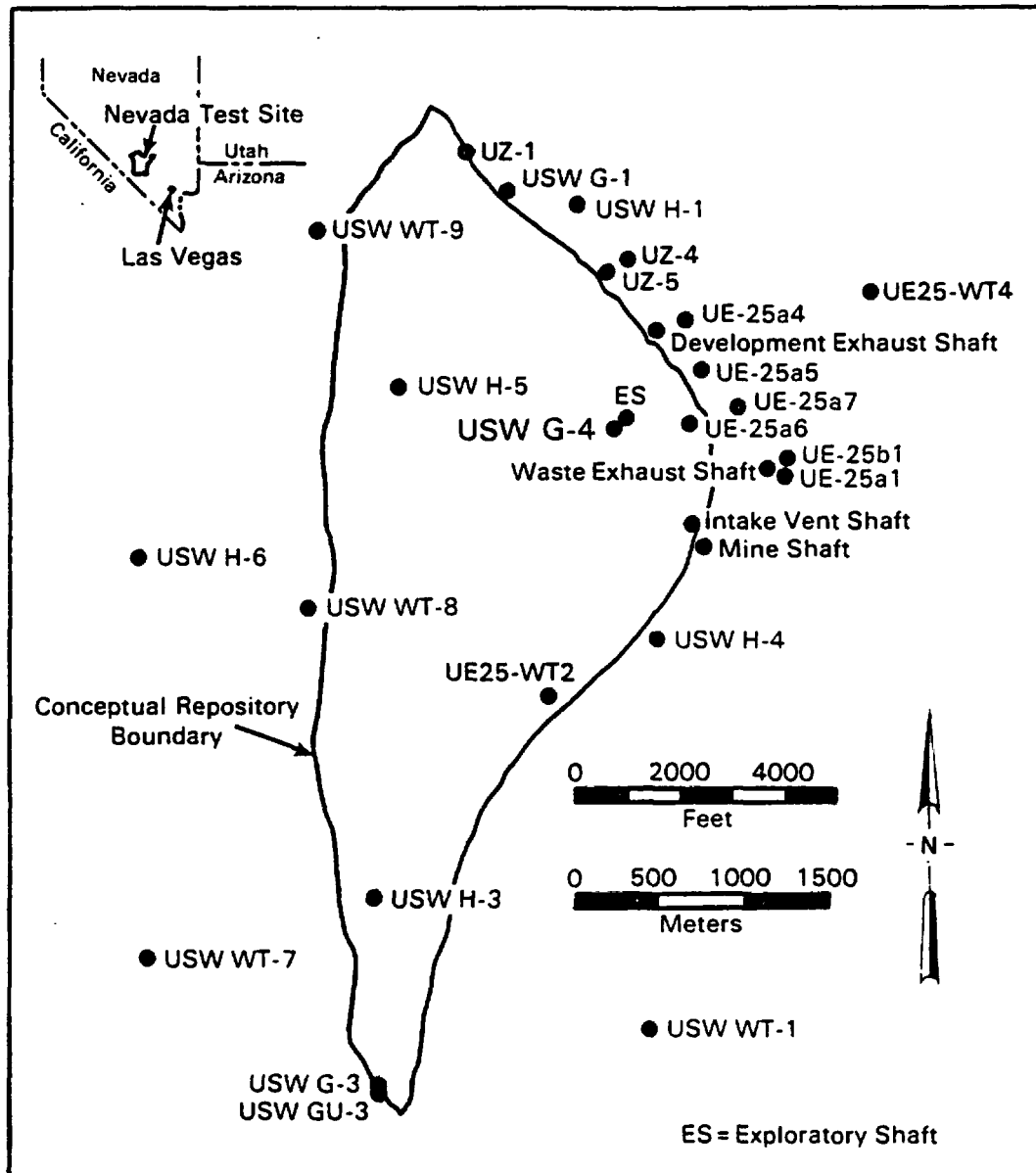
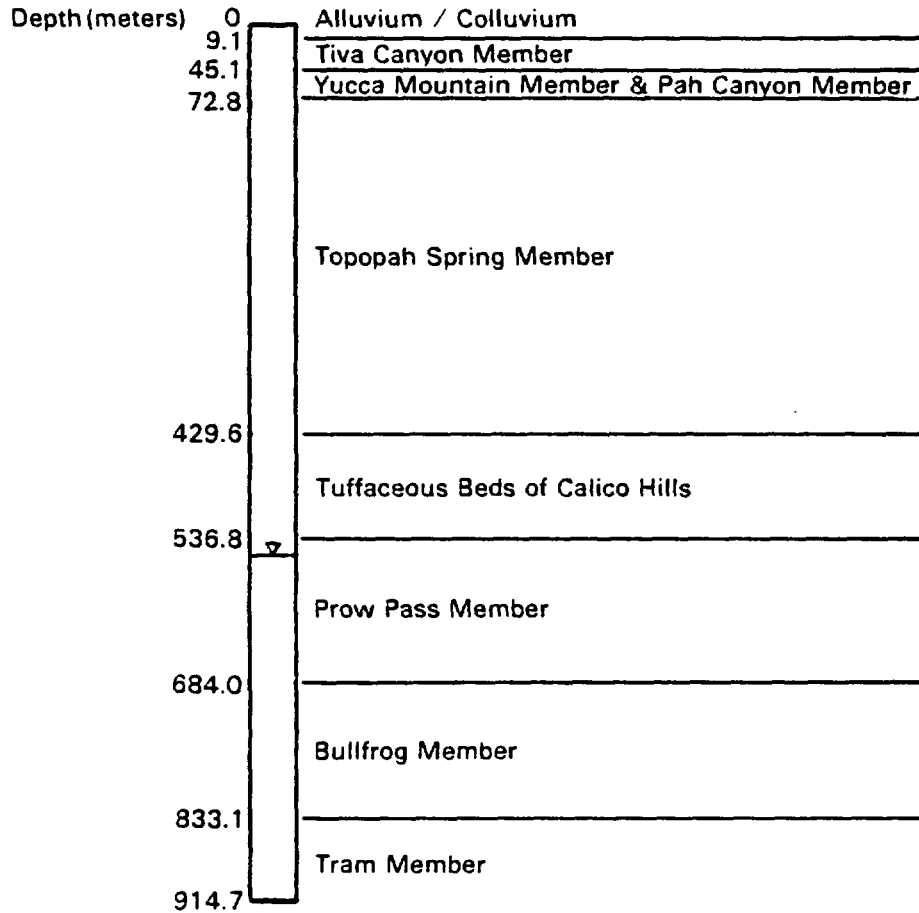


FIGURE 3. Location of USW G-4 and Other Wells Within and Adjacent to the Conceptual Repository Boundary at Yucca Mountain (after Fernandez and Freshley 1984)

Generalized Stratigraphic Log



Surface Elevation 1270 m (4166 ft)

Repository Horizon 1030 m (3379 ft)

FIGURE 4. Geologic Profile for Well USW G-4 (after Fernandez and Freshley 1984)

TABLE 1. Depths at Which Core Samples Were Taken from Well USW G-4
(from Peters et al. 1984)

<u>Sample PNL Code</u>	<u>Depth Below Surface (ft)</u>
G4-1	43
G4-2	123.5
G4-3	208
G4-5	246.5
G4-5	864 (dark section)
G4-6	1158
G4-7	1256
G4-8	1299
G4-9	1324
G4-10	1405
G4-11	1548
G4-12	1686
G4-13	1727.7
G4-14	1736.7
G4-15	1769.3
G4-16	1778
G4-17	1789
G4-18	1899
G4-19	2006
G4-20	2101
G4-21	2401
G4-22	1407

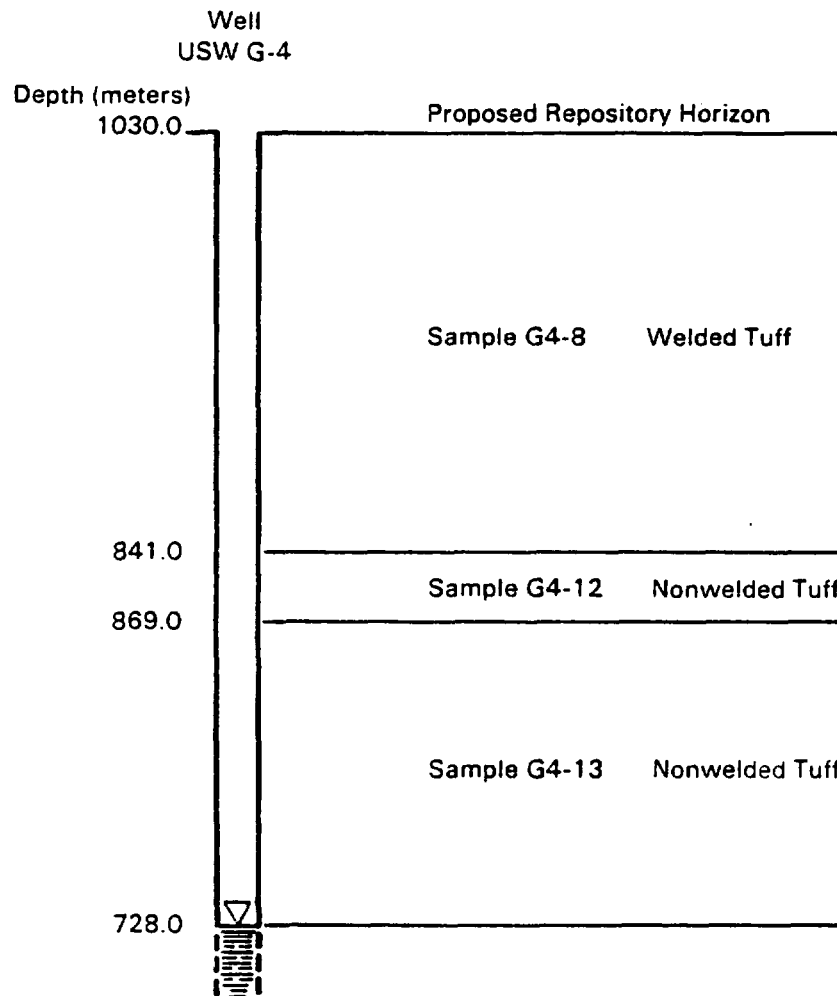


FIGURE 5. Simplified Stratigraphy for Modeling the One-Dimensional Profile Through Yucca Mountain

TABLE 2. Summary of Saturated Hydraulic Characteristics for Core Samples Used to Represent the One-Dimensional Yucca Mountain Profile (from Peters et al. 1984)

Sample	Interval (m)	Porosity	Saturated Hydraulic Conductivity (m/day)
G4-13 (NW) ^(a)	728-841	0.27	1.607×10^{-6}
G4-12 (NW)	841-869	0.37	1.132×10^{-6}
G4-8 (W)	869-1030	0.09	3.862×10^{-5}

(a) NW denotes nonwelded tuff, W denotes welded tuff.

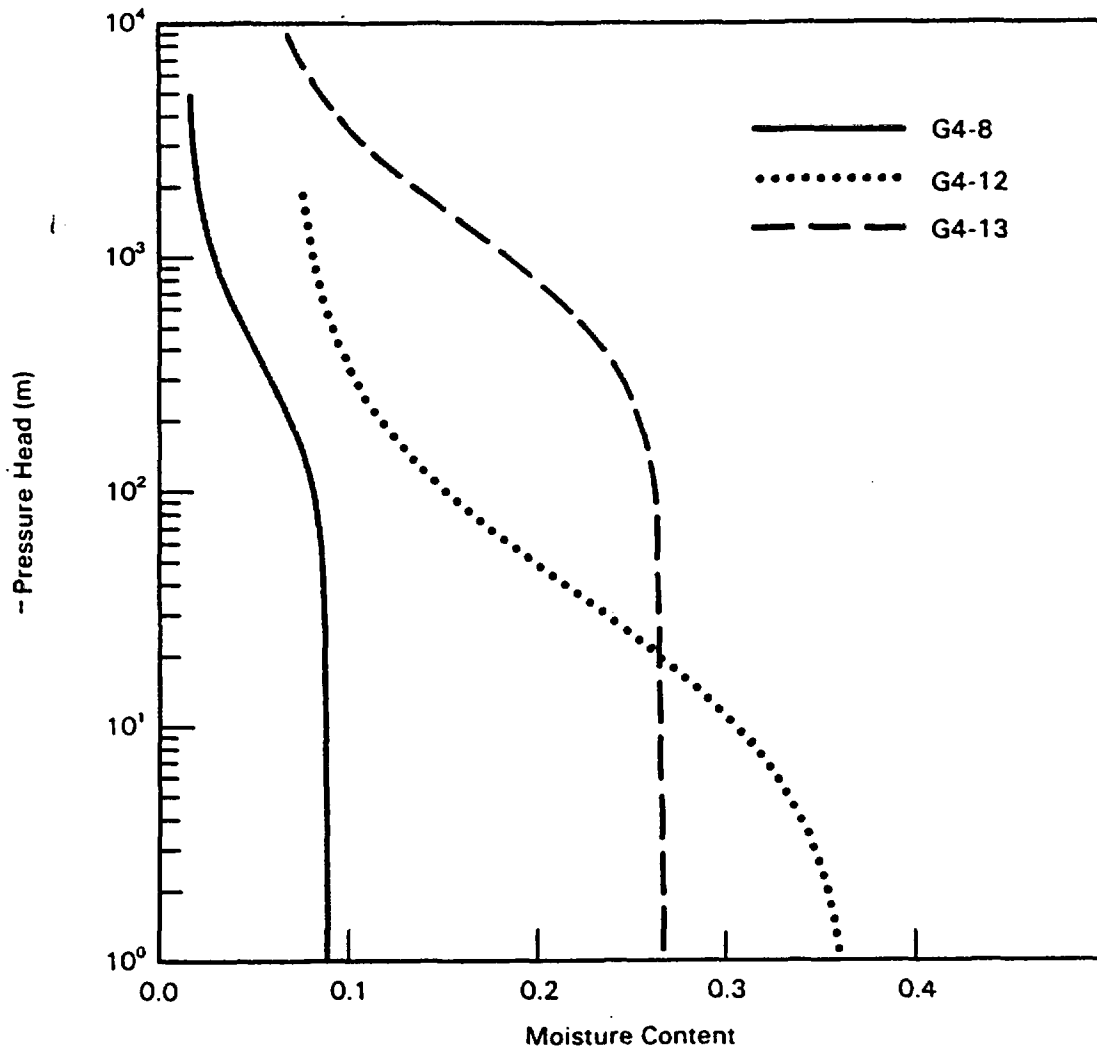


FIGURE 6. Moisture-Retention Characteristics Using Haverkamp's Formula for Core Samples Representing Stratigraphic Units in the One-Dimensional Yucca Mountain Profile

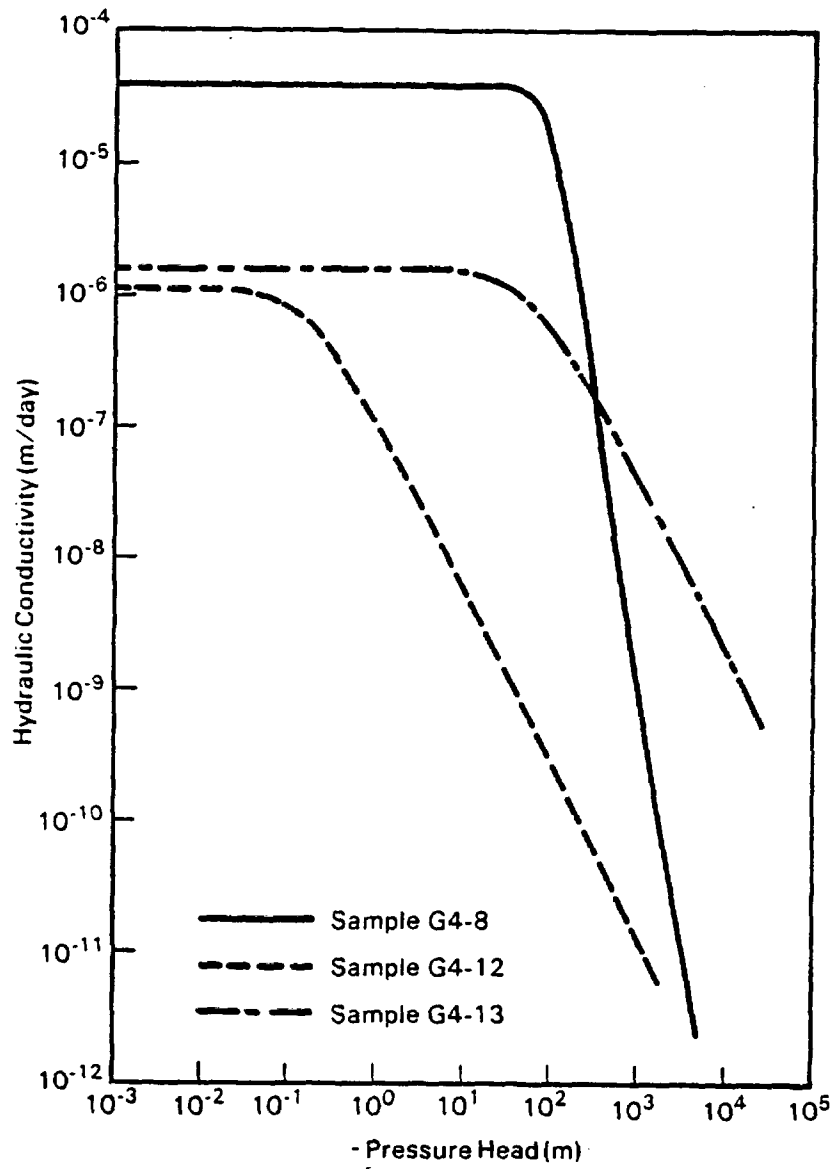


FIGURE 7. Unsaturated Hydraulic Conductivity for Core Samples G4-8, G4-12, and G4-13

The curves in Figure 7 were obtained by Haverkamp's formula (McKeon et al. 1983) for unsaturated hydraulic conductivity:

$$K(\psi) = K_s \frac{A}{A + |\psi|^B} \quad (10)$$

where K_s is the saturated hydraulic conductivity, and A, B are empirical coefficients used to fit the unsaturated hydraulic conductivity values.

To arrive at a baseline case for Yucca Mountain, saturations based on pressure heads estimated by the analytic solution were matched with saturations reported in Fernandez and Freshley (1984) (Table 3) to obtain a partial

TABLE 3. Generalized Stratigraphy and Saturations for Yucca Mountain (from Fernandez and Freshley 1984)

<u>Stratigraphic Unit</u>	<u>Saturation (%)</u>
Surficial Deposits	--
Paintbrush Tuff	
Tiva Canyon Member	33-50
Yucca Mountain Member	61-90
Pah Canyon Member	
Topopah Spring Member	17-91
Tuffaceous Beds of Calico Hills	82-100
Crater Flat Tuff	
Prow Pass Member	~100 ^(a)
Bullfrog Member	~100 ^(a)
Tram Unit	~100 ^(a)

(a) Assumed values below the static water level.

calibration of the analytic solution. The analytic solution was calibrated by adjusting the estimated percolation rate, rather than the measured hydraulic properties of the tuff. Although other values are reported in the literature, a percolation rate of 0.02 cm/yr gave the best calibration because saturations predicted by the analytical solution most closely matched the measured values. This percolation rate and the resulting distributions of pressure head and saturation were assumed to represent the baseline case for the uncertainty analysis. The total travel time from the proposed repository depth to the water tables for the baseline case is 2.17×10^5 years.

The distributions of moisture content, pressure head, and hydraulic head generated by numerical evaluation of the analytic solution are illustrated in Figures 8, 9, and 10, respectively. The resulting profile of travel time for the baseline case is illustrated by the solid line in Figure 11. The dashed lines in Figure 11 are profiles of travel time for different variations of the percolation rate.

Moisture content as illustrated by Figure 8 is not a continuous variable. Pressure head experiences a sharp jump across the lowest interface (Fig. 9). This contrast caused severe difficulties with numerical evaluation of the analytic solution. To overcome these difficulties, a grid spacing on the order of centimeters was required in the region near the interface. As illustrated in Figure 10, the steepest hydraulic-head gradients and the longest travel times occur in the lower nonwelded tuffs.

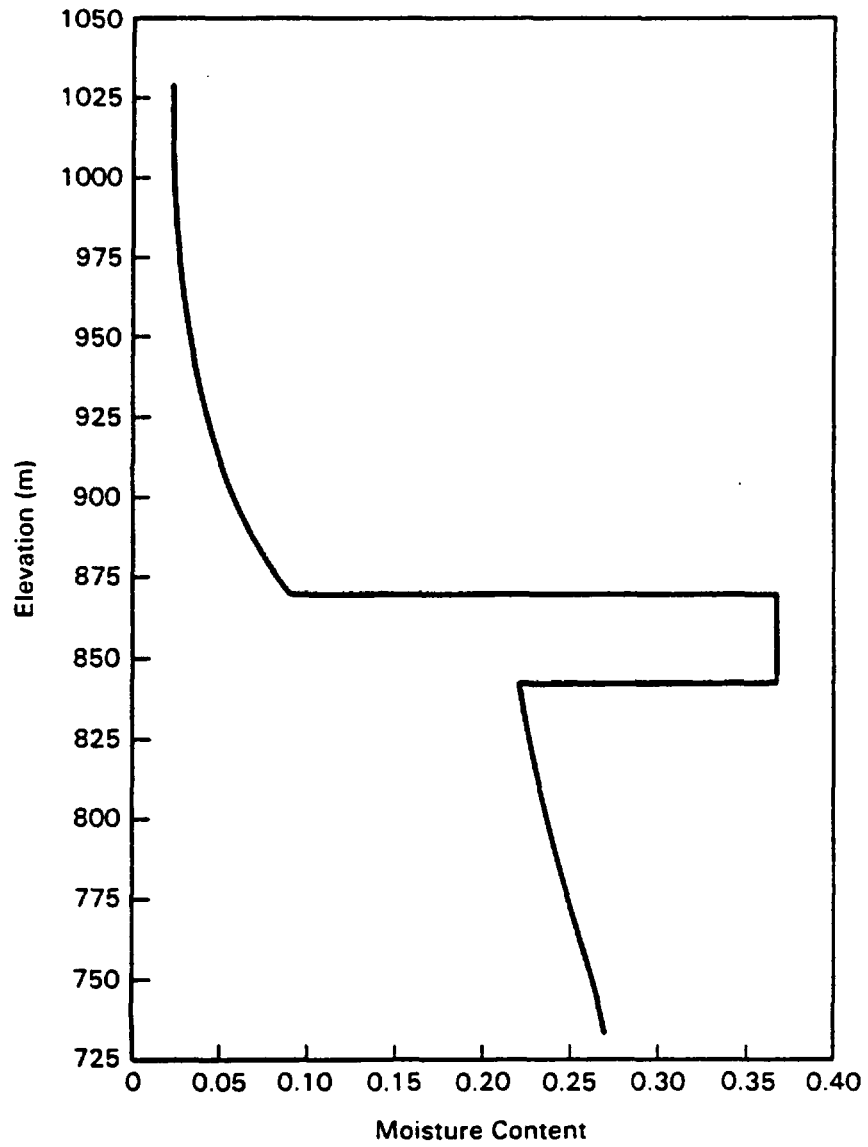


FIGURE 8. Moisture Content from Numerical Evaluation of the Analytic Solution for the One-Dimensional Yucca Mountain Profile

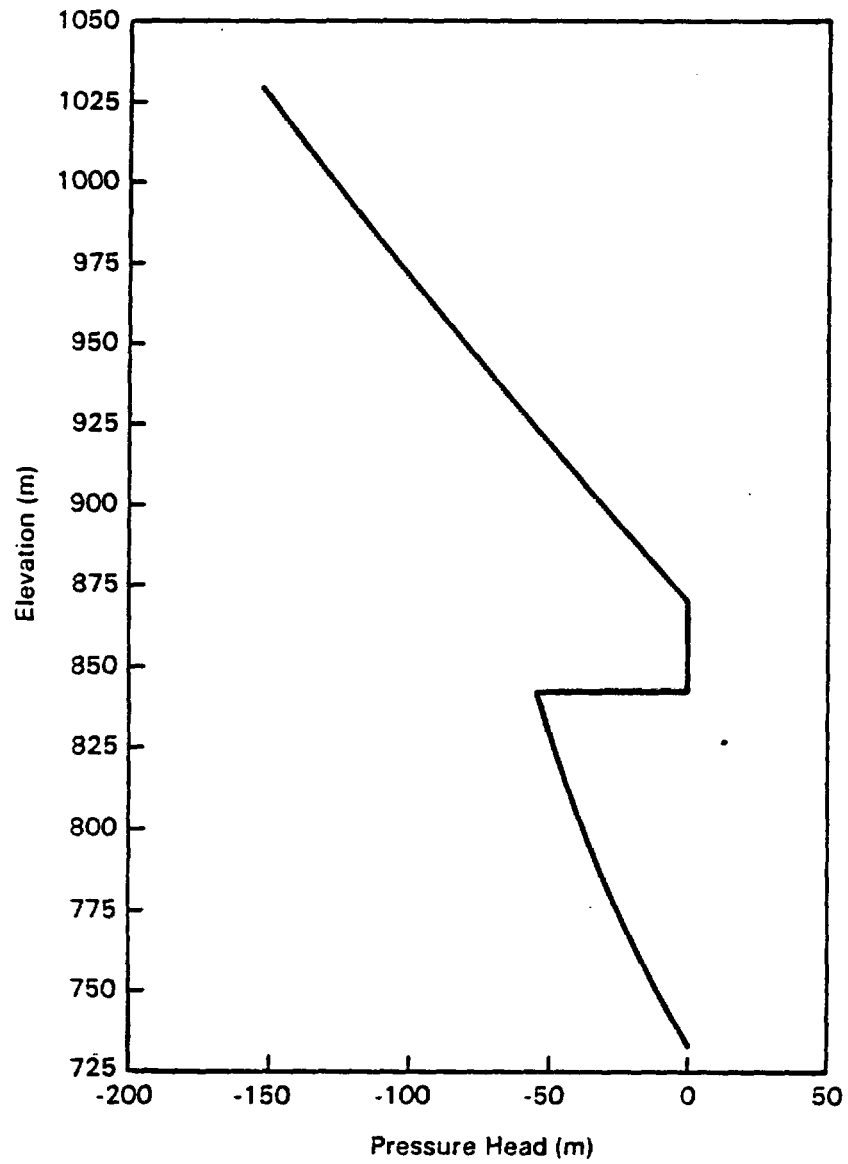


FIGURE 9. Pressure Head from Numerical Evaluation of the Analytic Solution for the One-Dimensional Yucca Mountain Profile

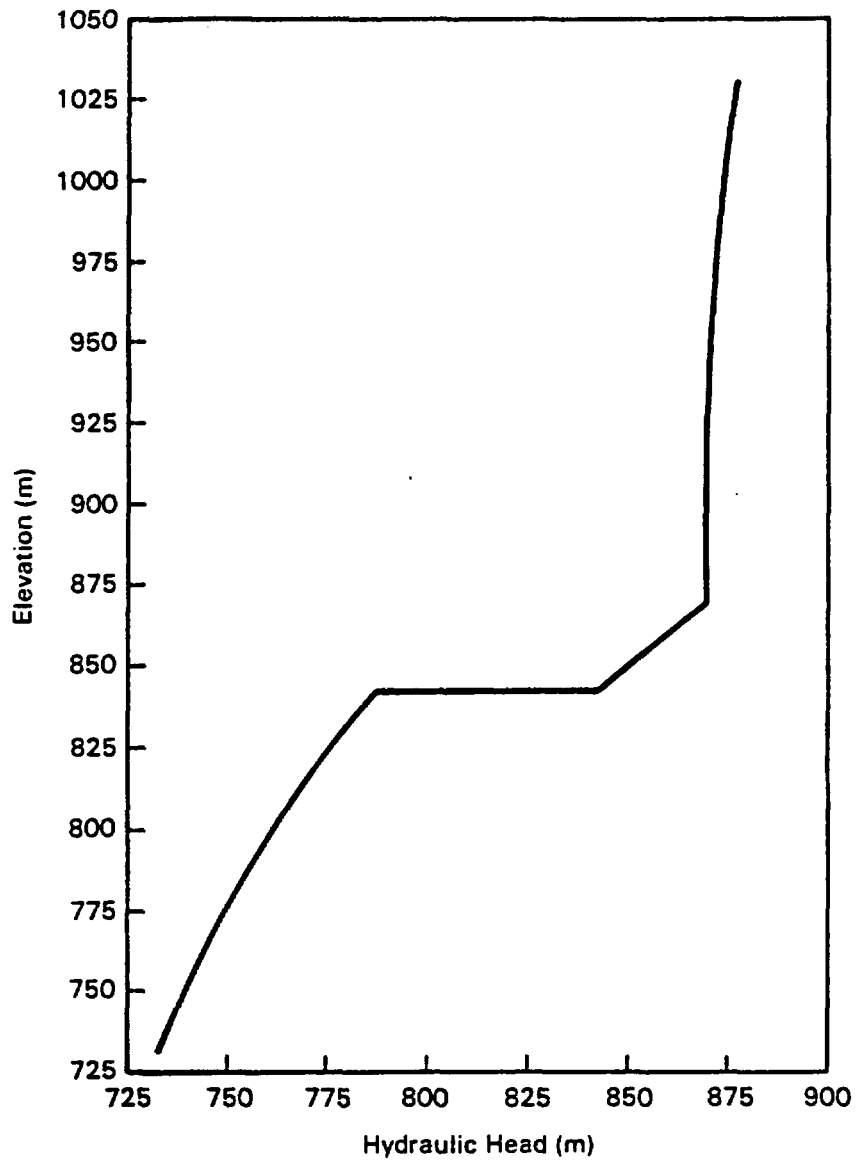


FIGURE 10. Hydraulic Head from Numerical Evaluation of the Analytic Solution for the One-Dimensional Yucca Mountain Profile

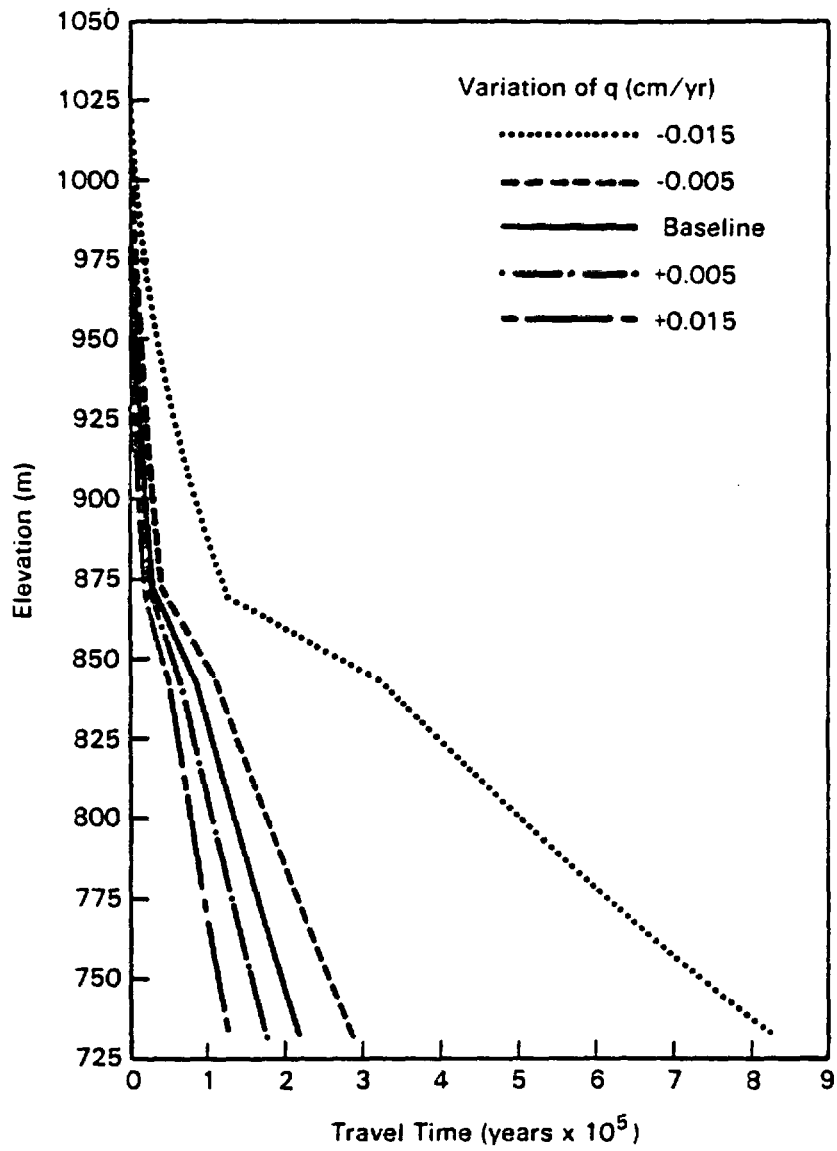


FIGURE 11. Travel Time of Water Through the One-Dimensional Yucca Mountain Profile for the Baseline Case and Variations of the Recharge Estimate

SENSITIVITY FOR INVESTIGATION OF PERCOLATION THROUGH YUCCA MOUNTAIN

Water travel time was the output function F for which uncertainty with respect to the parameter p_j , represented by the percolation rate, was investigated. Uncertainty of only one input parameter at a time was considered to contribute to the uncertainty in travel time. Variations to the baseline percolation rate of 0.02 cm/yr ranging from +0.015 cm/yr to -0.015 cm/yr (Table 4) were used to investigate the effect of the magnitude of perturbation in the input parameter on the resulting sensitivity coefficient. The total travel times from the prospective repository to the water table resulting from variations of the percolation rate are listed in Table 5. Sensitivity coefficients in Table 5 were calculated using Equation (B.4). The variation of travel time with change in percolation is illustrated in Figure 12. Variation of the sensitivity coefficient with change in percolation is illustrated in Figure 13.

Figures 12 and 13 were used to determine the appropriate sensitivity coefficient for the uncertainty analysis. Because we are considering sensitivity and uncertainty of travel time with respect to the baseline estimate, the sensitivity coefficient, which is the derivative of travel time with respect to percolation (see Fig. 12), should be calculated close to the baseline percolation estimate. When the percolation flux is small (large negative variation), both the unsaturated hydraulic conductivity $K(\psi)$ and the hydraulic gradient $\partial h/\partial z$ (or $\Delta h/\Delta z$) are small and, from Equation (2), the travel time is large (see Fig. 12). Conversely, when the percolation flux is high (large positive variation), $K(\psi)$ and $\partial h/\partial z$ are large, and travel time is small (see Fig. 12). Figure 13 illustrates that calculation of the sensitivity coefficient converges to -1.03×10^7 near 10^{-3} cm/yr perturbation of the percolation rate. When variation of the percolation rate is smaller than 5.0×10^{-4} cm/yr, some deviation from the sensitivity coefficient occurs, but the magnitude of change in S_j may be caused by numerical error.

TABLE 4. Variations from the Baseline Percolation Flux of 0.02 cm/yr and the Corresponding Flux for the Sensitivity Analysis

<u>Δq (cm/yr)</u>	<u>q (cm/yr)</u>	<u>q (m/day)</u>
+0.015	0.035	9.5890×10^{-7}
-0.015	0.005	1.3699×10^{-7}
+0.010	0.030	8.2192×10^{-7}
-0.010	0.010	2.7397×10^{-7}
+0.005	0.025	6.8493×10^{-7}
-0.005	0.015	4.1096×10^{-7}
+0.002	0.022	6.0274×10^{-7}
-0.002	0.018	4.9315×10^{-7}
+0.0015	0.0215	5.8904×10^{-7}
-0.0015	0.0185	5.0685×10^{-7}
+0.001	0.021	5.7534×10^{-7}
-0.001	0.019	5.2055×10^{-7}
+0.0008	0.0208	5.6986×10^{-7}
-0.0008	0.0192	5.2603×10^{-7}
+0.0007	0.0207	5.6712×10^{-7}
-0.0007	0.0193	5.2877×10^{-7}
+0.0006	0.0206	5.6438×10^{-7}
-0.0006	0.0194	5.3151×10^{-7}
+0.0005	0.0205	5.6164×10^{-7}
-0.0005	0.0195	5.3425×10^{-7}
+0.0002	0.0202	5.5342×10^{-7}
-0.0002	0.0198	5.4247×10^{-7}
+0.0001	0.0201	5.5068×10^{-7}
-0.0001	0.0199	5.4521×10^{-7}
+0.0005	0.02005	5.4932×10^{-7}
-0.0005	0.01995	5.4658×10^{-7}
0.0000	0.020	5.4795×10^{-7}

TABLE 5. Travel Times and Sensitivity Coefficients Corresponding to Variations from the Baseline Percolation Flux of 0.02 cm/yr

<u> \Delta q (cm/yr)</u>	<u>Tr₂ (yr) (Positive Variation)</u>	<u>Tr₁ (yr) (Negative Variation)</u>	<u>\Delta Tr (yr)</u>	<u>S_f</u>
0.015	128,526	825,710	-697,184	-2.324 x 10 ⁷
0.010	148,430	422,995	-274,565	-1.373 x 10 ⁷
0.005	176,146	286,174	-110,028	-1.100 x 10 ⁷
0.002	198,735	240,436	-41,701	-1.042 x 10 ⁷
0.0015	203,107	234,245	-31,138	-1.038 x 10 ⁷
0.001	207,684	228,377	-20,693	-1.035 x 10 ⁷
0.0008	209,577	226,115	-16,538	-1.034 x 10 ⁷
0.0007	210,536	225,002	-14,466	-1.033 x 10 ⁷
0.0006	211,505	223,900	-12,395	-1.033 x 10 ⁷
0.0005	212,483	222,809	-10,326	-1.033 x 10 ⁷
0.0002	215,476	219,601	-4,125	-1.031 x 10 ⁷
0.0001	216,493	218,554	-2,061	-1.030 x 10 ⁷
0.00005	217,001	218,034	-1,033	-1.033 x 10 ⁷

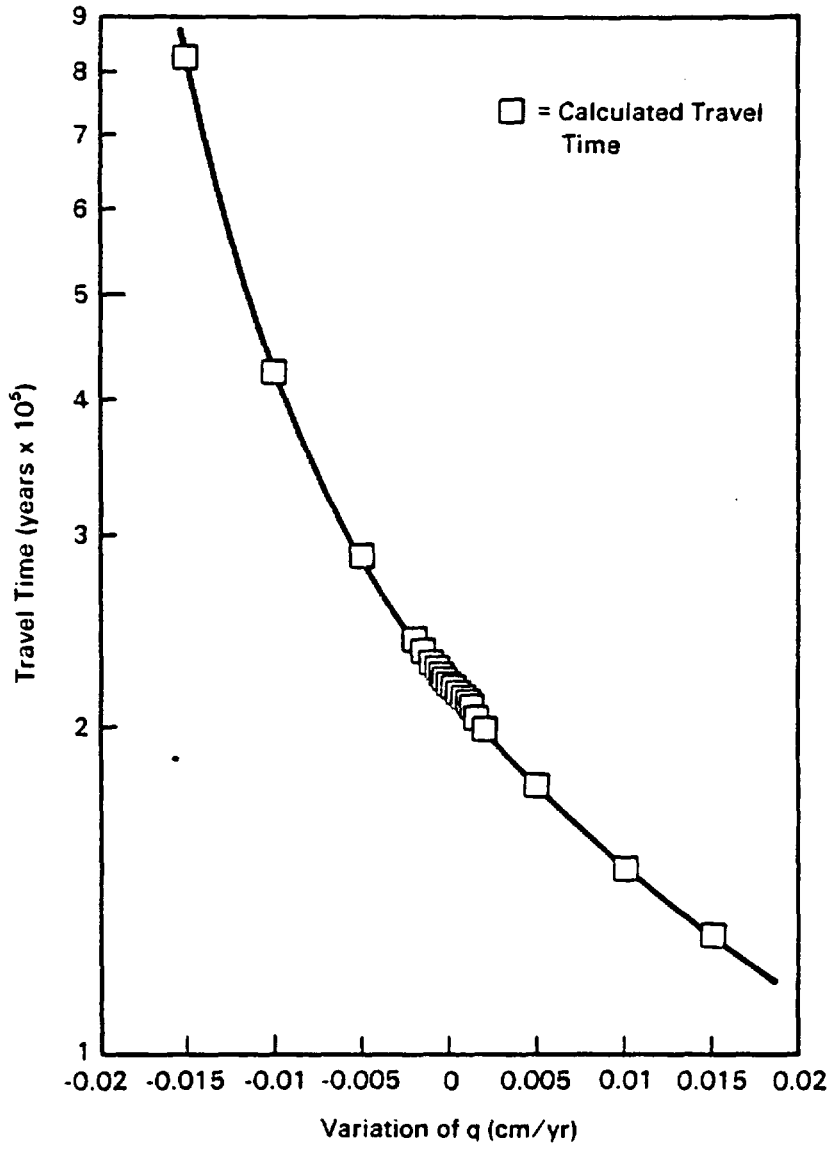


FIGURE 12. Travel Time Versus Variation from the Baseline Percolation Flux of a 0.02 cm/yr

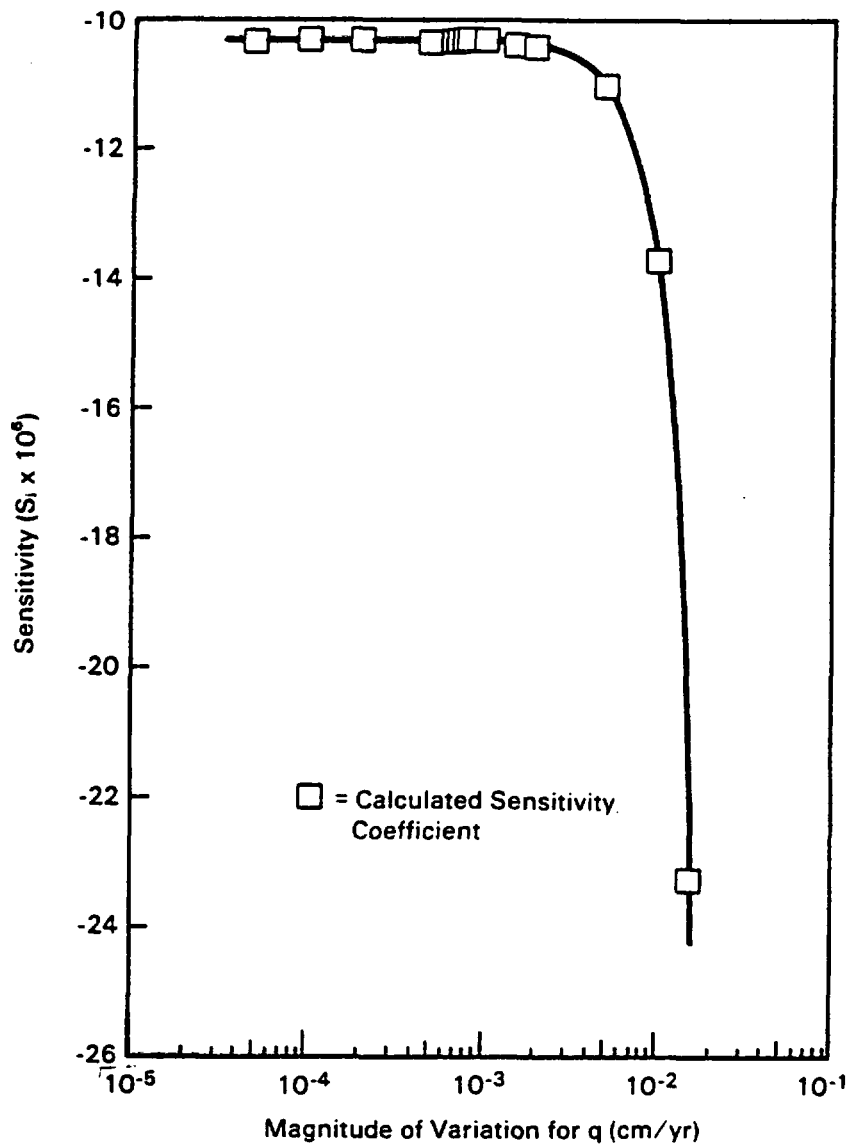


FIGURE 13. Sensitivity Versus Magnitude of Variation in the Percolation Flux

FIRST-ORDER UNCERTAINTY ANALYSIS FOR PERCOLATION

The uncertainty analysis began with an assumed range of percolation through Yucca Mountain. We assumed that percolation flux is bounded by recharge. Rice (1984) estimated recharge for regional modeling in the vicinity of Yucca Mountain to be less than 0.25 cm/yr. The U.S. Geological Survey

(USGS) suggests an upper limit to percolation of 0.4 cm/yr (Roseboom 1983), but evidence indicates that a value less than or equal to 0.1 cm/yr is more probable (Sinnock et al. 1984).

The assumed range of percolation was based on the following upper and lower bounds. The upper bound on the range of percolation was assumed to be 0.1 cm/yr, which resulted in a saturated profile from the analytic solution with the upper few meters showing noticeable drainage. Saturation was assumed to represent the limiting case.

The lower bound for the range of percolation was determined to be 3.0×10^{-3} cm/yr. This value was obtained from the graph of travel time versus perturbation of recharge (see Fig. 12). At a recharge rate of 3.0×10^{-3} cm/yr (perturbation of -0.02 cm/yr), travel time begins to approach infinity (see Fig. 12).

Because the range of percolation is not symmetric about the mean, we used natural logarithms of the values (Table 6). We assumed the estimates of percolation are lognormally distributed; variation of the logged values is more nearly symmetrical.

TABLE 6. Range of Percolation Estimates for the First-Order Uncertainty Analysis

Value of q (cm/yr)	$\ln^{(a)}(q)$	Differences between $\ln(q)$
0.003	-5.81	
		1.897
0.02	-3.91	
		1.609
0.10	-2.30	

(a) \ln denotes the natural logarithm.

We assumed 1.61, the smaller of the two differences in Table 6, represented a multiple of the standard deviation. The value selected is based on the upper bound on the range of percolation.

Properties of the lognormal distribution were used to examine the ranges $2\sigma_{\ln q} = 1.61$ and $3\sigma_{\ln q} = 1.61$, where $\sigma_{\ln q}$ represents the standard deviation

of the logged percolation. The number $2\sigma_{\ln q}$ means that 95.45 percent of the values are within the range $\ln(q_0) \pm 2\sigma_{\ln q}$ (Burington 1973), where q_0 denotes the baseline estimate of percolation. The number $3\sigma_{\ln q}$ means that 99.97 percent of the values are within the range $\ln(q_0) \pm 3\sigma_{\ln q}$.

If $2\sigma_{\ln q} = 1.61$, $\sigma_{\ln q} = 0.80$ and the variance of the $\ln q$ of q is $\text{Var}(\ln(q)) = (\sigma_{\ln q})^2 = 0.65$. According to Benjamin and Cornell (1970), the transformation of variance from natural logarithms to the unlogged values is

$$\text{Var}(q) = (q_0)^2 (\exp(\text{Var}(\ln q)) - 1) \quad (11)$$

For $\text{Var}(\ln(q)) = 0.65$,

$$\text{Var}(q) = 3.65 \times 10^{-4} \frac{\text{cm}^2}{\text{yr}^2}$$

Then, the variance of travel time, Tr , by Equation (6) is

$$\text{Var}(Tr) = 3.89 \times 10^{10} \text{ yr}^2$$

and the standard deviation is $\sigma_{Tr} = \sqrt{\text{Var}(Tr)} = 1.97 \times 10^5$ years.

If 1.61 is assumed to be three standard deviations of the logged percolation flux, the resulting variance and standard deviation of travel time are $1.42 \times 10^{10} \text{ yr}^2$ and 1.19×10^5 years, respectively.

The standard deviations of travel time for $2\sigma_{\ln q}$ and $3\sigma_{\ln q}$ are close to 100 and 50 percent of travel time for the baseline recharge.

FIRST-ORDER UNCERTAINTY ANALYSIS FOR HYDRAULIC CONDUCTIVITY

To compare uncertainty in travel time resulting from uncertainty in hydraulic conductivity with that caused by uncertainty in percolation through Yucca Mountain, an uncertainty analysis of travel time based on hydraulic

conductivity was performed. Inasmuch as most of the travel time through the unsaturated zone at Yucca Mountain occurs in the lower nonwelded tuff (see Fig. 11), this unit was selected for variation of hydraulic conductivity in the uncertainty analysis. The saturated hydraulic conductivity of Sample G4-13 in Figure 5 was varied in the analysis; changing the saturated hydraulic conductivities shifts the unsaturated hydraulic conductivity curves up or down, depending on the sign of the change

The saturated hydraulic conductivity of the lowermost stratigraphic unit of the profile was considered in the uncertainty analysis of travel time for comparison with the uncertainty analysis based on estimates of percolation. It would be possible to consider functional variation of unsaturated hydraulic conductivity as well, provided the functional relationship is known.

To determine the sensitivity coefficient for travel time with respect to hydraulic conductivity, a wide range of variations to a baseline hydraulic conductivity of 0.06 cm/yr was considered (Table 7). The travel times and sensitivity coefficients associated with variations of the hydraulic conductivity are listed in Table 8. From Table 8, the sensitivity coefficient appears to converge near $-1.76 \times 10^5 \text{ yr}^2/\text{cm}$ at small variations of hydraulic conductivity. The lower limit of hydraulic conductivity was assumed to be 0.02 cm/yr, which is the baseline percolation flux for this study and results in a saturated profile. The upper limit was assumed to be an order of magnitude larger than the baseline hydraulic conductivity; Freeze and Cherry (1979) state that order-of-magnitude estimates of hydraulic conductivity are reasonable.

Hydraulic conductivities are generally accepted as being lognormally distributed (Davis 1969), so we used logarithms of hydraulic conductivity to describe the variations used in the uncertainty analysis (Table 9). We assumed the difference that includes the lower limit was representative because the lower limit of the range for hydraulic conductivity is based on the Yucca Mountain flow system, namely that hydraulic conductivity that yields a saturated profile.

TABLE 7. Variations of Saturated Hydraulic Conductivity (K_s) of Sample G4-13 for Calculating the Sensitivity Coefficient for Travel Time with Respect to Hydraulic Conductivity

Percent Variation	Variation of K_s (cm/yr)	Variation of K_s (m/day)	K_s (m/day)
90	0.0528	-1.45 x 10 ⁻⁶ +1.45 x 10 ⁻⁶	(saturated profile)
50	0.0293	-8.04 x 10 ⁻⁷ +8.04 x 10 ⁻⁷	8.04 x 10 ⁻⁷ 2.41 x 10 ⁻⁶
30	0.0176	-4.82 x 10 ⁻⁷ +4.82 x 10 ⁻⁷	1.12 x 10 ⁻⁶ 2.09 x 10 ⁻⁶
20	0.0117	-3.21 x 10 ⁻⁷ +3.21 x 10 ⁻⁷	1.29 x 10 ⁻⁶ 1.93 x 10 ⁻⁶
10	0.0059	-1.61 x 10 ⁻⁷ +1.60 x 10 ⁻⁷	1.45 x 10 ⁻⁶ 1.77 x 10 ⁻⁶
5	0.0029	-8.04 x 10 ⁻⁸ +8.04 x 10 ⁻⁸	1.53 x 10 ⁻⁶ 1.69 x 10 ⁻⁶

TABLE 8. Travel Times and Sensitivity Coefficients Corresponding to Variations of the Saturated Hydraulic Conductivity of Sample G4-13

Percent Variation	Variation of K_s (cm/yr)	Tr_2 (yr) (Positive Variation)	Tr_1 (yr) (Negative Variation)	S_i
50	0.0293	213,900	226,445	-2.137 x 10 ⁵
30	0.0176	215,059	221,683	-1.882 x 10 ⁵
20	0.0117	215,757	220,009	-1.817 x 10 ⁵
10	0.0059	216,566	218,646	-1.763 x 10 ⁵
7	0.0041	216,835	218,285	-1.768 x 10 ⁵
5	0.0029	217,022	218,056	-1.783 x 10 ⁵

TABLE 9. Range of Saturated Hydraulic Conductivities Used in the First-Order Uncertainty Analysis

<u>Value of K_s (cm/yr)</u>	<u>$\ln(K_s)$</u>	<u>Differences Between $\ln(K_s)$</u>
0.02	-3.912	
		1.082
0.059	-2.830	
		2.302
0.59	-0.528	

If $2\sigma_{\ln K} = 1.08$, $\sigma_{\ln K} = 0.54$, and $\text{Var}(\ln K) = 0.29$, then, based on the transformation of variance from logged to unlogged values by Equation (11),

$$\text{Var}(K) = 1.18 \times 10^{-3} \frac{\text{cm}^2}{\text{yr}^2}$$

The variance of travel time for $2\sigma_{\ln K} = 1.08$ is, by Equation (6),

$$\text{Var}(Tr) = 3.68 \times 10^7 \text{ yr}^2$$

and the standard deviation is $\sigma_{Tr} = 6.07 \times 10^3$ years.

If 1.08 is assumed to be three standard deviations of the logged saturated hydraulic conductivity, the resulting variance and standard deviation of travel time are $1.50 \times 10^7 \text{ yr}^2$ and 3.88×10^3 years, respectively.

The standard deviations for $2\sigma_{\ln K}$ and $3\sigma_{\ln K}$ are much less than the magnitude of the baseline travel time.

COMPARISON OF THE UNCERTAINTY ANALYSES FOR PERCOLATION AND HYDRAULIC CONDUCTIVITY

By comparing the uncertainty analyses we can determine whether percolation or saturated hydraulic conductivity contributes more to uncertainty of water travel time through the unsaturated zone at Yucca Mountain. The variances of travel time indicate that uncertainty in the estimates of percolation through

Yucca Mountain contributes much more to uncertainty in travel time than uncertainty in saturated hydraulic conductivity for the range of values considered. We calculated a travel-time variance of about 100 percent of the baseline value resulting from variance of percolation, whereas, the variance of saturated hydraulic conductivity of the lowermost, nonwelded tuff in the Yucca Mountain profile produced a 5 percent travel-time variance.

The sensitivity coefficients (see Tables 5 and 8) indicate that changes in travel time are greater for changes in the percolation estimate than for changes in hydraulic conductivity. Consequently, travel time is more sensitive to the percolation rate than to saturated hydraulic conductivity of the lowermost layer of the profile by two orders of magnitude. The negative sign of the sensitivity coefficients indicates that, as the percolation flux and saturated hydraulic conductivity increase, travel time decreases. This result is consistent because travel time is inversely proportional to both the hydraulic conductivity and percolation flux. The variances of percolation flux and hydraulic conductivity demonstrate opposite behavior from the sensitivity coefficients. The assumed variance of the unlogged recharge estimate was an order of magnitude smaller than that assumed for hydraulic conductivity. However, in the equation for travel-time uncertainty [Equation (6)], the sensitivity coefficient is squared and has a greater influence on travel-time variance than the parameter variance. This causes the uncertainty in travel time resulting from uncertainty in the estimate of percolation to be larger than that resulting from uncertainty in saturated hydraulic conductivity of the lowermost layer of the profile.

UNCERTAINTY ANALYSIS OF GROUND-WATER TRAVEL TIME
IN THE SATURATED ZONE

In steady-state ground-water flow systems, ground-water travel time along a given pathline is a function of 1) hydraulic gradient, 2) transmissivity (or hydraulic conductivity), and 3) effective thickness (or effective porosity). Uncertainty in numerical predictions of ground-water travel time arises from lack of knowledge about the spatial variations of these hydrogeologic properties. Additional sources of uncertainty may be caused by the lack of knowledge about the boundary conditions, sources, sinks, and conceptual models. In this study, only the uncertainty in ground-water travel time caused by the uncertainty in hydrogeologic parameters is addressed because insufficient information was available about the boundary conditions, sources, and sinks to treat them in a statistical manner. In this section, two techniques (Monte Carlo and first-order analysis) are used to calculate the uncertainty in ground-water travel time caused by uncertainty in transmissivity and effective thickness (effective porosity times the thickness of the aquifer).

Given estimates of the mean, variance, and probability density distribution for each of the two hydrologic parameters, a Monte Carlo technique was used to calculate the ground-water travel-time uncertainty for seven cases. The different cases varied in the treatment of the hydrologic information.

The calculation of uncertainty in ground-water travel time by a first-order analysis requires an estimate of the mean and variance of the hydrologic parameters together with an estimate of the first derivative of travel time with respect to the hydrologic parameters. The first derivative is also called the sensitivity coefficient. A sensitivity analysis was applied to the four cases with the most reasonable hydrologic parameters to observe the sensitivity of the ground-water travel times to each hydrologic parameter and obtain the information necessary for the calculation of uncertainty in travel time from a first-order analysis.

The estimates of ground-water travel time uncertainty as calculated by the Monte Carlo and first-order methods are compared and discussed in this section. Also discussed is how the mean travel time and its variance is influenced by

the distribution of hydraulic head, spatial variability of the effective porosity, and uncertainty associated with the effective porosity.

NUMERICAL CALCULATION OF GROUND-WATER TRAVEL TIME

Ground-water flow in the study area is treated as two dimensional and in steady state. The governing equation for two-dimensional steady-state flow in heterogeneous isotropic media with no sources or sinks is given by

$$\nabla \cdot (\underline{T} \nabla h) = 0 \quad (12)$$

where ∇ is the two-dimensional gradient operator, \underline{T} is the transmissivity tensor, and h is hydraulic head. The solution of Equation (12) is subject to constant hydraulic head and/or constant flux boundary conditions. Following the solution of Equation (12), the ground-water travel time can be calculated from

$$Tr = \int_L \frac{dL}{|\underline{q}_s|} \quad (13)$$

where Tr is the ground-water travel time and L is the path length of interest. The seepage velocity \underline{q}_s (defined as the Darcy velocity divided by the effective porosity) is a vector quantity that is calculated from Darcy's law and is given by

$$\underline{q}_s = - \frac{\underline{T} \nabla h}{n_e b} \quad (14)$$

where n_e is the effective porosity and b is the thickness of the saturated zone. The product $n_e b$ may be called the 'effective thickness' (Leonhart et al. 1983; Clifton et al. 1983) and represents the area of pore space in a vertical plane of the flow system of unit width and thickness b . Equation (13) may be rewritten using Equation (14) as follows:

$$Tr = \int_L \frac{n_e b}{T \sqrt{vh}} dL \quad (15)$$

Ground-water travel time may be calculated by Equation (15) if the path length, spatial distribution of transmissivity, boundary conditions, and spatial distribution of effective thickness are specified.

For this analysis, Equation (12) is solved numerically by the finite difference Variable Thickness Transient (VTT) ground-water flow code (Reisenauer 1979). In the finite difference discretization of the flow domain, the spatial distribution of transmissivity is represented by parameter values assigned to each node. However, when there is insufficient information about the spatial variability of transmissivity to assign differing parameter values to each finite difference node, the flow domain must be divided into zones consisting of a group of nodes with a uniform transmissivity. The numerical solution to Equation (15) for ground-water travel time is obtained by approximating the steady-state seepage velocities over the flow domain from Equation (14) and integrating these velocities along the path of interest. To obtain travel time, the spatial distribution of effective thickness (or effective porosity) must also be represented in some discrete manner over the flow domain.

ANALYSIS OF UNCERTAINTY IN GROUND-WATER TRAVEL TIME

The aquifer parameters necessary for calculating ground-water travel-time--the transmissivity and effective thickness--can be treated stochastically by considering them as random variables with known mean, variance, and probability density distribution. The boundary conditions necessary to solve Equation (7) may also be treated stochastically if sufficient statistical information is available. Based on the uncertainties in the input parameters, the mean and variance of ground-water travel-time may be calculated by a Monte Carlo or first-order analysis to quantify the uncertainty in the travel times.

Correlation Among Parameters

In a given geologic formation, it is generally accepted that hydraulic conductivities and transmissivities are lognormally distributed parameters, whereas porosities are usually reported to be normally distributed (Davis 1969; Freeze 1975; Neuman 1982). If the thickness of the aquifer is constant (as assumed in this study), the effective thickness ($n_e b$) will also be normally distributed.

Because the permeability (ease of fluid flow) depends on interconnected (effective) porosity, we expect correlation between these two parameters. Permeability, which is related to properties of the geologic medium, is generally correlated with hydraulic conductivity, which is a function of the properties of both the geologic medium and the fluid. If the properties of the fluid are constant, a correlation between hydraulic conductivity and effective porosity is likely because of the correlation between permeabilities and effective porosity. In addition, a correlation between transmissivity and effective porosity can be assumed because transmissivity is the product of hydraulic conductivity and the saturated thickness, and the saturated thickness is assumed constant over the flow domain for this study.

Brace et al. (1982) studied the relationship between porosity and permeability in granite, basalt, and tuff and concluded that permeability generally does not correlate directly with effective porosity. For example, the porous rock permeabilities of granite and shale are about the same, whereas the porosity of granite is typically less than half a percent and porosity of shale is usually 10 percent or greater. Brace et al. (1982) suggest that pore dimension accounts for the apparent discrepancy. Thus, for a geologic formation composed of one material with a characteristic distribution of pore size, the permeability may be correlated with effective porosity.

Brace et al. (1982) discuss the relationship between porosity and permeability for flow through isotropic porous rock and flow through rough parallel fractures and found that for porous rock, the following expression for permeability is widely applicable:

$$k = \frac{m^2}{k_0} n_e^3 \quad (16)$$

where k_0 is a dimensionless constant that can vary between 2 and 3, n_e is the effective porosity, and m is one fourth of the diameter of a cylindrical pore. For fractures the permeability is given by

$$k = \frac{b^3}{12J} \quad (17)$$

where b is the aperture of the fractures and J is the spacing between fractures. Because, b/J is the fracture porosity, n_f , the permeability may be expressed as

$$k = \frac{b^2}{12} n_f \quad (18)$$

Assuming that n_f is the effective porosity in flow through fractures, a comparison of Equations (16) and (18) clearly demonstrates the difference in the role played by effective porosity in flow through porous versus fractured media. Based on these relationships between permeability and porosity, we can assume that hydraulic conductivity (transmissivity) and effective porosity are correlated parameters for a given type of geologic material.

APPLICATION TO AQUIFER NEAR YUCCA MOUNTAIN

As previously discussed, the ground-water flow system in the vicinity of Yucca Mountain was modeled as a single-layer aquifer. The region modeled is shown in Figure 14 and lies between long. 116°37'W and long. 116°11'W and between lat. 37°00'N and lat. 36°40'N. To estimate ground-water travel time from the proposed repository in Yucca Mountain to the accessible environment (defined at a distance of 10 km from the repository), seven pathlines were considered with their starting points located between Wells USW G-1 and USW H-3 (see Fig. 14) and their end points on a line just south of Well J12.

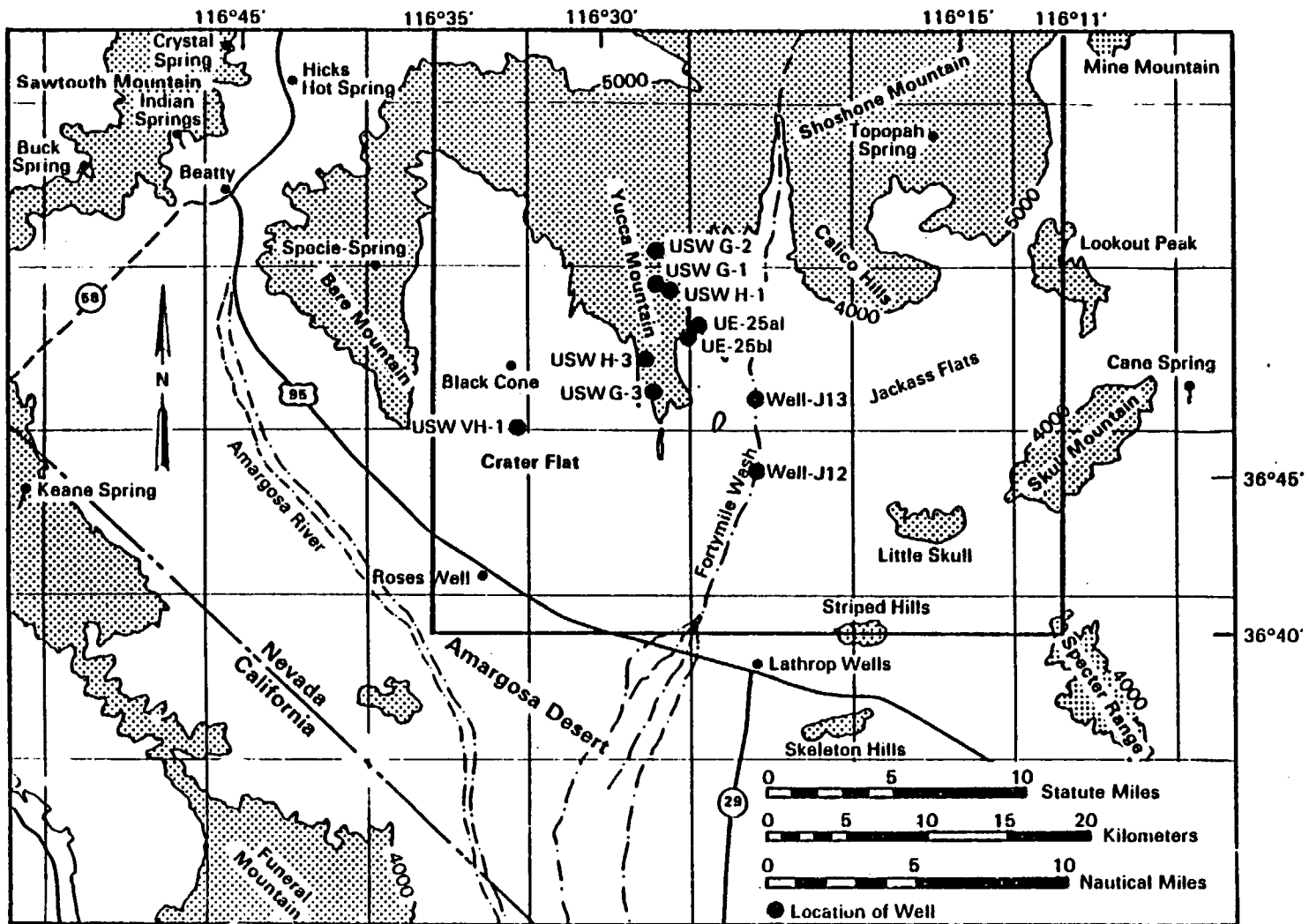


FIGURE 14. Study Area for Saturated Flow

Travel times calculated along these pathlines were averaged to obtain a representative travel time. Although only the local ground-water flow system within a radius slightly in excess of 10 km from the tentative repository location was involved in the calculation of travel times, a ground-water flow model of the larger region was used to estimate the distribution of hydraulic head and thereby minimize the effect of boundary conditions on the computed hydraulic heads within the area of interest.

A square finite difference grid composed of 47 rows and 49 columns with approximately one-half-mile node spacing was superimposed over the study area. Transmissivities considered representative of the area surrounding each node were assigned to each node. The flow region was divided into nine zones of constant transmissivity (Fig. 15). No recharge was assumed over the area. Constant hydraulic heads were imposed at all boundaries based on a USGS interpretation of steady-state hydraulic heads.^(a) Given the boundary conditions and estimates of the hydraulic parameters, the distribution of steady-state hydraulic head distribution within the study area was calculated to determine the corresponding ground-water travel time.

Seven Specific Cases for Uncertainty Analysis

The uncertainty in ground-water travel time was calculated for seven different cases that varied in the treatment of the hydrologic information (Table 10). The various combinations of hydrologic parameters were chosen in order to investigate the effect on travel-time uncertainty of 1) the use of simulated hydraulic heads from the aquifer parameters versus a fixed distribution of hydraulic head that may not reflect a mass balance solution for the flow system, 2) the representation of effective porosity by either one value over the entire flow domain or differing values in selected zones to allow for spatial variability, and 3) the treatment of the effective porosity as a deterministic parameter (known values with no uncertainty) or a random parameter. In all seven cases, transmissivity was treated as a spatially varying, random parameter.

(a) Written communication from USGS, Denver Office, to PNL, March 31, 1982.

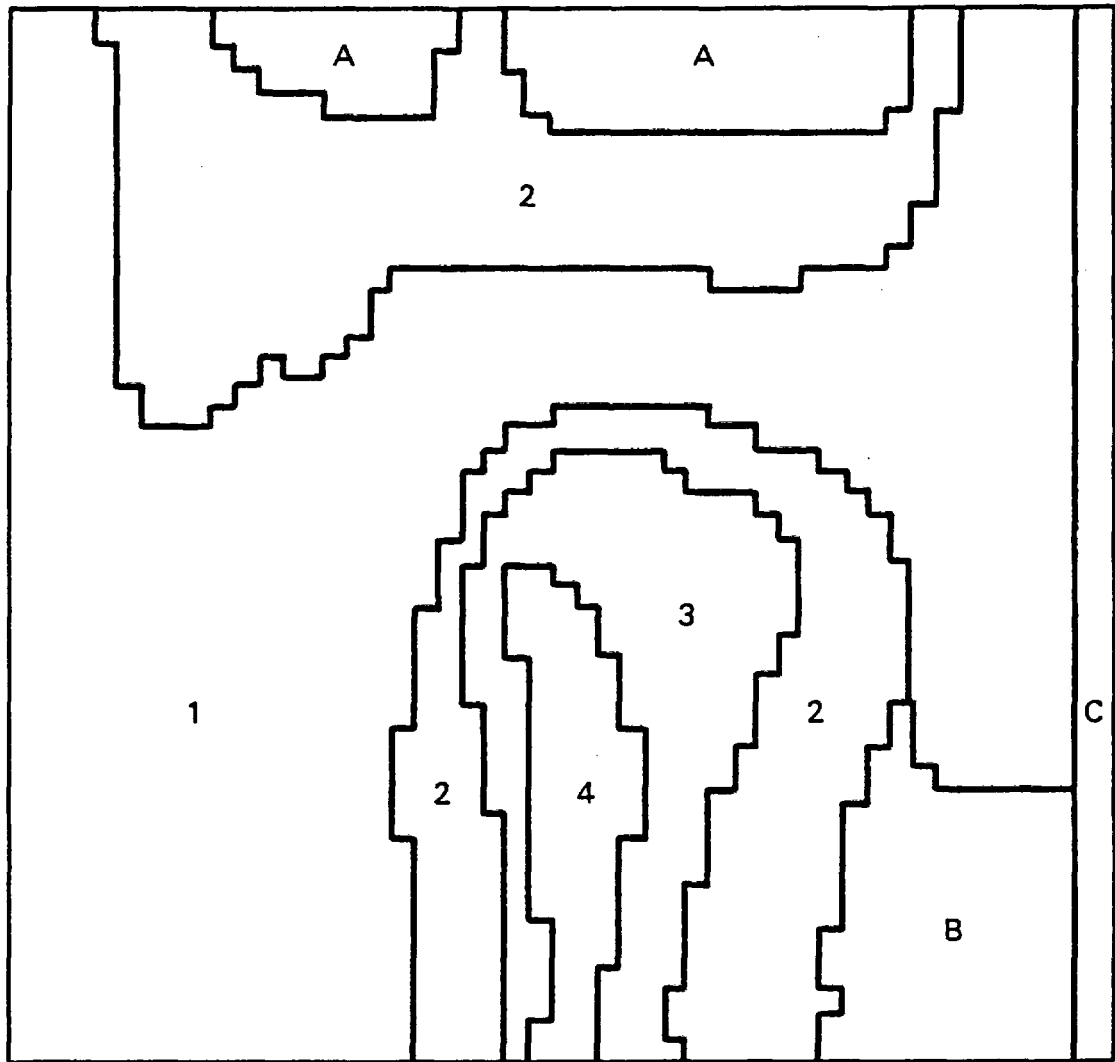


FIGURE 15. Transmissivity Zonation Pattern for the Study Area

Statistical Properties of Transmissivity

The transmissivity zonation pattern illustrated in Figure 15 was determined by considering 1) the transmissivity zones used in the USGS two-dimensional, regional ground-water flow model (Waddell 1982), 2) the transmissivity distribution from the regional flow model presented by Rice (1984), and 3) the transmissivity pattern calculated using a stream-tube technique

TABLE 10. Hydrologic Information Used in Each of the Seven Cases for Which Uncertainty in Ground-Water Travel Time was Calculated

TABLE 10. Hydrologic Information Used in Each of the Seven Cases for Which Uncertainty in Ground-Water Travel Time was Calculated

Case Number	Transmissivity Spatially Varying and Random	Hydraulic Heads			Effective Porosity			
		USGS Interpretation	Simulated for Each Realization of Transmissivities	Simulated from Mean Transmissivities	Uniform		Spatially Variable	
					Constant	Random	Constant	Random Correlated with Transmissivities
1	X	X			X			
2	X		X		X			
3	X		X			X		
4	X	X					X	
5	X			X			X	
6	X		X				X	
7	X		X					X

described in Thompson et al. (1984). Only large-scale spatial variability is represented by the transmissivity zones shown in Figure 15. The aquifer thickness is assumed to be a constant value of 81 m (Thompson et al. 1984) because of the lack of information on the spatial variability of the thickness of the saturated zone.

Zones A, B, and C (see Fig. 15) are not along any pathline from the proposed repository site. Thus, the transmissivity values in these zones were held constant in all the simulations and were not considered in the uncertainty analysis. The mean transmissivity values for each of the seven zones were determined based on estimates presented in the three studies mentioned previously. Inasmuch as transmissivity is generally considered to be lognormally distributed, the mean and standard deviation of the common logarithm (base 10) of transmissivity ($\log T$) must be determined. First a mean value of transmissivity was estimated for each zone and then the log of that mean value was used to calculate the mean value of $\log T$ (i.e., $\bar{T}_1 = 5 \text{ m}^2/\text{day}$, thus $\log \bar{T}_1 = 0.7$). The range in magnitude of the values of \log transmissivity over the zone was used to estimate the standard deviation by the following method. With a range in T_1 values from $2.0 \text{ m}^2/\text{day}$ to $12.6 \text{ m}^2/\text{day}$, the corresponding range in $\log T_1$ values is 0.30 and 1.10. Assuming that the total range represents two standard deviations ($2 \sigma_{\log T_1}$) on either side of the mean value, then $\sigma_{\log T_1} = 0.8/4 = 0.20$ is the estimate of the standard deviation. For a normal (i.e., Gaussian) distribution, 95.5% of the values are within two standard deviations on either side of the mean value. The estimates of mean and standard deviation of the \log transmissivity in each zone is listed in Table 11.

Generation of Realizations of Transmissivity

Realizations of the transmissivity distribution were generated by first generating realizations of \log transmissivity. Because \log transmissivity was assumed to be normally distributed, Gaussian errors, e , were generated for each zone of transmissivity and multiplied by the corresponding standard deviation ($\sigma_{\log T}$). This product was added to the mean of the \log transmissivity ($\log T + \sigma_{\log T} \cdot e$) to obtain a realization of the value of \log transmissivity. The corresponding value of transmissivity was obtained by taking the antilogarithm of the \log transmissivity. This procedure was followed to obtain

TABLE 11. Estimates of Mean and Standard Deviation of Log Transmissivity for Each Zone

Zone	Mean Transmissivity	Mean Log Transmissivity	Standard Deviation log Transmissivity
	$\bar{T}(\text{m}^2/\text{day})$	$\log \bar{T}$	$\sigma_{\log T}$
1	5.0	0.70	0.20
2	20.0	1.3	0.30
3	100.0	2.0	0.15
4	1200.0	3.08	0.30
A	40.0	-	-
B	50.0	-	-
C	1.0	-	-

100 realizations of the transmissivity distribution. The procedure did not consider correlation among the transmissivities. The correlation structure can be included in the process of generating realizations (Clifton and Neuman 1982); however, currently available information on correlation of transmissivity values between the zones is insufficient for this type of analysis. Therefore, for this study the transmissivities in each of the zones were considered to be independent of those in other zones.

The Monte Carlo approach to uncertainty analysis requires the generation of enough realizations to reproduce the statistical properties of the hydrologic parameters. Because the purpose of this study is to demonstrate the use of various approaches to uncertainty analysis and not to produce a definitive analysis of the Yucca Mountain system, only 100 realizations of the spatial distribution of transmissivity were generated. The mean, standard deviation, and probability density distribution of the Gaussian errors in each zone were calculated to determine how accurately the 100 realizations reproduced the assumed values of the statistics of the log transmissivities. The resulting distribution of Gaussian errors is plotted in Figure 16a through Figure 16d for each zone. The calculated means and standard deviations are all within 6 percent of the assumed values of the statistics. However, under ideal conditions, these values should be closer to the assumed values. This lack of

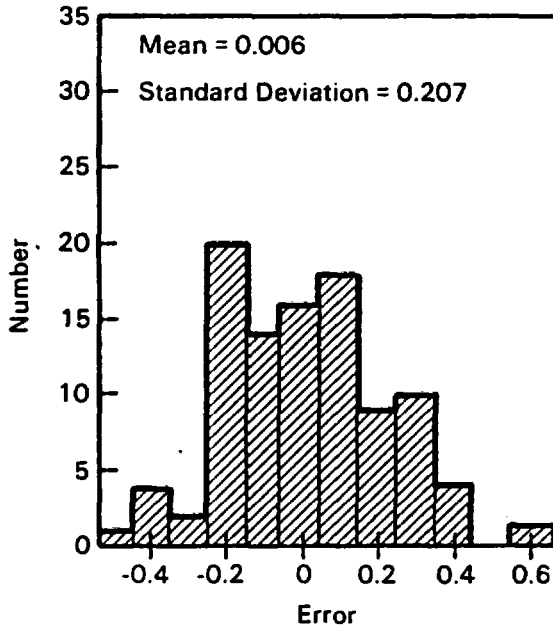


FIGURE 16a. Distribution of Gaussian Errors for Transmissivity Zone 1 ($\bar{T}_1 = 5 \text{ m}^2/\text{day}$)

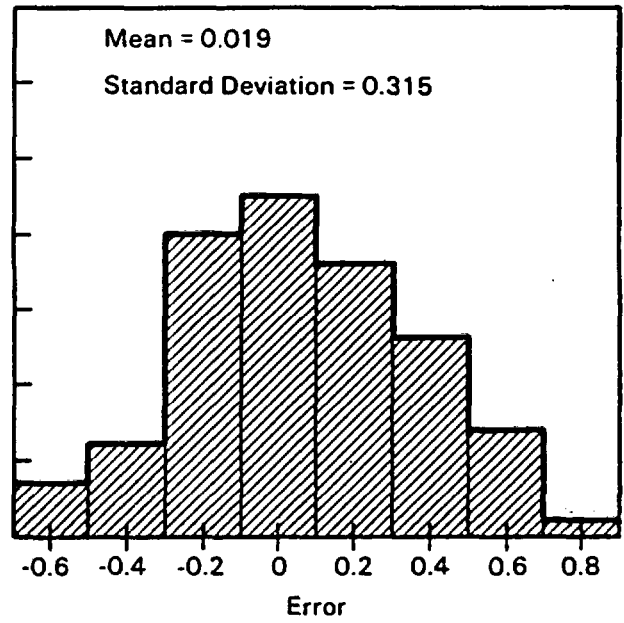


FIGURE 16b. Distribution of Gaussian Errors for Transmissivity Zone 2 ($\bar{T}_2 = 20 \text{ m}^2/\text{day}$)

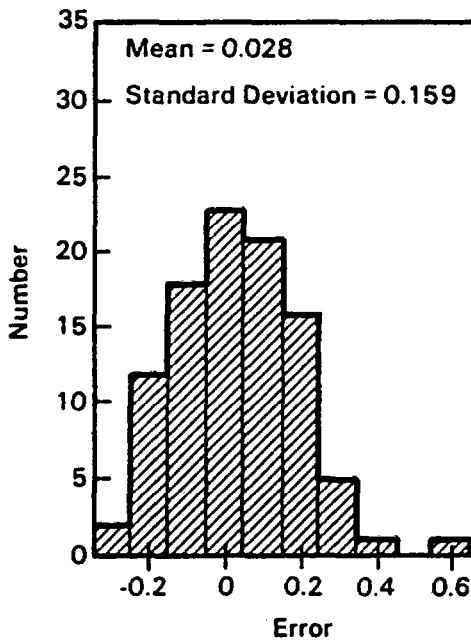


FIGURE 16c. Distribution of Gaussian Errors for Transmissivity Zone 3 ($\bar{T}_3 = 100 \text{ m}^2/\text{day}$)

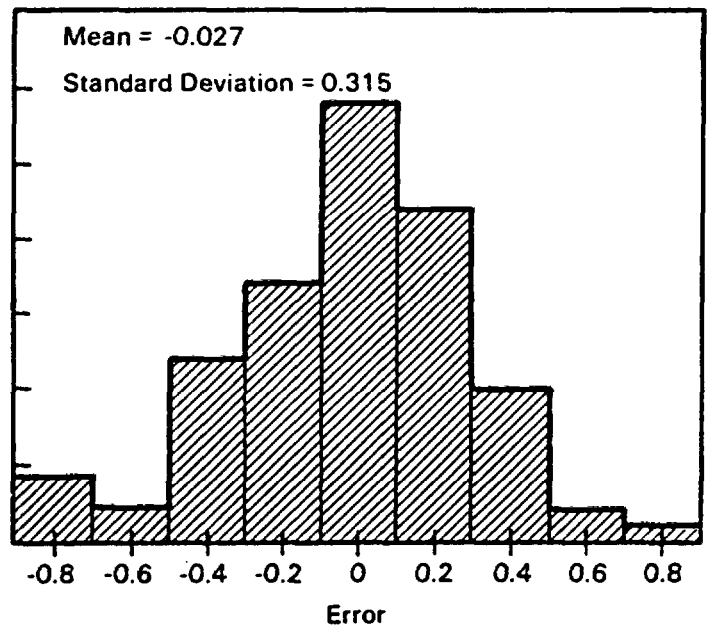


FIGURE 16d. Distribution of Gaussian Errors for Transmissivity Zone 4 ($\bar{T}_4 = 1200 \text{ m}^2/\text{day}$)

fit indicates that a larger number of realizations would be needed to reproduce the assumed values for a truly rigorous application of the Monte Carlo technique.

Statistical Properties of Effective Porosity

In order to calculate the ground-water travel time from Equations (12) and (15), the effective porosity must be known. At this time limited information is available about the values, let alone the spatial variability of effective porosity near Yucca Mountain. To investigate the effect of uncertainty in effective porosity on travel time uncertainty, two models of the spatial variability of effective porosity were considered. In the first model, the effective porosity was assumed to be uniform over the entire study area, whereas in the second model the effective porosity was assumed to be constant in each of the transmissivity zones labeled 1, 2, 3, and 4 in Figure 15. For this study, effective porosity was assumed to be normally distributed.

The first model estimates of the mean and standard deviation were based on information from Peters et al. (1984), Thompson et al. (1984), Bentley (1984), Rush et al. (1983), and Lobmeyer et al. (1983). The mean effective porosity was estimated to be 0.15 with a standard deviation of 0.06 using the same procedure as used to estimate the statistical properties of transmissivity.

In the second model, the effective porosity was assumed to be uniform in each of the zones (1, 2, 3, 4) of transmissivity. The estimate of mean and standard deviation in each zone was based on reports by Bentley (1984), Lobmeyer et al. (1983) and Rush et al. (1983). The measurements of Peters et al. (1984) for small cores indicate a positive correlation between porosity and hydraulic conductivity for welded and nonwelded-nonzeolitized tuffs (Fig. 17). Based on this information, the mean value of effective porosity was assumed to increase as the transmissivity increased. The standard deviations were estimated using the range in values and the same procedure used to estimate the statistical properties of the transmissivities. The assumed means and standard deviations for each of the zones are listed in Table 12.

The mean effective porosity values for both models are representative of porous flow equivalence of bulk rock properties. Available porosity data

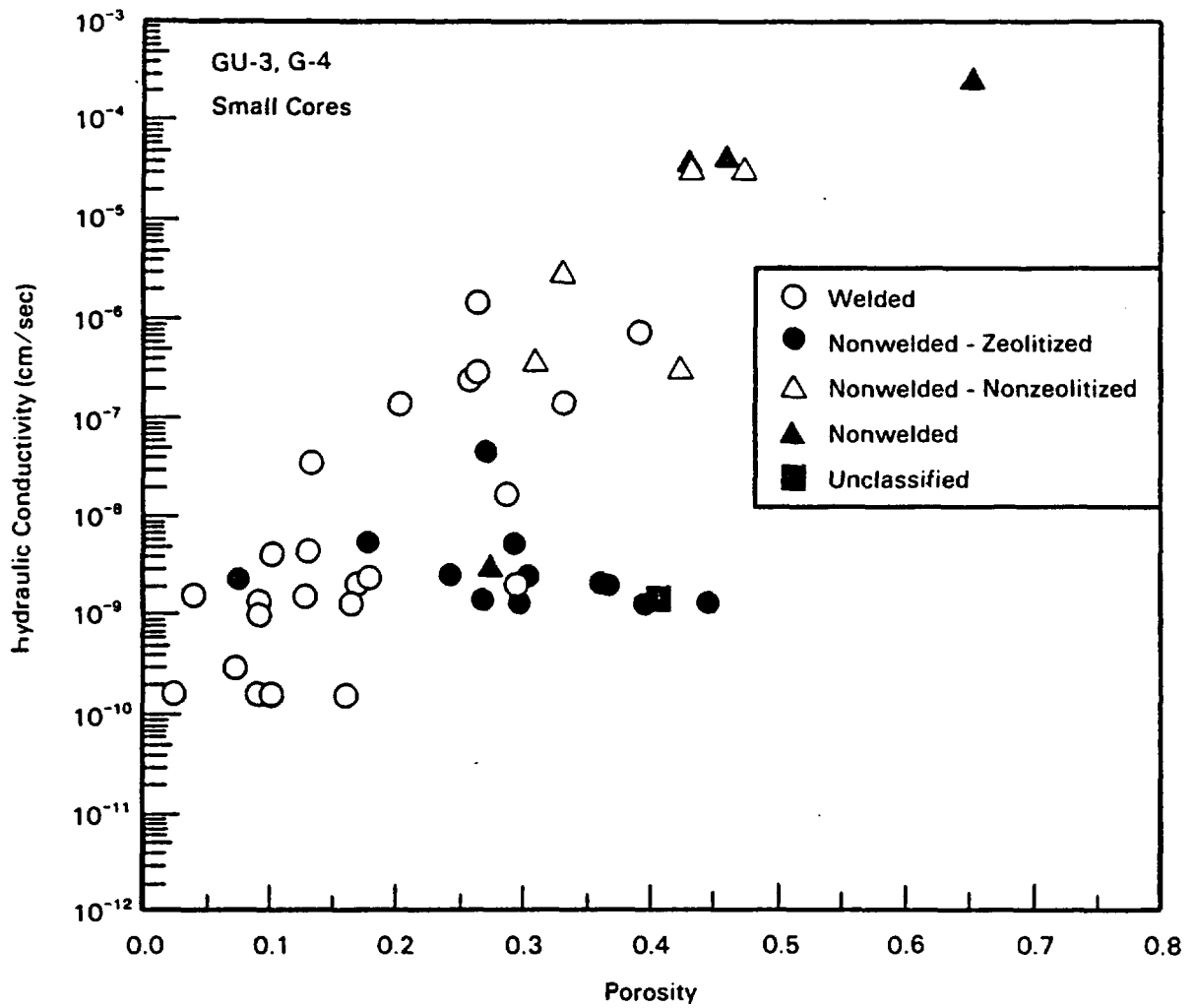


FIGURE 17. Correlation Between Porosity and Hydraulic Conductivity for Small Cores USW GU-3 and USW G-4 (from Peters et al. 1984)

TABLE 12. Estimates of Mean and Standard Deviation of Effective Porosity for Each Zone

Zone	Mean Transmissivity (m ² /day)	Mean Effective Porosity	Standard Deviation Effective Porosity
1	5	0.10	0.02
2	20	0.15	0.03
3	100	0.20	0.04
4	1200	0.32	0.04

corresponds to rock matrix pores in welded and nonwelded tuff. Preliminary information indicated that porosity values for the Topopah Spring Member of the Paintbrush Tuff Formation were generally less than 5 percent. This welded tuff unit was known to be fractured. Under saturated conditions, the Topopah Spring Member could produce at least 600 gallons-per-minute (gpm) to a well with relatively low drawdown (Winograd and Thordarson 1975). Well productions of this magnitude are more characteristic of either higher porosity materials than 5 percent or fracture flow. Thus, the bulk effects of fractured, low porosity rock was considered to be adequately represented by a higher porosity, equivalent porous flow medium.

Currently, it is difficult to obtain estimates of the effective porosity of fractures for use in transport problems. The definition of porosity used in Equation (18) for fracture flow depends only on the aperture of the fractures and the spacing between the fractures. Inasmuch as the effective porosity is the parameter necessary for transport calculations, some measure of the degree of interconnectiveness of the fractures must be obtained. Thus, estimating only fracture aperture and spacing between fractures is not sufficient to obtain a value of effective porosity for use in transport calculations.

Generation of Realizations of Effective Porosity

For the model with uniform effective porosity, the effective porosity can be treated as either a randomly varying or constant parameter. For the example in which effective porosity was treated as a random parameter, 100 realizations were generated using the same procedure as discussed for log transmissivities. No correlation between transmissivity and effective porosity was assumed. The distribution of the Gaussian errors for effective porosity is shown in Figure 18. The sample mean of the 100 realizations is within 11 percent of the assumed mean, and the sample standard deviation is within 7 percent of the assumed value. As with log transmissivity, this lack of fit between sample values and the assumed values indicates that additional realizations are needed.

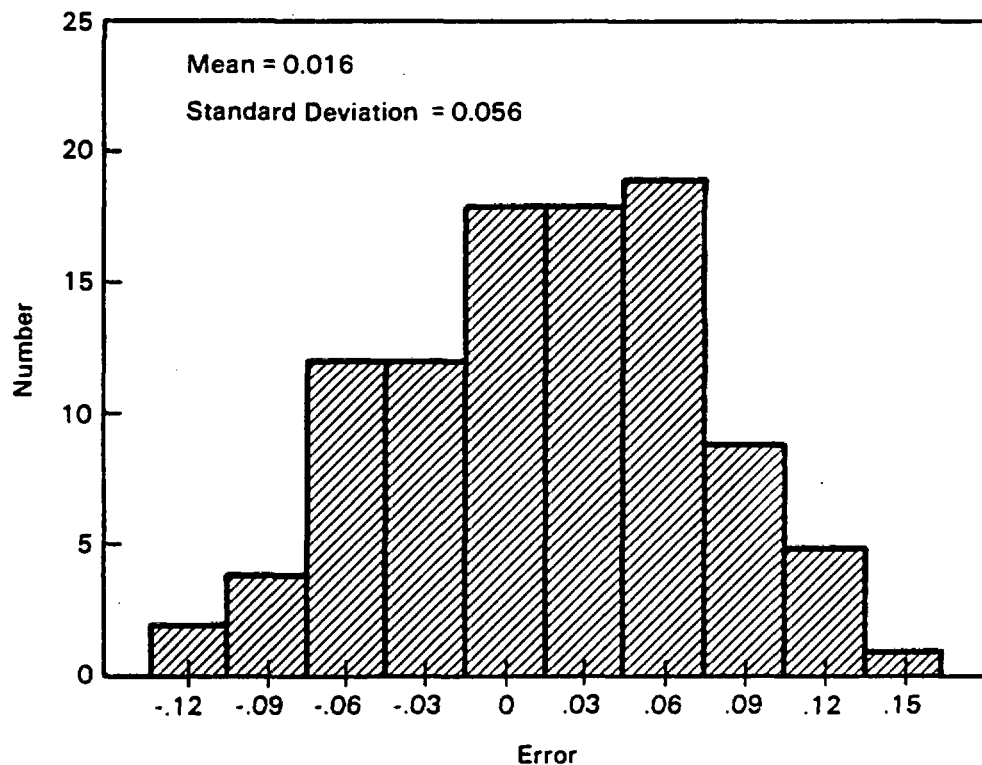


FIGURE 18. Distribution of Gaussian Errors for Effective Porosity ($\bar{n}_e = 0.15$)

For the second model, the effective porosities in each of the zones were treated as either random or as constant parameters. Assuming the effective porosity is random within each zone, effective porosity in each zone was generated for each of the 100 realizations of log transmissivity. To investigate the effect of correlation between the hydrologic parameters, a correlation coefficient equal to one was assumed between effective porosity and log transmissivity in each zone, and no correlation was assumed between zones. For each zone, the realizations of effective porosity were obtained from the Gaussian error in the corresponding realization of log transmissivity; i.e., if the log transmissivity in a zone was increased by one standard deviation, then the corresponding effective porosity was also increased by one standard deviation. Inasmuch as the same Gaussian errors were used to generate the realizations of both effective porosity and log transmissivity, the distribution of errors plotted in Figure 16 also applies to the effective porosities.

UNCERTAINTY ANALYSIS FOR THREE CASES WITH UNIFORM EFFECTIVE POROSITY

The uncertainty of ground-water travel time was calculated for the first three cases using the model of uniform effective porosity. The first case involved calculating 100 average travel times using the constant mean effective porosity value of 0.15, the hydraulic-head distribution obtained from the USGS interpretation, and 100 realizations of transmissivity. This case was included to investigate the effects of using a fixed hydraulic head distribution that may not reflect a mass balance solution to the flow system. The second case investigated the uncertainty in travel time when the hydraulic heads were obtained by simulating the flow system for each realization of transmissivity and fixed boundary conditions. The results from these simulations were used together with the mean effective porosity to calculate the ground-water travel times. In the third case, the effective porosity was assumed to be random. Thus, for each of the ground-water flow simulations, a new, uniform effective porosity was used to calculate travel time.

Monte Carlo Analysis with Uniform Effective Porosity

The contours of hydraulic head obtained from the USGS interpretation are shown in Figure 19. For steady-state flow, the location of pathlines is determined by the spatial distribution of hydraulic head. Thus, the location of the seven pathlines shown in Figure 19 is the same for all 100 realizations in Case 1. The histogram of the resulting ground-water travel times is illustrated in Figure 20. The sample mean travel time was calculated to be 3600 years with a sample standard deviation of 1040 years. The histogram is skewed to the higher values of travel time, which may be because transmissivities are lognormally distributed. The coefficient of variation is defined as the standard deviation divided by the mean and may be used as an indication of the magnitude of uncertainty in the mean value. For example, a coefficient of variation of 0.30 indicates that the standard deviation is 30 percent of the mean value, whereas a value of 1.0 indicates the standard deviation is 100 percent of the mean value. The coefficient of variation is equal to 0.29 for Case 1. A plot of the cumulative histogram of ground-water travel times for Case 1 is shown in Figure 21 and, based on these results, the median travel

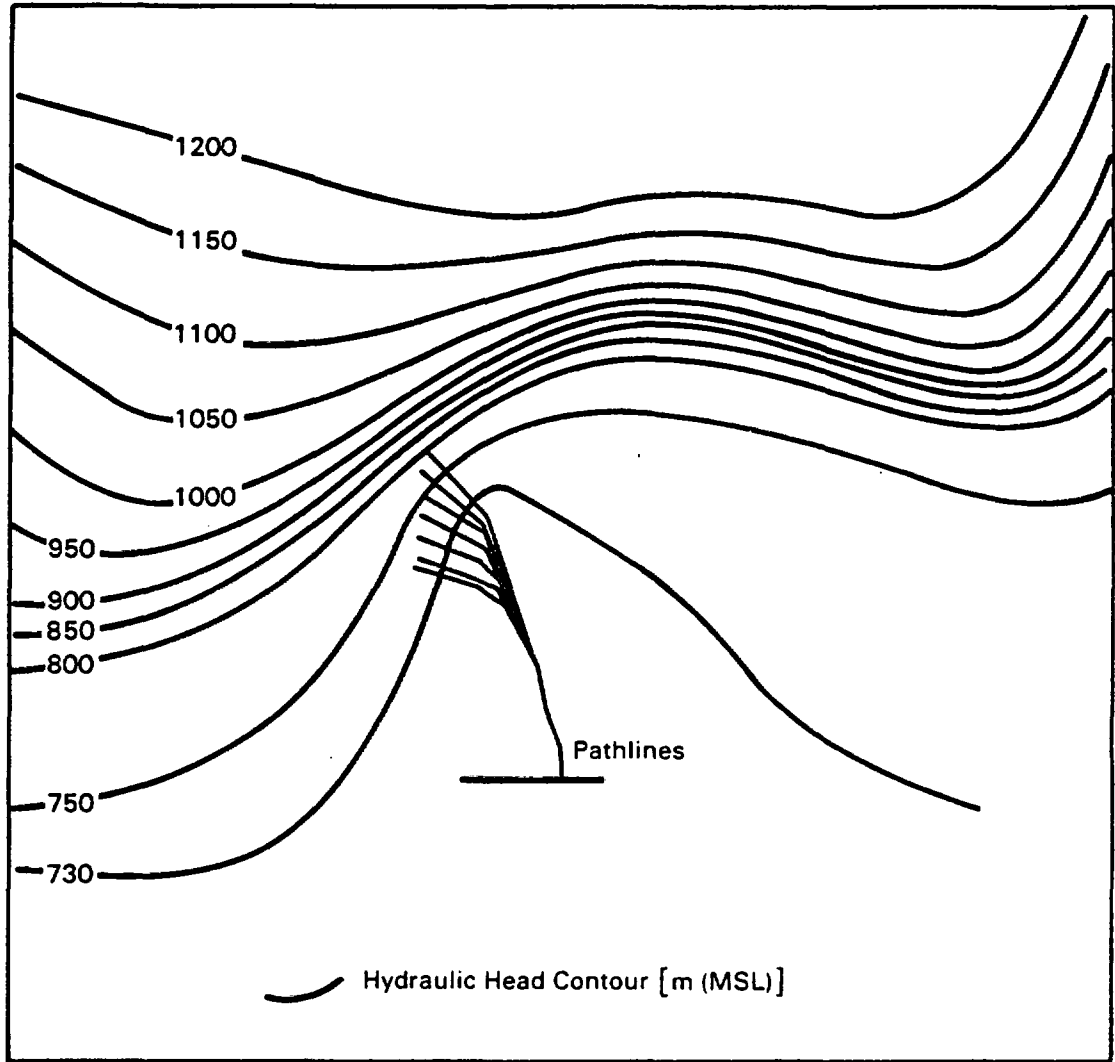


FIGURE 19. Contours of Hydraulic Heads Obtained from the U.S. Geological Survey Interpretation

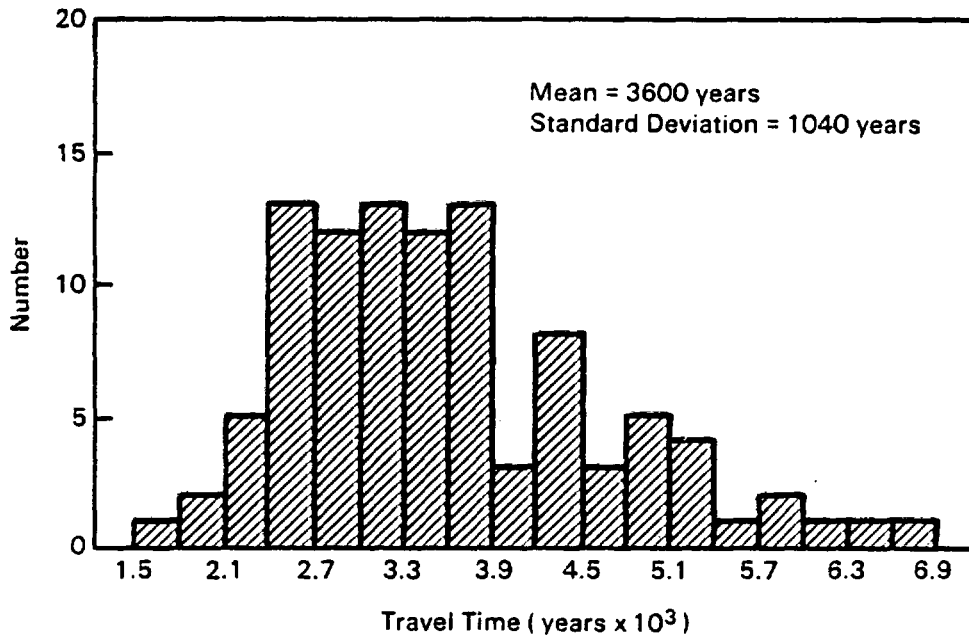


FIGURE 20. Histogram of Ground-Water Travel Time for Case 1

time (i.e., 50 percent point) is equal to 3370 years. This median value is less than the sample mean of 3600 years because the distribution is skewed to higher values.

When consistent hydraulic heads are obtained for each realization by simulating the ground-water flow system, as was done in Case 2, the travel times are more representative of the physical system. Contours of hydraulic heads obtained from a simulation using the mean transmissivity values, transmissivity realization number 14, and realization number 88 are shown in Figures 22, 23 and 24, respectively. The hydraulic head distributions produced by realizations 14 and 88 are presented because they corresponded to short (440 years) and long (1815 years) travel times, respectively, for Case 2. A comparison of the contours in Figures 22, 23, and 24 demonstrates variations in the hydraulic heads produced by changes in the transmissivity values. The corresponding values of transmissivity are given in Table 13 for the four zones traversed by the pathlines. The histogram of ground-water travel times for Case 2 is presented in Figure 25. The sample mean is 840 years with a sample standard

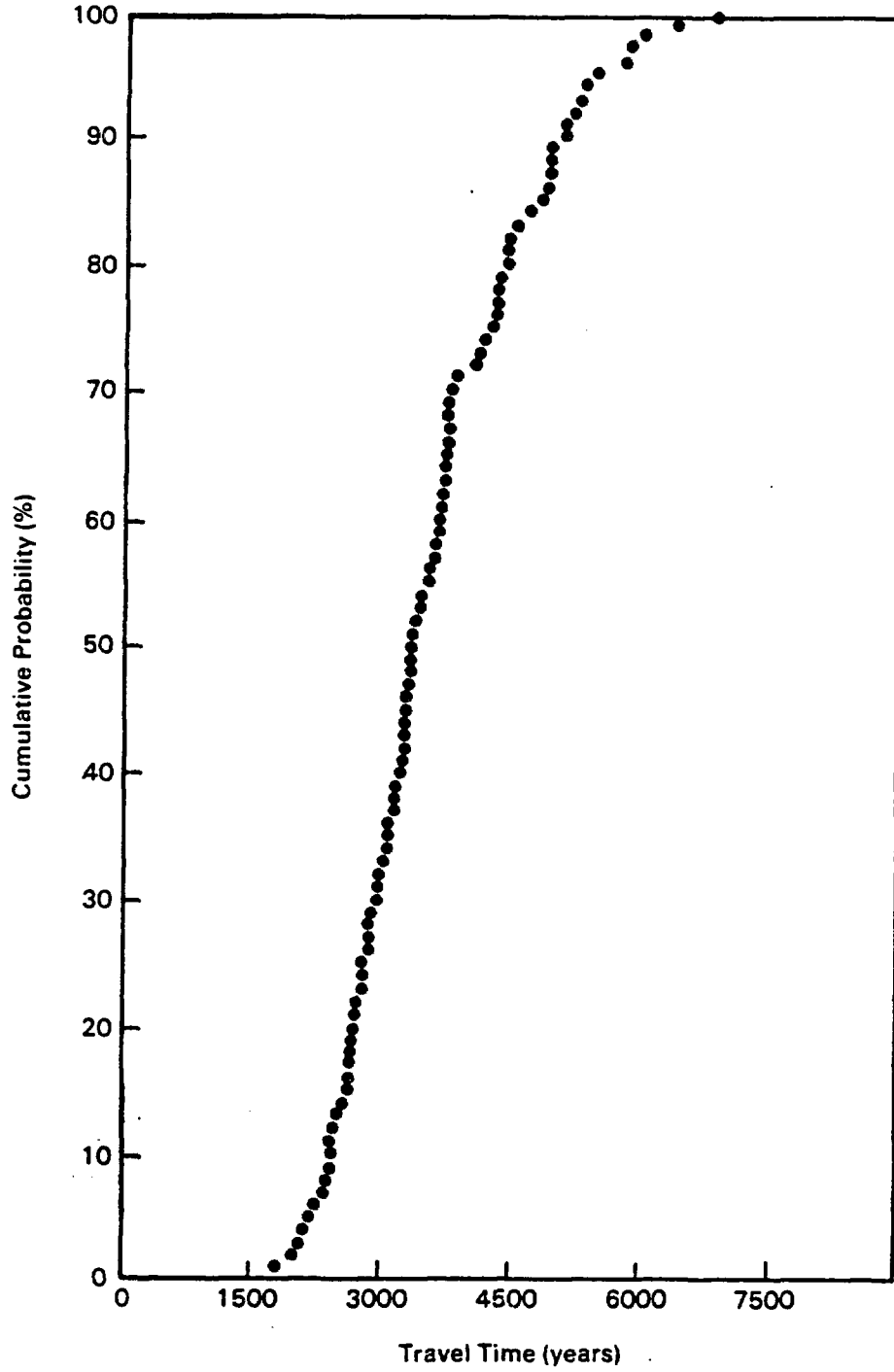


FIGURE 21. Cumulative Histogram of Ground-Water Travel Time for Case 1

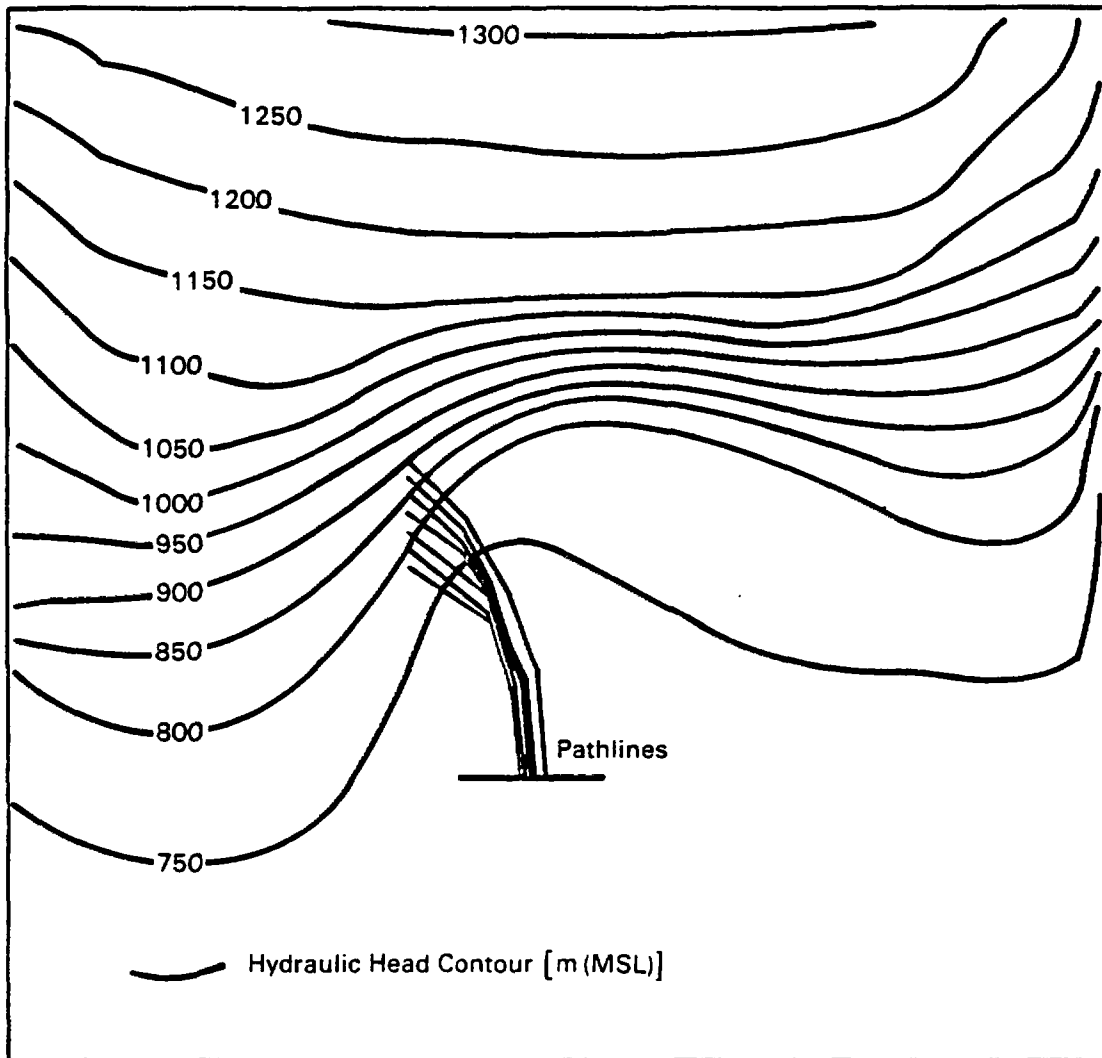


FIGURE 22. Contours of Hydraulic Head Obtained from the Ground-Water Flow Simulation Using the Mean Transmissivity Values

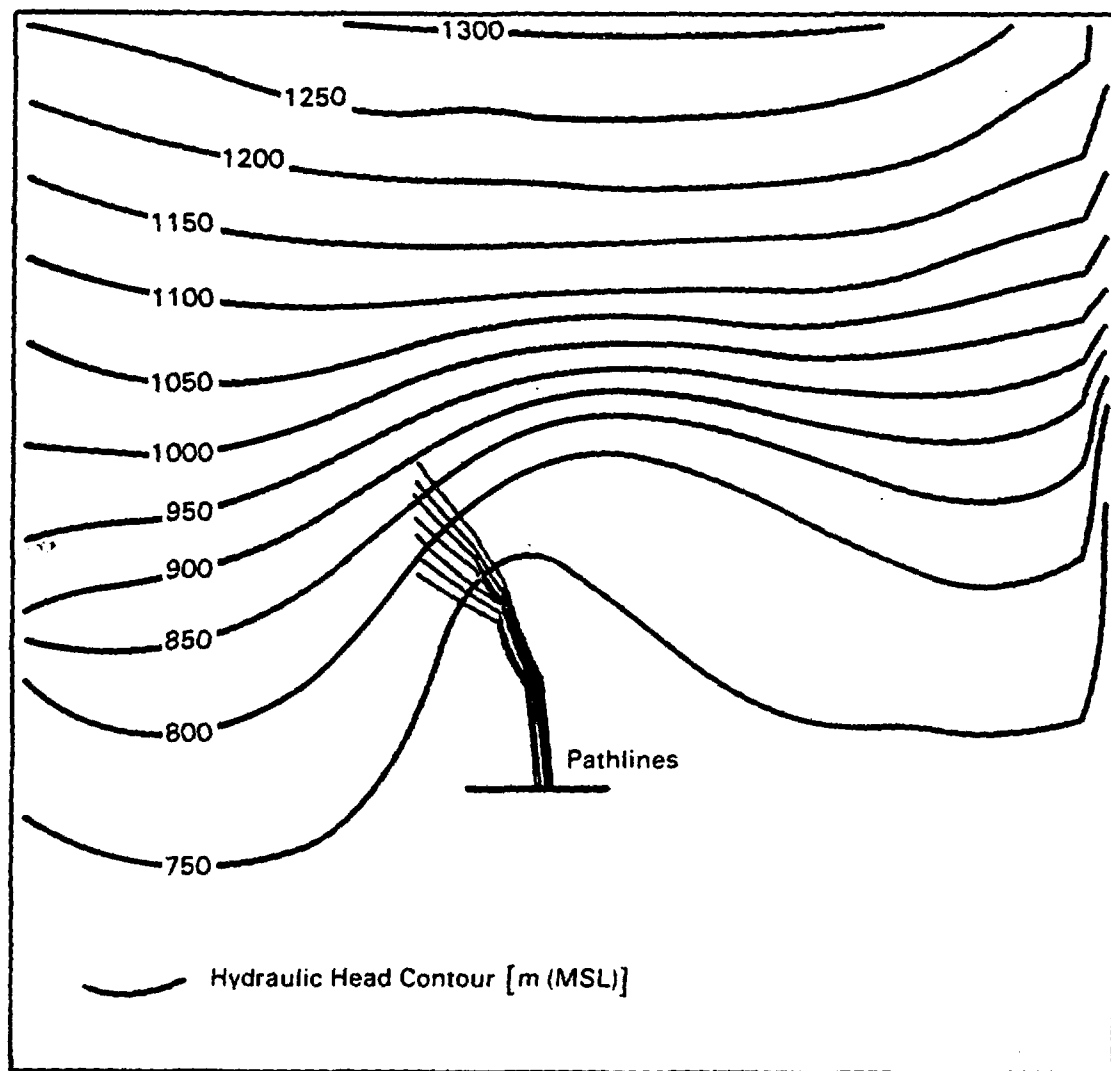


FIGURE 23. Contours of Hydraulic Head Obtained from the Ground-Water Flow Simulation Using Transmissivity Realization Number 14

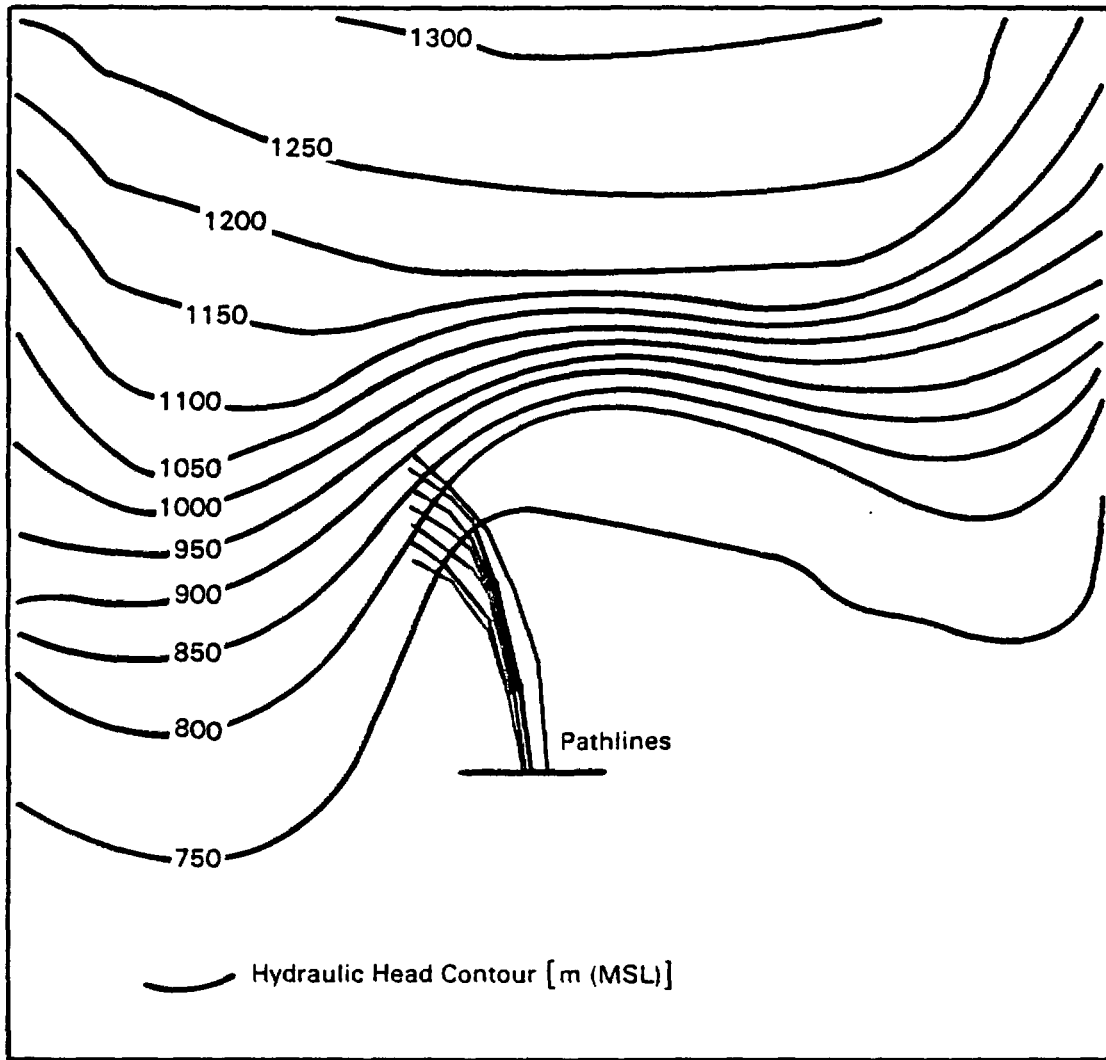


FIGURE 24. Contours of Hydraulic Head Obtained from the Ground-Water Flow Simulation Using Transmissivity Realization Number 88

TABLE 13. Zonal Transmissivity Values Corresponding to the Mean, Realization 14, and Realization 88

<u>Zone</u>	<u>Mean Transmissivity (m²/day)</u>	<u>Realization 14 Transmissivity (m²/day)</u>	<u>Realization 88 Transmissivity (m²/day)</u>
1	5	10.2	2.0
2	20	21.2	9.8
3	100	90.7	86.9
4	1200	1953.0	504.8

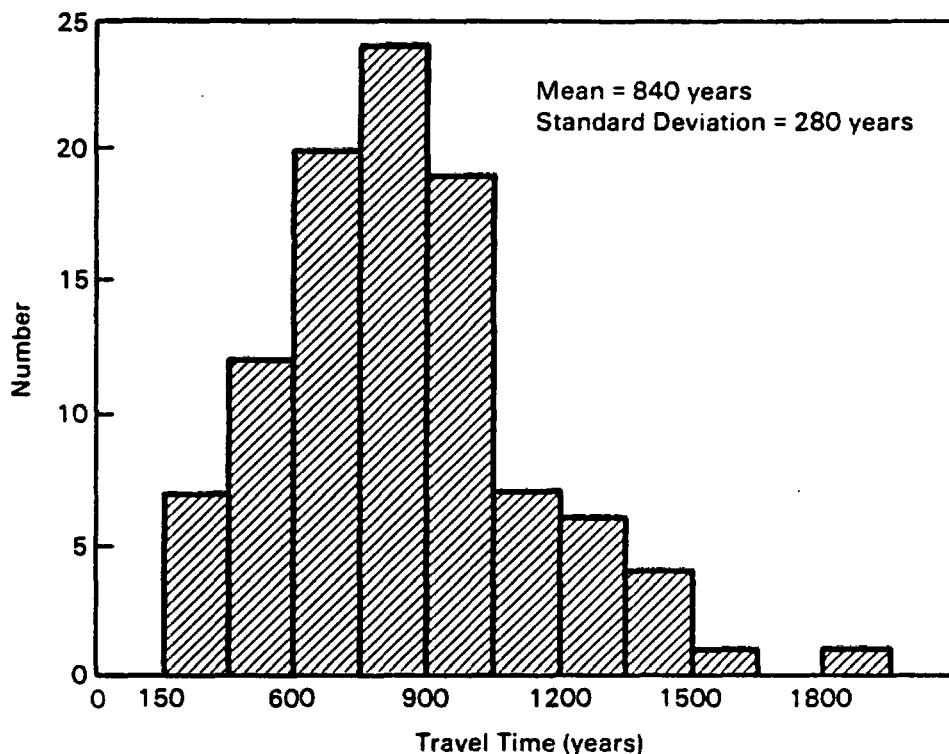


FIGURE 25. Histogram of Ground-Water Travel Time for Case 2

deviation of 280 years. The histogram appears to be skewed to higher values of travel time similar to Case 1. The mean value of travel time for Case 2 (840 years) is more than four times smaller than the mean travel time for Case 1 (3600 years). Thus for this data set, use of the USGS-interpreted hydraulic heads leads to an overestimation of ground-water travel time. The coefficient of variation was equal to 0.34, which is larger than the value obtained from Case 1. The cumulative histogram of travel time is presented in Figure 26 for Case 2. The median value of travel time is equal to 820 years, which is less than the sample mean and is due to the skew toward higher values.

In Case 3 the hydraulic heads obtained by simulating the flow system for each realization of transmissivity were used together with random effective porosities to calculate ground-water travel time. The effective porosity was treated as a random parameter in order to calculate the ground-water travel time uncertainty when both the values of transmissivity and effective porosity

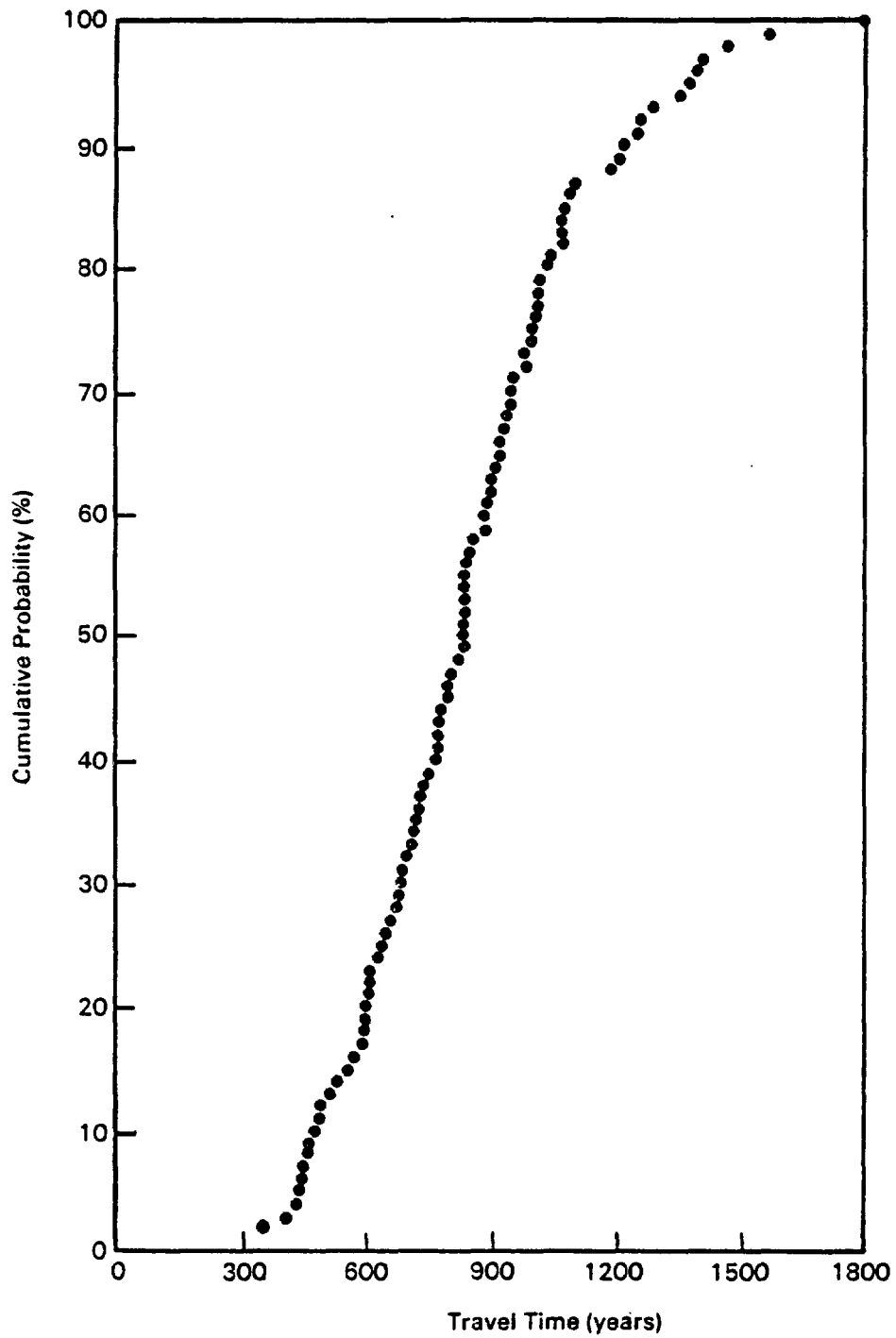


FIGURE 26. Cumulative Histogram of Ground-Water Travel Time for Case 2

were uncertain. The histogram of ground-water travel time for Case 3 is shown in Figure 27 and has a sample mean of 920 years with a standard deviation of 460 years. The coefficient of variation is equal to 0.50. The shape of the histogram shows a skew toward higher values of travel time as also observed for Cases 1 and 2. The cumulative histogram of travel times for Case 3 is shown in Figure 28. The median ground-water travel time is equal to 890 years, which is smaller than the sample mean value.

The sample mean values of travel time together with the sample standard deviations, corresponding coefficients of variation, and the median values of travel time for Cases 1, 2, and 3 are summarized in Table 14. The histogram of travel time can be considered an approximation of the probability density distribution of travel time. The histograms for all three cases exhibited a skew toward higher values, which suggests that the travel time may be lognormally

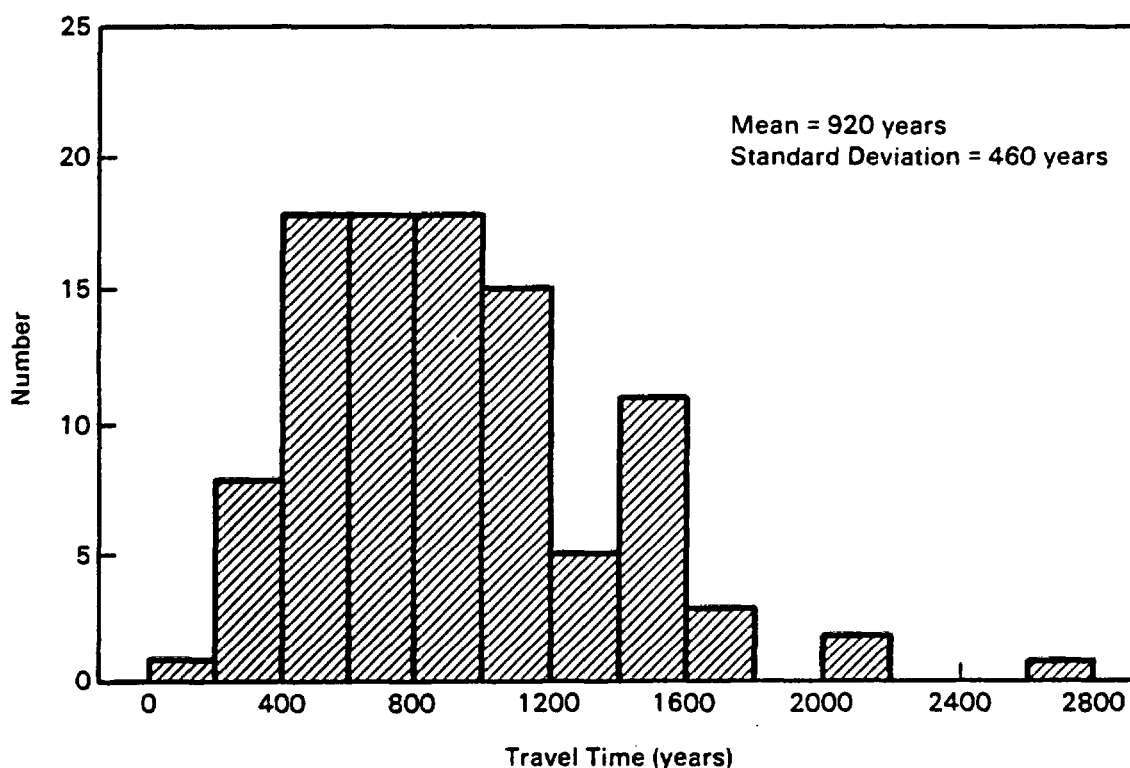


FIGURE 27. Histogram of Ground-Water Travel Time for Case 3

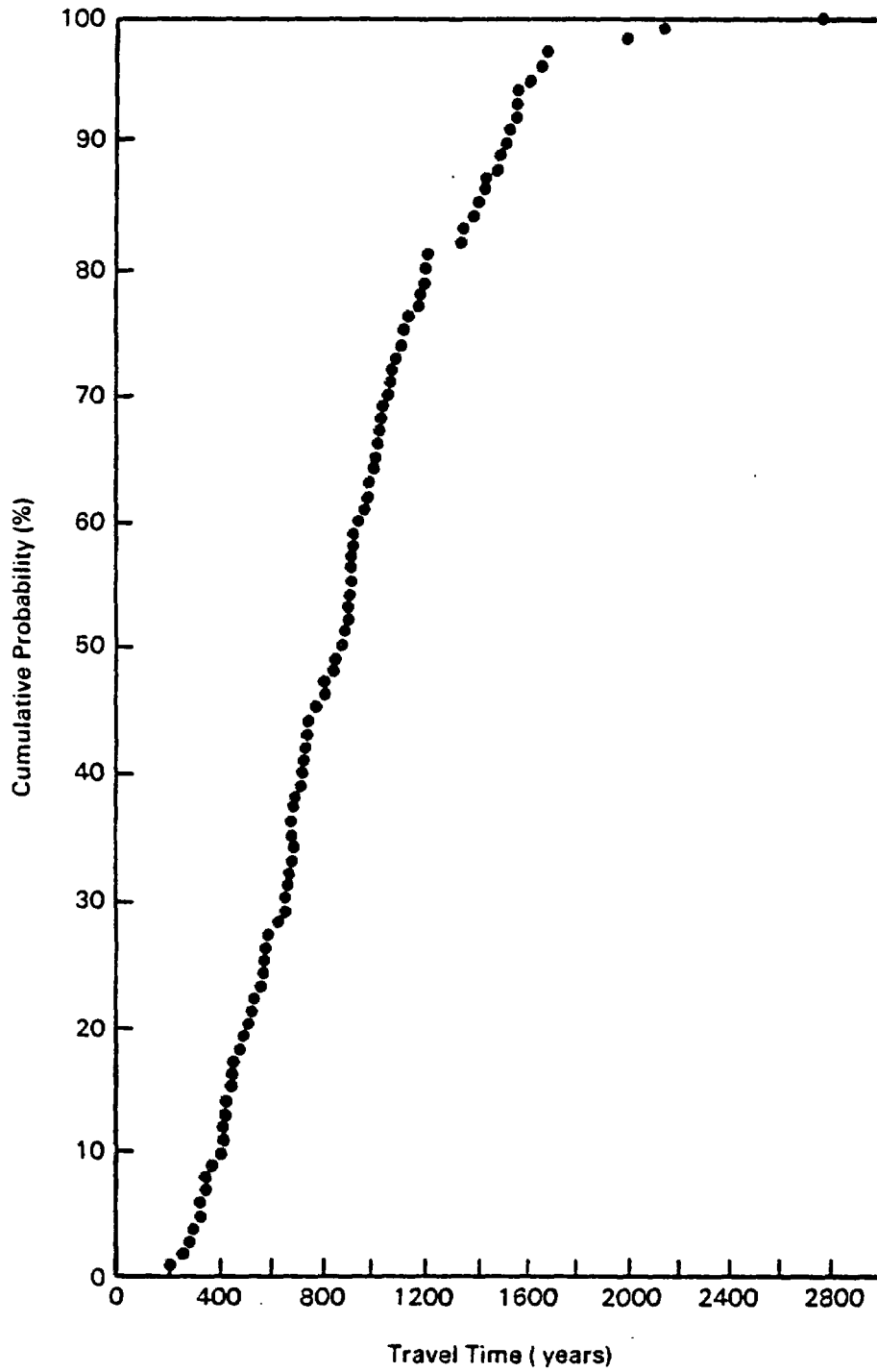


FIGURE 28. Cumulative Histogram of Ground-Water Travel Time for Case 3

TABLE 14. Sample Means, Sample Standard Deviations, Coefficient of Variations and Medians of Ground-Water Travel Time Obtained from Monte Carlo Analysis for Cases 1, 2, and 3

<u>Case</u>	<u>Sample Mean (yr)</u>	<u>Median (yr)</u>	<u>Sample Standard Deviation (yr)</u>	<u>Coefficient of Variation</u>
1	3600	3370	1040	0.29
2	840	820	280	0.34
3	920	890	460	0.50

distributed. If this observation is correct, a more representative value of the expected travel time would be the median rather than the sample mean. In all three cases, the median travel time is less than the sample mean; therefore, the expected travel time could be overestimated if the sample mean were used rather than the more representative median.

A comparison of the magnitudes of the sample means of ground-water travel time for Cases 1, 2, and 3 shows that when the USGS hydraulic head interpretation was used (Case 1), the travel times were four times larger than when consistent hydraulic head data were used (Cases 2 and 3). When the effective porosity was treated as a random parameter (Case 3), the sample mean travel time was only 9 percent larger than for Case 2 where effective porosity was assumed to be a deterministic parameter. However, comparing the coefficients of variation for Cases 2 and 3 shows that the uncertainty in travel time for Case 3 was much larger than for Case 2. Thus, treating the effective porosity as a random parameter caused the uncertainty in travel time to increase while having only a small affect on the sample mean travel time. The coefficient of variation was smallest for Case 1, which indicates the least uncertainty; however, recall that use of the USGS hydraulic head interpretation produces travel times that are not representative of the ground-water flow system. Given the current state of knowledge of the hydrologic parameters, Case 3 contains the most physically realistic assumptions for estimating uncertainty in travel time when the effective porosity is assumed to be uniform over the flow region.

The sample mean together with the sample standard deviations of travel time are plotted versus the number of realizations in Figures 29, 30, and 31

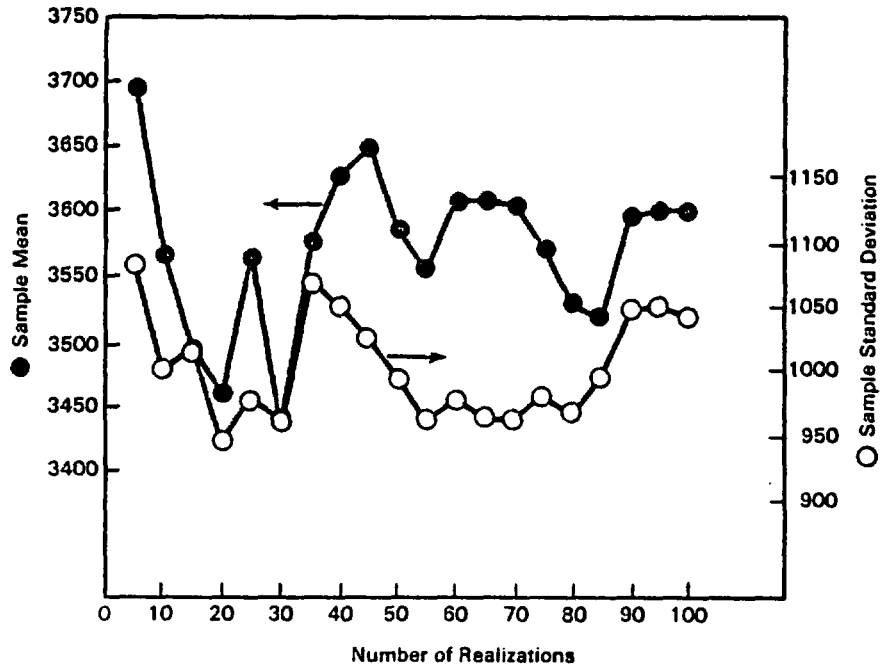


FIGURE 29. Sample Mean and Sample Standard Deviation of Ground-Water Travel Time Versus Number of Realizations for Case 1

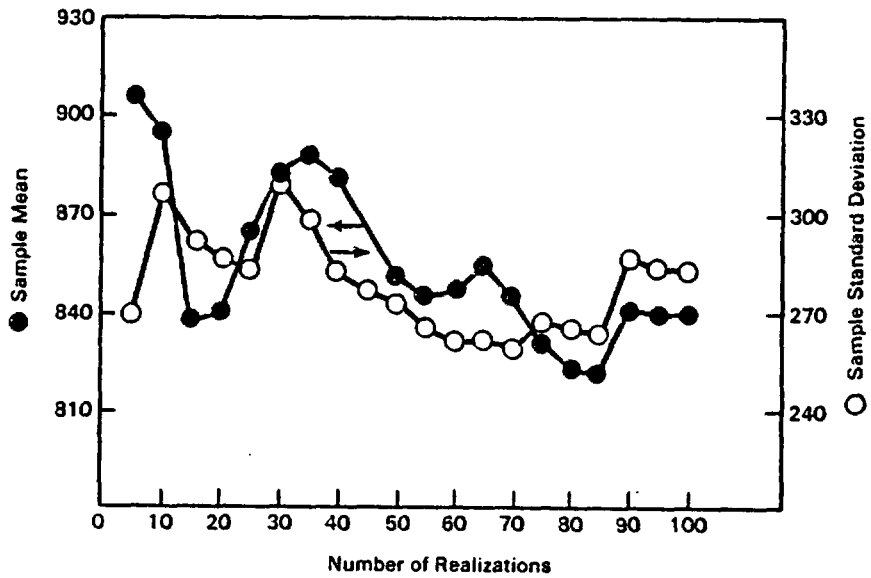


FIGURE 30. Sample Mean and Sample Standard Deviation of Ground-Water Travel Time Versus Number of Realizations for Case 2

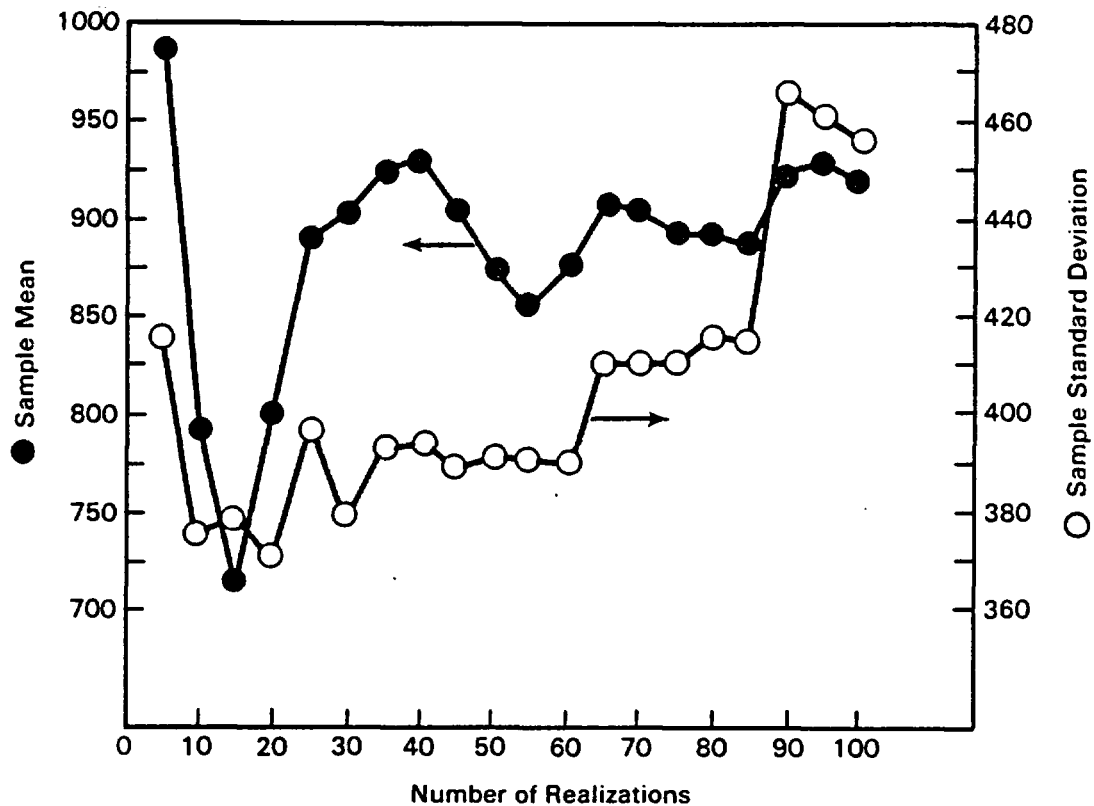


FIGURE 31. Sample Mean and Sample Standard Deviation of Ground-Water Travel Time Versus Number of Realizations for Case 3

for Cases 1, 2, and 3, respectively. If a sufficient number of realizations have been considered, the values of the sample statistics should converge to specific values as the number of realizations is increased. The figures illustrate that 100 realizations were not sufficient for the statistics to converge to their final value. The sample statistics for Cases 1 and 2 show indications of converging, but for Case 3 only the sample mean may be converging, while the sample standard deviation is still variable. These results suggest that, in general, the sample mean appears to converge more quickly than the sample standard deviation. Also, for cases with larger uncertainties in the hydrologic parameters (i.e., Case 3), it is necessary to consider a larger number of realizations in a Monte Carlo analysis in order to obtain convergence of the sample statistics.

Sensitivity Analysis with Uniform Effective Porosity

A sensitivity analysis was conducted for Cases 2 and 3 that were based on simulation of the ground-water flow system. Case 1 with the USGS hydraulic heads was not used because it is not representative of the flow system.

The sensitivity coefficients were calculated by a perturbation method as discussed in Appendix B. The log transmissivity in each zone and the effective porosity were varied about their mean values by an amount equal to ± 5 percent of their corresponding standard deviations. The 5 percent variation in the parameters was chosen in order to ensure that the corresponding travel times had measurable variation in their magnitudes, while maintaining the parameter values close to their means. A reasonably accurate estimate of the sensitivity coefficients should be obtained by using the 5 percent variation of the input parameters because ground-water travel time appears to vary slowly as the magnitude of the input parameters changes. The parameters were varied one at a time, and the sensitivity coefficients were calculated using Equation (2). The travel times and sensitivity coefficients obtained in this study are given in Table 15. Also listed are the normalized sensitivity coefficients (S_{n_j}) calculated by Equation (3). Because of different magnitudes of the parameters, the normalized sensitivity coefficients must be used to indicate which parameters most affect the calculation of travel time.

TABLE 15. Travel Times, Sensitivity Coefficients (S_j), and Normalized Sensitivity Coefficients (S_{n_j}) Corresponding to Variations of the Log Transmissivity in the Four Zones and Effective Porosity

<u>Delta Change in Parameter</u>	<u>Tr₂ (yr) (Positive Variation)</u>	<u>Tr₁ (yr) (Negative Variation)</u>	<u>ΔTr (yr)</u>	<u>S_j</u>	<u>S_{n_j}</u>
Δlog T ₁ = 0.02	749.2	768.3	-19.1	-955.0	-0.88
Δlog T ₂ = 0.03	755.5	765.1	-9.6	-320.0	-0.55
Δlog T ₃ = 0.015	760.2	760.6	-0.4	-26.7	-0.07
Δlog T ₄ = 0.03	750.8	754.4	-3.6	-120.0	-0.49
Δn _e = 0.006	775.3	744.9	30.4	5066.7	1.0

In a sensitivity analysis of Case 2 where the effective porosity was treated as deterministic, the only parameters varied were log transmissivities in each of the four zones. A comparison of the normalized sensitivity coefficients for the log transmissivities shows that log transmissivity in Zone 1 has the most influence on the calculation of travel time. Zones 2 and 4 have S_{n_i} of similar magnitude, while Zone 3 has the least influence on travel times. Because the log transmissivity value in Zone 1 is smaller in magnitude than those in the other three zones, it produces the most effect on the ground-water flow system near Yucca Mountain, and travel time is most sensitive to this parameter. Note that the sensitivity coefficients are negative, which indicates that travel time decreases with an increase in the log transmissivity values. This result is expected because travel time is inversely proportional to transmissivity in Equation (15).

In a sensitivity analysis for Case 3, both the log transmissivities and the uniform effective porosity were varied. Comparing all the normalized sensitivity coefficients listed in Table 15 shows that the effective porosity had a slightly larger influence on the estimates of travel time than the log transmissivity value in Zone 1. This result was expected because the smaller transmissivity value in Zone 1 had the most effect on the flux through the flow system near Yucca Mountain, and the effective porosity directly influences the magnitude of the seepage velocity [Equation (15)]. Note that the normalized sensitivity coefficient for effective porosity is positive, while those for log transmissivity are negative. This difference in sign is because travel time is directly proportional to effective porosity, whereas it is inversely proportional to transmissivity.

First-Order Analysis with Uniform Effective Porosity

A first-order approach to estimating uncertainty in ground-water travel time was applied to Cases 2 and 3. The first partial derivatives of travel time with respect to the hydrologic parameters (i.e., sensitivity coefficients)

were determined from the sensitivity analyses of Cases 2 and 3. These estimates of the derivatives together with the estimates of the variance of the parameters were used to calculate travel time uncertainty from Equation (6). The mean value of travel time was calculated from Equation (4).

The mean ground-water travel time for Case 2 is 760 years, the standard deviation is 220 years, and the corresponding coefficient of variation is 0.29. Because each term in Equation (6) for variance of travel time depends on only one parameter, a comparison of the magnitudes of the terms that are products of the sensitivity coefficients squared and the variance of parameters indicates which parameters contribute most to the travel time uncertainty. For Case 2, 78 percent of the uncertainty (represented by variance) in travel time was due to the uncertainty in log transmissivity in Zone 1. This result means that a reduction in the parameter uncertainty for this zone would have the maximum effect on the travel time uncertainty.

The mean ground-water travel time for Case 3 is 760 years, the standard deviation is 370 years, and the coefficient of variation is 0.49. For this case, 66 percent of the uncertainty (variance) in travel time is due to the uncertainty in effective porosity, whereas 26 percent of the travel time uncertainty is due to the uncertainty in log transmissivity in Zone 1.

Comparison of Monte Carlo and First-Order Results Using Uniform Effective Porosity

The estimates of mean and standard deviation of travel time for Cases 2 and 3 obtained by the Monte Carlo and first-order analyses are listed in Table 16. The first-order analysis underestimated the mean and standard deviation when compared to those determined by the Monte Carlo approach for both cases. Only the coefficients of variation for Case 3 are similar. This discrepancy between the estimates of the mean and standard deviation for the two approaches indicates that either the second-order and higher derivatives cannot be neglected in the Taylor series expansion for the first-order analysis or the Taylor series expansion is not appropriate to use for an uncertainty analysis. In general, a rigorous Monte Carlo analysis yields the more accurate

TABLE 16. Values of Mean, Standard Deviation, and Coefficient of Variation of Travel Time Obtained from Monte Carlo and First-Order Analysis for Cases 2 and 3 with Uniform Effective Porosity

Case	Mean		Standard Deviation		Coefficient of Variation	
	Travel Time (yr)		Travel Time (yr)			
	Monte Carlo	First-Order	Monte Carlo	First-Order	Monte Carlo	First-Order
2	840	760	280	220	0.34	0.29
3	920	760	460	370	0.50	0.49

estimate of uncertainty in model output because the generation of realizations of input parameters allows more complete representation of the statistical properties of the input parameters.

Although the first-order approach is an efficient method of calculating the uncertainty in ground-water travel time, application of this approach yields no information concerning the probability density distribution of ground-water travel time. On the other hand, the histogram obtained from a Monte Carlo analysis can be used to approximate the probability density distribution of travel time. However, the first-order analysis may give an indication of which parameters are contributing the most to the travel time uncertainty. This information cannot be obtained from the Monte Carlo approach.

UNCERTAINTY ANALYSIS FOR FOUR CASES WITH SPATIALLY VARYING EFFECTIVE POROSITY

The uncertainty in ground-water travel time was calculated for four cases (labeled 4, 5, 6, and 7) in which the value of effective porosity varied in the different zones near Yucca Mountain. In Case 4, the deterministic (i.e., constant) spatially varying effective porosities were used along with the 100 realizations of transmissivities, and the USGS interpretation of hydraulic heads. This case was included to observe the effect on travel time of using spatially varying porosities together with a fixed hydraulic head distribution. A comparison of the results of Cases 1 and 4 should indicate the influence on travel time of the two models of effective porosity (i.e., uniform versus

spatially varying). The distribution of hydraulic head calculated from the mean values of transmissivity was used in Case 5 to represent more consistent hydraulic head data. Cases 6 and 7 were based on hydraulic head data obtained by simulating the ground-water flow system for each realization of transmissivity. The spatially varying effective porosities were treated as deterministic in Case 6, whereas in Case 7 they were considered to be random but correlated with log transmissivity.

Monte Carlo Analysis with Spatially Varying Effective Porosity

A statistical analysis of the ground-water travel time calculated for Case 4 yielded a sample mean travel time of 4600 years, a sample standard deviation of 1590 years, and corresponding coefficient of variation of 0.35. The histogram and cumulative histogram of ground-water travel time are not presented because their shapes are very similar to those obtained for Case 1. The median travel time for Case 4 is 4270 years, which is less than the sample mean and due to a skew in travel time toward higher values. A comparison of the sample means, medians, and standard deviations of travel time for Cases 1 and 4 indicates that the effect of spatially varying effective porosity is to increase the values of the statistical quantities. In addition, the coefficient of variation is larger for Case 4, which suggests that spatially varying effective porosities (whose values have been chosen to consider correlation with the transmissivities) cause an increase in the uncertainty associated with calculating travel time when the USGS hydraulic head distribution is used.

The hydraulic heads calculated from the mean values of transmissivity are more representative of the flow system than the values obtained from the USGS interpretation. Thus, the estimate of travel time uncertainty obtained from Case 5 can be directly compared to the other cases in which the flow system was simulated for each realization of transmissivity. The histogram of ground-water travel times for Case 5 is given in Figure 32. The sample mean of travel time is 1090 years with a sample standard deviation of 390 years and coefficient of variation of 0.36. The cumulative histogram of ground-water travel time for Case 5 is plotted in Figure 33. The median travel time observed from the cumulative histogram is equal to 990 years. The histogram of travel time (see Fig. 32) displays the largest skew to higher values when

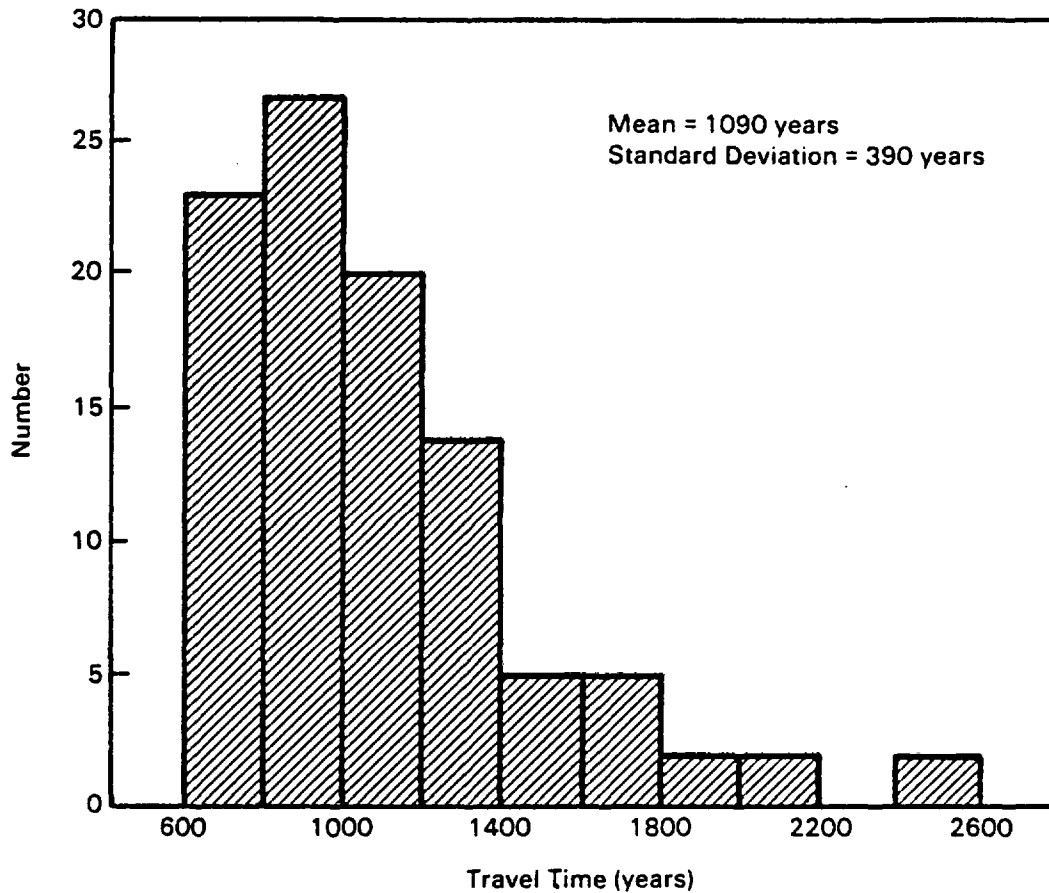


FIGURE 32. Histogram of Ground-Water Travel Time for Case 5

compared to the histograms for the other cases. In addition, the difference between the sample mean and median of travel time is also the largest for Case 5, which supports the previous observation concerning the skew. The magnitude of the sample mean travel time for Case 4 is over four times larger than that obtained for Case 5. Thus, the travel times are overestimated when based on the USGS hydraulic head data as compared to the case when more representative hydraulic head data are used. However, the coefficients of variation for Cases 4 and 5 are very similar, which indicates that the uncertainty in travel time is comparable for the two cases.

The histogram of ground-water travel times for Case 6, which involves simulating the ground-water flow system for each realization of transmissivity is given in Figure 34. The sample mean and standard deviation for ground-water

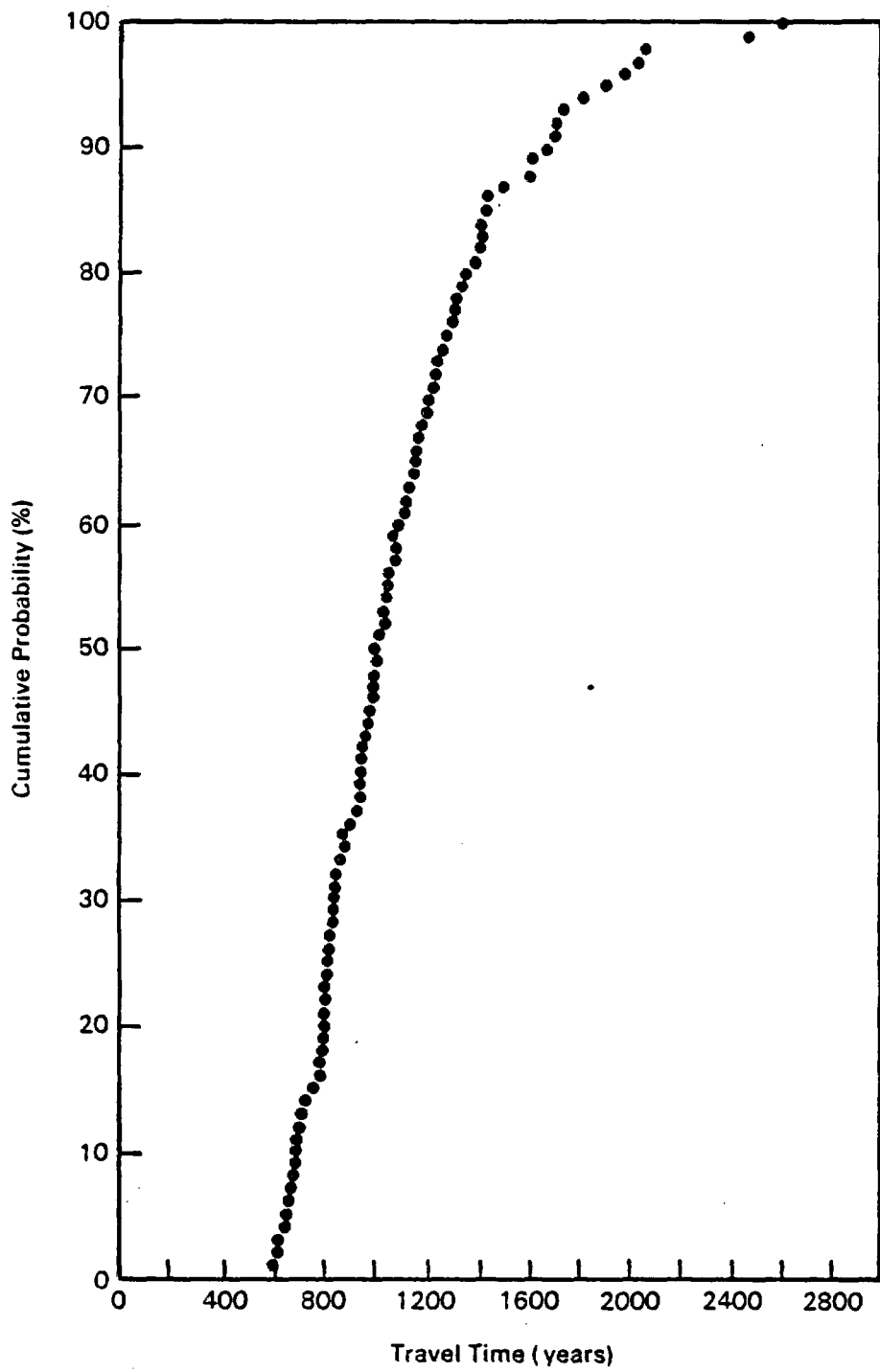


FIGURE 33. Cumulative Histogram of Ground-Water Travel Time for Case 5

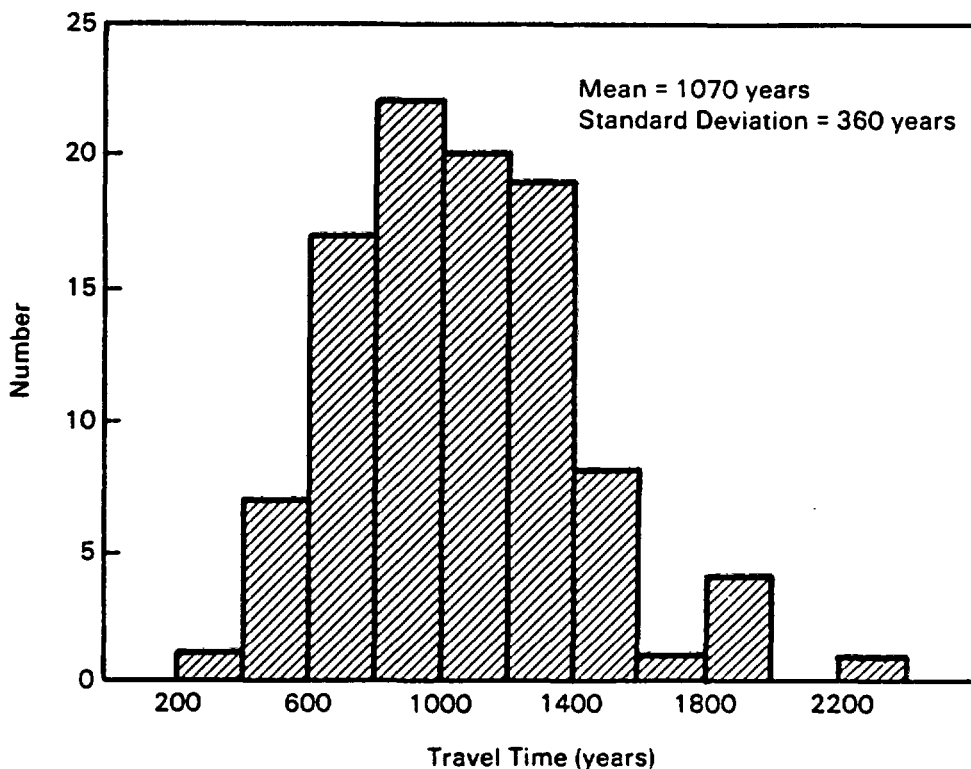


FIGURE 34. Histogram of Ground-Water Travel Time for Case 6

travel time were determined to be 1070 years and 360 years, respectively, and the corresponding coefficient of variation was equal to 0.34. A median travel time value of 1030 years was observed from the cumulative histogram of ground-water travel time given in Figure 35. Although the histogram exhibits a skew toward higher travel times, it is not as large a skew as observed in other cases. The results of Case 6 can be compared to those obtained from Case 2 to observe the effect of spatially varying effective porosities. The sample mean travel time of 840 years is smaller for the case with uniform effective porosity (Case 2); however, the coefficients of variation are the same, indicating that the same degree of uncertainty is observed for both cases. The larger sample mean travel time for Case 6 can be attributed to the influence of larger effective porosity values in two of the four zones.

In Case 7, the hydraulic heads were obtained by simulating the ground-water flow system for each realization, and the travel times were calculated

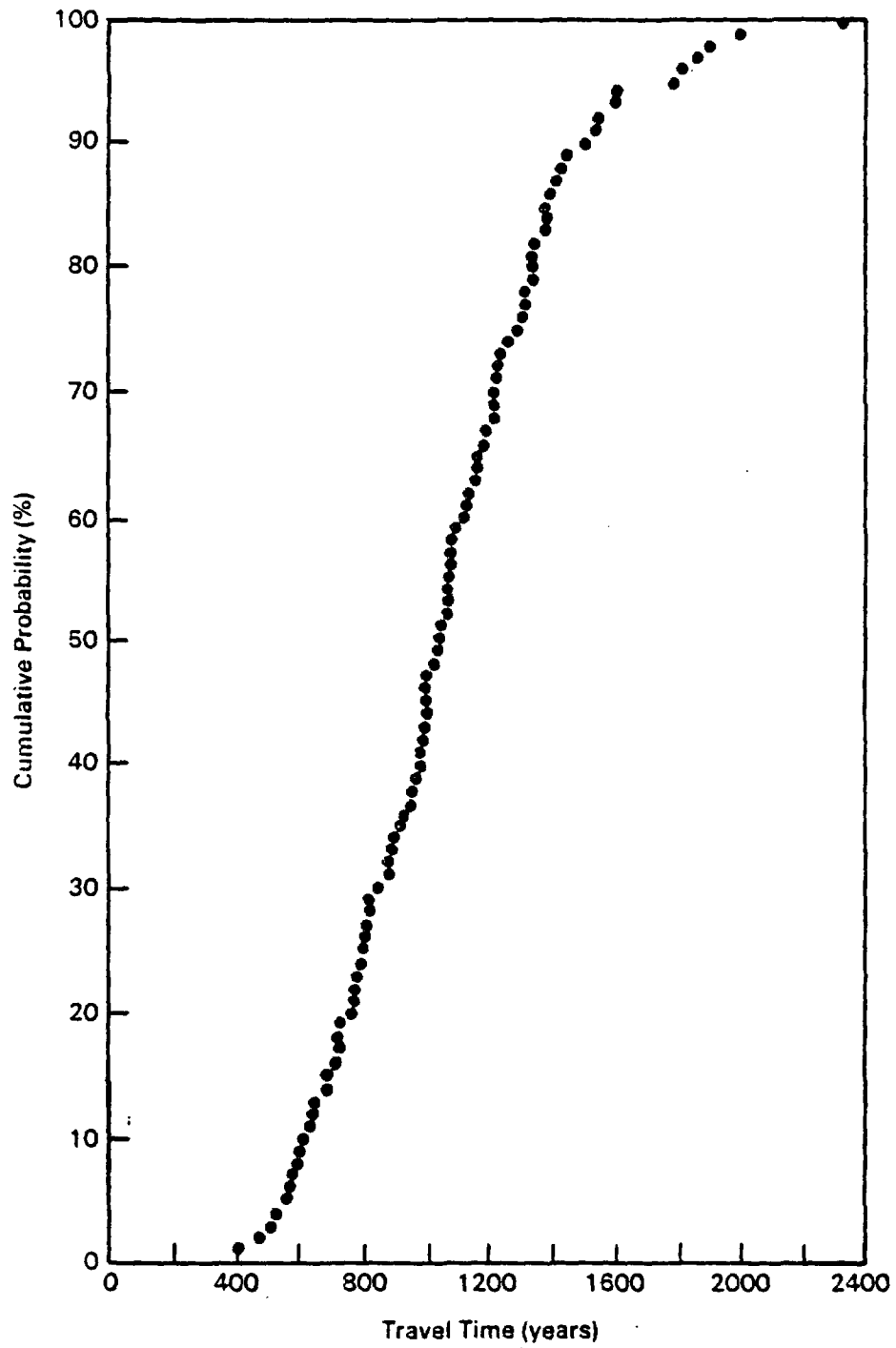


FIGURE 35. Cumulative Histogram of Ground-Water Travel Time for Case 6

using random effective porosities in each zone. These random effective porosities were correlated with the log transmissivity values in each zone with a correlation coefficient assumed to be equal to one. The histogram of ground-water travel times for Case 7 is given in Figure 36. The histogram shows a skew toward higher values of travel time similar to that observed in the histograms for the other cases. The sample mean and standard deviation are 1090 years and 340 years, respectively.

The coefficient of variation for Case 7 is 0.31, which is a smaller value than that obtained for Case 6. In the model with uniform effective porosity, the coefficient of variation increased when effective porosity was treated as a random variable (see Table 14, Cases 2 and 3). However, for Case 7, with spatially varying effective porosity, the coefficient of variation decreased when effective porosity was treated as a random parameter. This result is caused by imposing the one-to-one correlation between effective porosity and

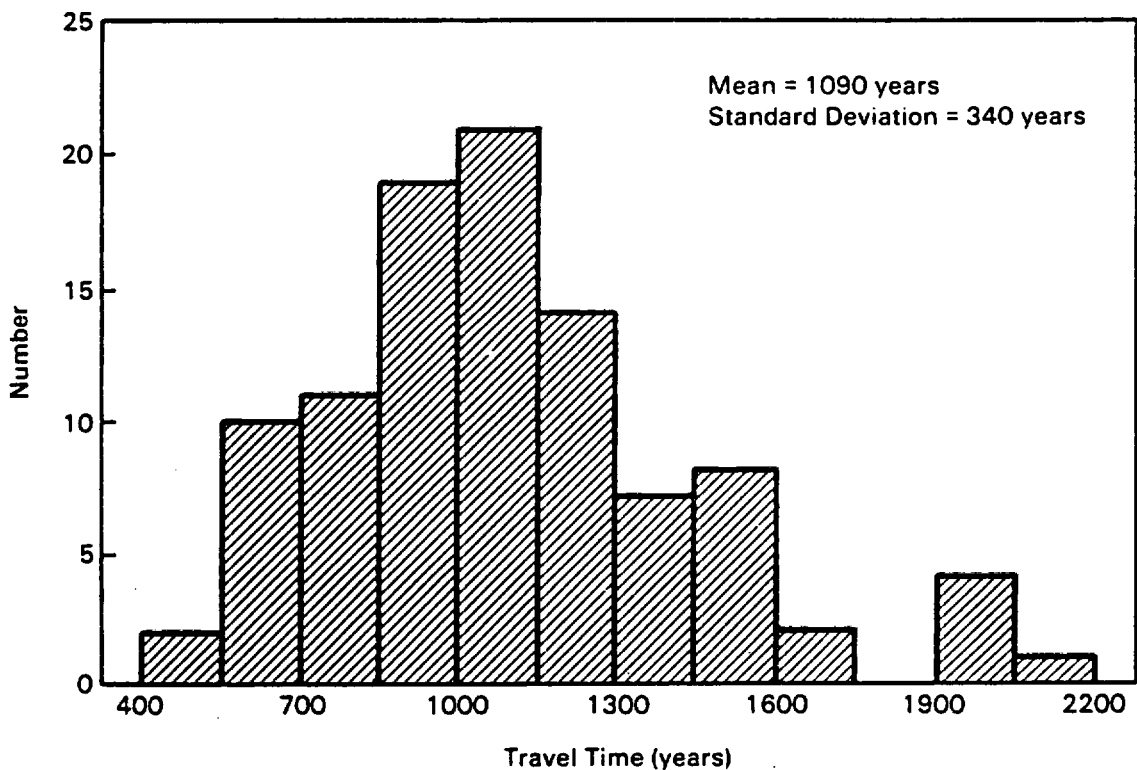


FIGURE 36. Histogram of Ground-Water Travel Time for Case 7

log transmissivity. If no correlation were assumed, the coefficient of variation would probably increase with the effective porosity treated as a random parameter. The median ground-water travel time for Case 7 is 1060 years as observed from the cumulative histogram given in Figure 37. This median value is also less than the sample mean travel time, as is observed for all the other cases.

The values of sample mean, sample standard deviation, coefficients of variation obtained for Cases 4, 5, 6, and 7 are listed in Table 17. Also, a comparison of the sample mean travel times for Cases 5, 6, and 7 shows little variation in the magnitudes; however, the median values for the three cases are more variable. The coefficients of variation for the four cases are of similar magnitude.

To observe the effect of the number of realizations on the statistics, the sample mean together with the sample standard deviation of travel time are plotted versus the number of realizations in Figures 38, 39, and 40 for Cases 5, 6, and 7, respectively. Analysis of the sample statistics as the number of realizations increased indicated that 100 realizations were not sufficient for the mean and standard deviation to converge to their final value. However, the sample mean and standard deviation for Cases 5 and 6 show indications of converging, while those for Case 7 show definite signs of converging. This result for Case 7 suggests that when the effective porosities are highly correlated with log transmissivities in the four zones, 100 realizations may be sufficient to evaluate the statistical properties of the travel time.

Sensitivity Analysis with Spatially Varying Effective Porosity

A sensitivity analysis was conducted for Cases 6 and 7 that involved simulating the ground-water flow system for each realization. Cases 4 and 5 were not analyzed because they used hydraulic heads that were not completely representative of the ground-water flow system.

The sensitivity coefficients for the analysis with spatially varying effective porosity were calculated by the perturbation method as before. The log transmissivity and effective porosity values in each zone were varied about

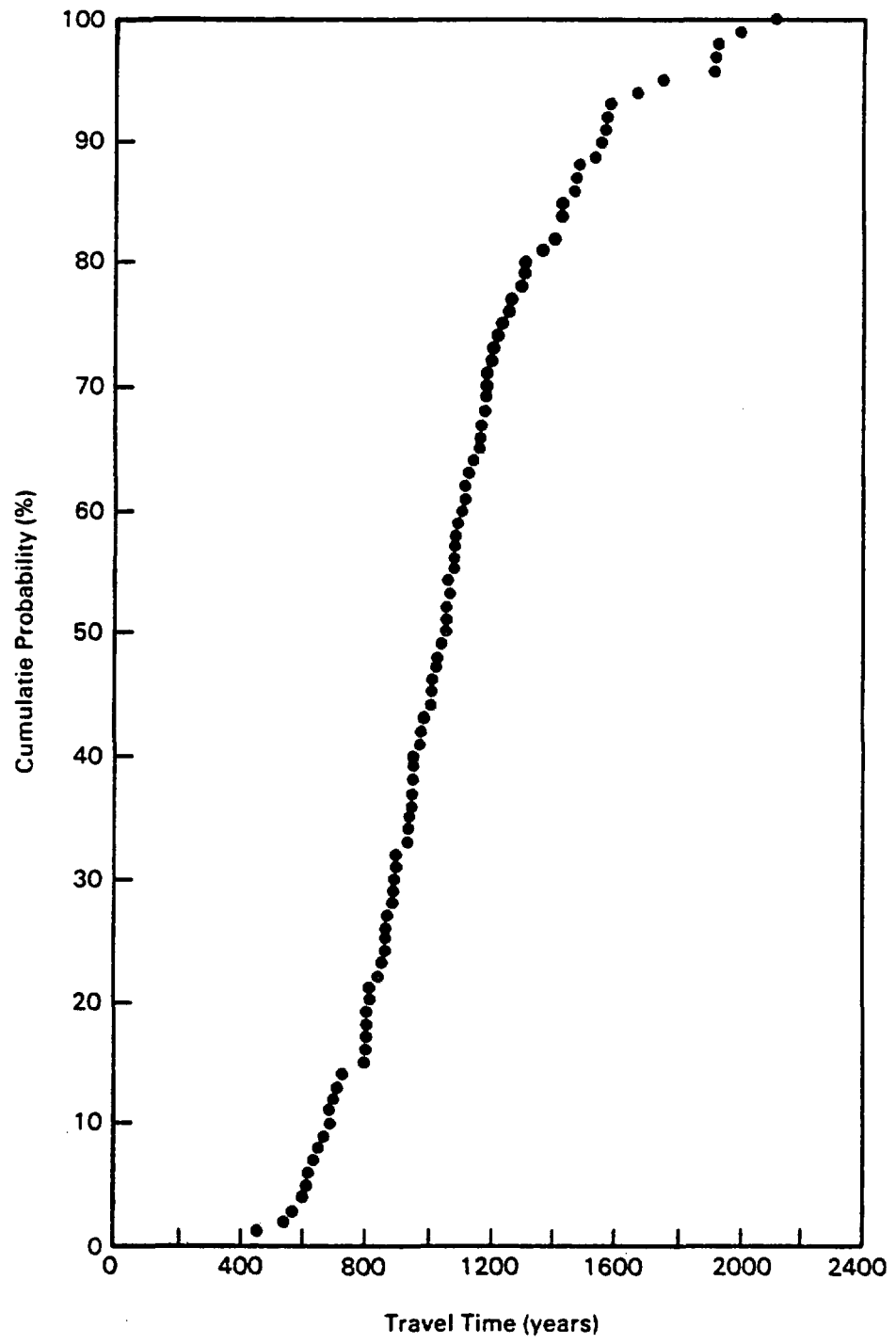


FIGURE 37. Cumulative Histogram of Ground-Water Travel Time for Case 7

TABLE 17. Sample Means, Sample Standard Deviations, Coefficients of Variations, and Medians of Ground-Water Travel Time Obtained from Monte Carlo Analysis for Cases 4, 5, 6, and 7

Case	Sample Mean (yr)	Median (yr)	Sample Standard Deviation (yr)	Coefficient of Variation
4	4600	4270	1590	0.35
5	1090	990	390	0.36
6	1070	1030	360	0.34
7	1090	1060	340	0.31

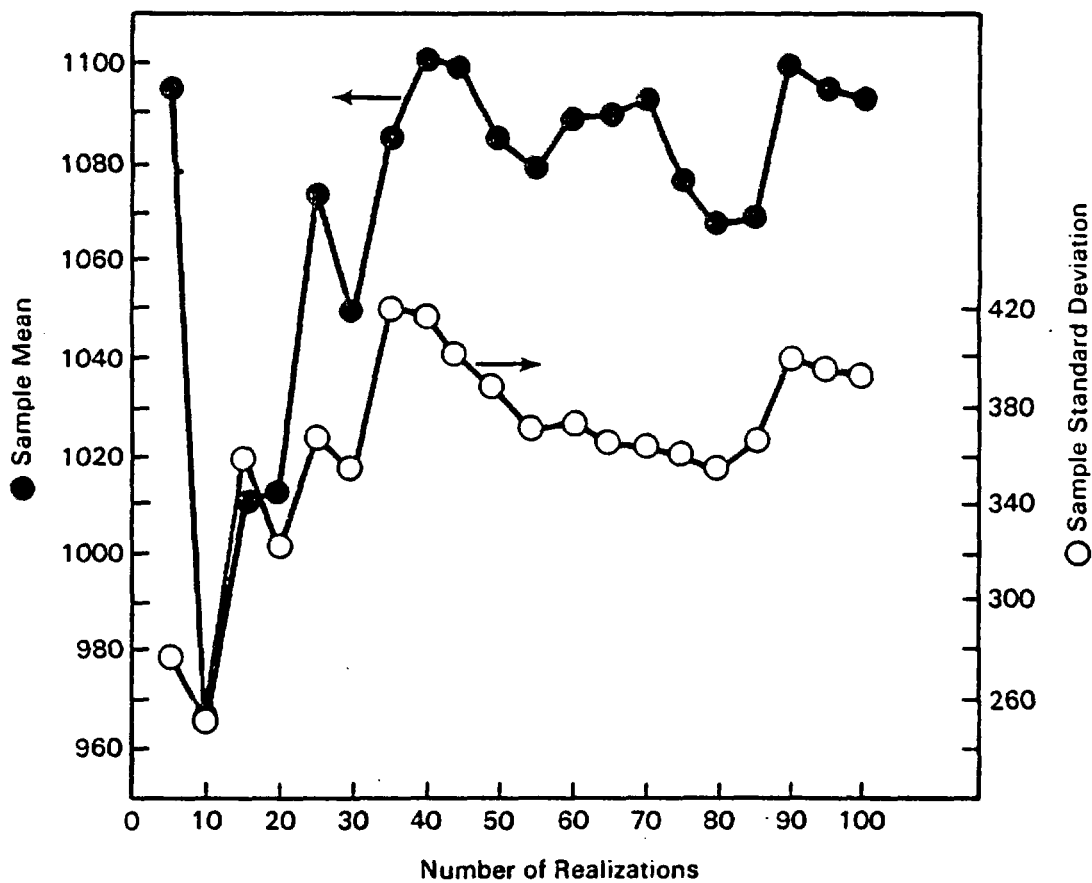


FIGURE 38. Sample Mean and Sample Standard Deviation of Ground-Water Travel Time Versus Number of Realizations for Case 5

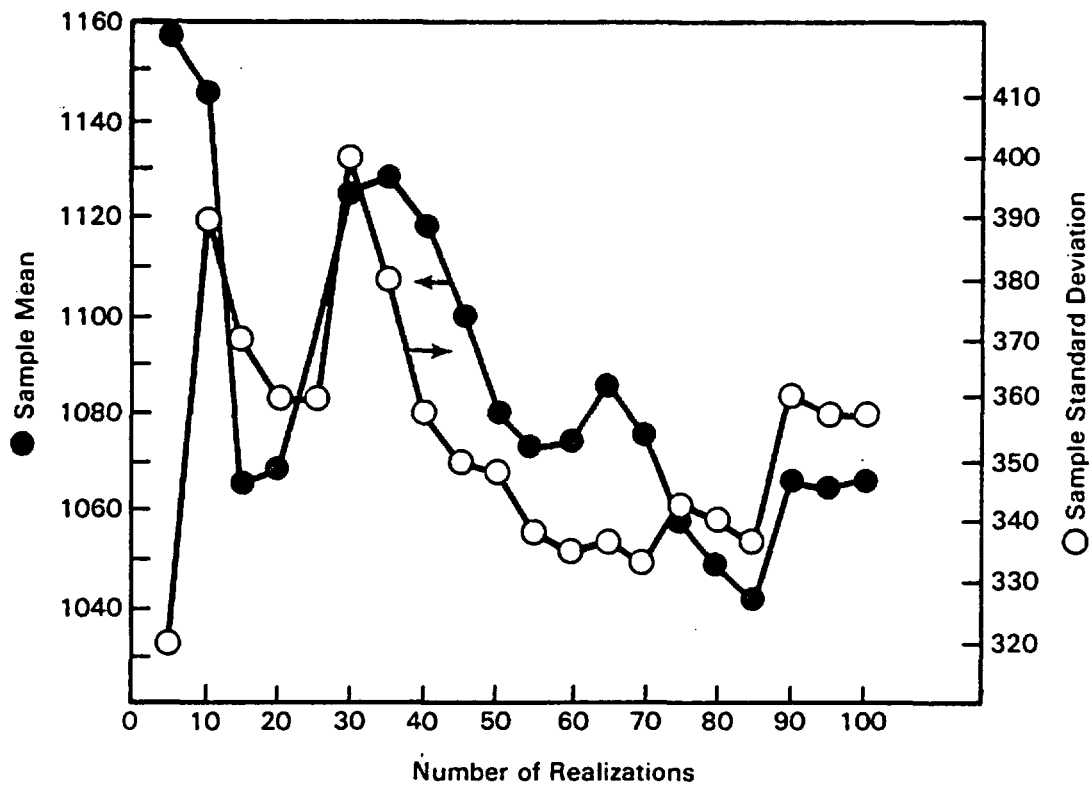


FIGURE 39. Sample Mean and Sample Standard Deviation of Ground-Water Travel Time Versus Number of Realizations for Case 6

their mean values by an amount equal to ± 5 percent of their corresponding standard deviations. The 5 percent variation in the parameters was chosen in order to ensure that the corresponding travel times had measurable variation in their magnitudes while maintaining the parameter values close to their means. The parameters were varied one at a time, and the sensitivity coefficients calculated using Equation (2). The sensitivity coefficients for the log transmissivities and effective porosities are listed in Table 18. The normalized sensitivity coefficients (S_{n_j}) calculated by Equation (3) are also listed in Table 18 and are used to determine which parameters most affect the calculation of travel time.

In the sensitivity analysis for Case 6, the only variable parameters were the log transmissivities in each of the four zones because the spatially

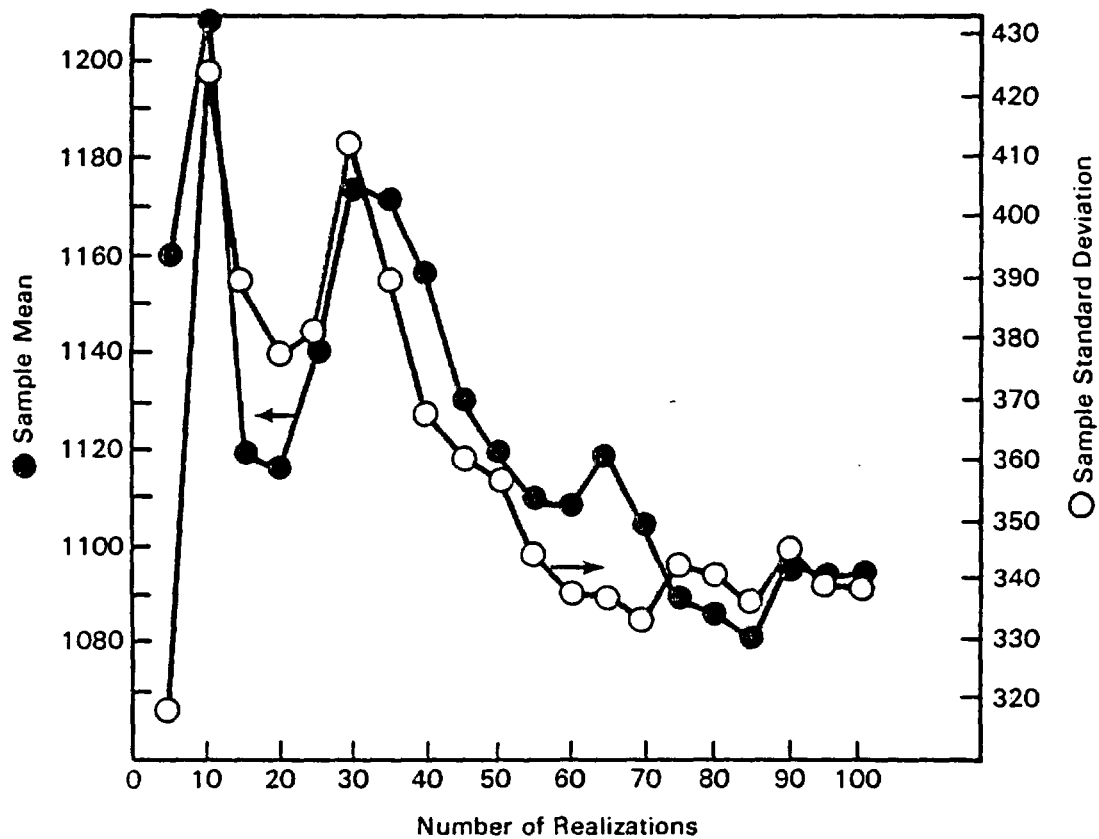


FIGURE 40. Sample Mean and Sample Standard Deviation of Ground-Water Travel Time Versus Number of Realizations for Case 7

varying effective porosities were held constant. A comparison of the normalized sensitivity coefficients corresponding to the log transmissivities in Table 18 shows that the log transmissivity in Zone 1 has the greatest impact on calculation of ground-water travel time. The log transmissivity in Zone 2 produces the next largest effect, and the log transmissivity in Zone 4 has the least influence on the value of travel time. Because travel time is inversely proportional to transmissivity, the sensitivity coefficients for Case 6 are negative; thus, as this parameter is increased, the travel time decreases.

A comparison of the results of the sensitivity analysis for Case 2 with constant uniform effective porosity (see Table 15) and Case 6 with spatially varying effective porosity (see Table 18) shows that in both instances the log transmissivity value in Zone 1 has the most influence on travel time. This

TABLE 18. Travel Times, Sensitivity Coefficients (S_i), and Normalized Sensitivity Coefficients (Sn_i) Corresponding to Variations of the Log Transmissivity and Spatially Varying Effective Porosity in the Four Zones

<u>Delta Change in Parameter</u>	<u>Tr₂ (yr) (Positive Variations)</u>	<u>Tr₁ (yr) (Negative Variations)</u>	<u>Tr (yr)</u>	<u>S_i</u>	<u>Sn_i</u>
log T ₁ = 0.02	975.9	997.7	-21.8	-1090.0	-0.77
log T ₂ = 0.03	983.6	995.4	-11.8	-393.3	-0.52
log T ₃ = 0.015	989.3	991.3	-2.0	-133.3	-0.27
log T ₄ = 0.03	975.6	976.4	-0.8	-26.6	-0.08
n _{e1} = 0.002	991.5	988.5	3.0	1500.0	0.15
n _{e2} = 0.003	991.2	988.8	2.4	800.0	0.12
n _{e3} = 0.004	993.0	987.0	6.0	1500.0	0.30
n _{e4} = 0.004	992.6	987.4	5.2	1300.0	0.42

result is expected because the smaller transmissivities govern the magnitude of the flux through the ground-water flow system near Yucca Mountain.

In the sensitivity analysis for Case 7, both the log transmissivities and the effective porosities were varied. A comparison of all the normalized sensitivity coefficients listed in Table 18 shows that the values of log transmissivity in Zones 1 and 2 and the values of effective porosity in Zone 4 have the largest influence on the calculation of travel time. Again, this result can be attributed to the fact that the smaller transmissivities (i.e., in Zone 1 and 2) govern the magnitude of the ground water flux, while the effective porosity has its largest value in Zone 4 and thus has the most affect on the magnitude of the ground-water travel time [see Equation (15)].

A comparison of the results of the sensitivity analyses for Cases 3 and 7 shows that in Case 3, the normalized sensitivity coefficient is largest for the uniform effective porosity, while in Case 7, the coefficient is largest for log transmissivity in Zone 1. Thus, consideration of spatially varying effective porosities reduced the influence of effective porosity on the travel time. Note that, as before, the normalized sensitivity coefficients for effective porosity are positive because travel time is directly proportional to effective

porosity, while coefficients for log transmissivity are negative because travel time is inversely proportional to transmissivity.

First-Order Analysis with Spatially Varying Effective Porosity

The first-order approach previously described for estimating uncertainty in ground-water travel time was applied to Cases 6 and 7. The first partial derivatives (sensitivity coefficients) were determined from the sensitivity analyses of Cases 6 and 7. These approximations of the derivatives together with estimates of variance of log transmissivity (see Table 10) and effective porosity (see Table 11) were used to calculate the ground-water travel time uncertainty from Equation (6) for Case 6 and Equation (5) for Case 7. Recall that Equation (6) is the expression for variance of ground-water travel time when the parameters are independent, while Equation (5) was used for Case 7 because the parameters were assumed to be correlated. The mean value of travel time was calculated from Equation (4) for both cases.

The mean travel time for Case 6 calculated from the first-order analysis is 990 years and the standard deviation is 250 years with a corresponding coefficient of variation of 0.25. As before, because each term in Equation (6) for the variance of ground-water travel time depends only on one parameter, a comparison of the magnitudes of the terms indicates which parameters contribute most to the travel time uncertainty. For Case 6, 77 percent of the uncertainty (variance) in travel time was caused by the uncertainty of log transmissivity in Zone 1. Thus, reducing the uncertainty in log transmissivity for Zone 1 would produce the maximum effect on the uncertainty in ground-water travel time.

The mean travel time calculated from the first-order analysis for Case 7 is 990 years, and the standard deviation is 240 years with a corresponding coefficient of variation of 0.24. For Case 7, the first-order estimate of variance was calculated from Equation (5)

$$\begin{aligned} \text{Var} (Tr) = & \sum_i \left(\frac{\partial Tr}{\partial p_i} \right)^2 \text{Var} (p_i) \\ & + \sum_i \sum_{\substack{j \\ i > j}} \text{Cov} [p_i, p_j] \left(\frac{\partial Tr}{\partial p_i} \right) \left(\frac{\partial Tr}{\partial p_j} \right) \end{aligned}$$

Because some terms in Equation (5) involve more than one parameter, it is more difficult to determine which parameters cause the most uncertainty in travel time. However, based on the magnitude of the terms which involve the uncertainty of log transmissivity in Zone 1, we can state that this parameter produces a large percentage of the travel time uncertainty.

Comparison of Monte Carlo and First-Order Results for Spatially Varying Effective Porosity

The estimates of mean, standard deviation, and coefficient of variation for travel time calculated from the Monte Carlo and first-order analyses are summarized in Table 19 for Cases 6 and 7. The first-order analysis underestimated the mean, standard deviation, and coefficient of variation when compared to the values determined by the Monte Carlo approach for both cases (see Table 19). The first-order estimates of mean travel time are also less than the median values of travel obtained from the Monte Carlo analysis (see Table 17). The fact that the coefficients of variation obtained from the first order analysis are smaller than the values calculated from the Monte Carlo approach indicates that the first-order analysis underestimates the travel time uncertainty. The discrepancy between the estimates of the statistics for the two approaches suggests that the second-order or higher derivatives cannot be neglected in the Taylor series expansion for the first-order analysis or the use of a Taylor series expansion in an uncertainties analysis is not appropriate.

TABLE 19. Values of Mean, Standard Deviation, and Coefficient of Variation of Travel Time Obtained from Monte Carlo and First-Order Analysis for Cases 6 and 7 with Spatially Varying Effective Porosity

Case	Mean Travel Time (yr)		Standard Deviation Travel Time (yr)		Coefficient of Variation	
	Monte Carlo	First- Order	Monte Carlo	First- Order	Monte Carlo	First- Order
	6	1070	990	360	250	0.34
7	1090	990	340	240	0.31	0.24

DISCUSSION AND CONCLUSIONS

The uncertainty in travel time of water through both the unsaturated and saturated zones can be discussed in terms of the types of uncertainty outlined by Benjamin and Cornell (1970) and Dettinger and Wilson (1981), namely model and parameter (both natural and statistical) uncertainty. Model uncertainty is caused by the limitations in the mathematical and numerical models used to simulate the hydrogeologic system. In this study, contributions to model uncertainty for the unsaturated flow system originate from the following: 1) assumptions necessary for formulating the analytic solution, in particular the steady-state assumption; 2) material characteristic selection and one-dimensional model development; and 3) the relatively poor representation of those material characteristics (see Fig. 5, 6, and 7). For the saturated flow system, model uncertainty is related to the assumptions of steady-state two-dimensional flow, no recharge, constant hydraulic head boundary conditions, and the coarse representation of the spatial variability of transmissivity and effective porosity. Model uncertainty is difficult to quantify for both the unsaturated and saturated zones (Dettinger and Wilson 1981) and was not considered in this study.

Data or parameter uncertainty is caused by 1) random and/or systematic measurement errors in the data used to make parameter estimates for a model, 2) incomplete knowledge of the spatial or temporal variations of some of the data used to make parameter estimates, and 3) heterogeneities within the hydrogeologic system that have not been detected during collection of the data. Parameter uncertainty may be classified as natural or statistical. For example, natural uncertainty in estimates of percolation through Yucca Mountain originates from variability of events contributing to recharge. Nonuniformity of precipitation events, rain-shadow effects, concentration of runoff in arroyos and washes, and variation of precipitation with elevation and temporal variation all contribute to the natural uncertainty of recharge. Statistical uncertainty arises from difficulties of measurement. These measurement difficulties may be caused by frequency of measurements, accuracy of measurements and detection limits of instrumentation. Additionally, statistical uncertainty may be used to represent the relative accuracy of point or areal

measurements. When sufficient statistical information about the parameters is not available, additional uncertainty may be introduced because of the selection of reasonable ranges for the parameters.

In this study, the uncertainty in travel time of water through both the unsaturated and saturated zones was estimated by considering uncertainty in the hydrogeologic parameters. Uncertainty analyses of travel time were conducted separately for the unsaturated and saturated zones.

Based on the first-order analysis of uncertainty in the unsaturated zone using the analytic solution for water flow through Yucca Mountain, uncertainty in the percolation estimate contributes significantly more to uncertainty in travel time than does uncertainty in estimates of hydraulic conductivity. This supports the importance of accurate estimates of the present and future percolation through Yucca Mountain in assessing the performance of a high-level nuclear waste repository. Consequently for performance assessment of a nuclear waste repository in Yucca Mountain, uncertainty in travel time through the unsaturated zone can be reduced by decreasing the uncertainty in the estimate of percolation. However, because of complexity of the infiltration process at the ground surface, reducing uncertainty in estimates of percolation through the mountain will be a difficult, expensive, and time-consuming process.

Two approaches, Monte Carlo and first-order, were used to investigate uncertainty in ground-water travel time through the saturated zone. The Monte Carlo approach shows that using hydraulic head data that is not representative of the ground-water flow system (Cases 1 and 4) leads to incorrect estimates of mean travel time. The hydraulic head distribution calculated using the mean values of transmissivity (Case 5) is more representative of the flow system and yields a mean ground-water travel time that was similar in magnitude to the travel time obtained by using hydraulic head distribution calculated from simulating the ground water flow system for each realization (Case 6). Although the mean travel time for Case 5 is representative, the coefficient of variation is larger than for Case 6, which is based on simulations of the flow system. For Case 5, this larger coefficient of variation indicates a higher degree of uncertainty in ground-water travel time, which is due to the

correlation between the log transmissivities and the distribution of hydraulic heads that has been neglected by not simulating the flow system for each realization.

In the saturated zone, two models of effective porosity--uniform versus spatially varying--were used to determine their effects on mean travel time and its uncertainty. The values of spatially varying effective porosity were determined based on an assumed correlation between the effective porosity and log transmissivity (i.e., larger effective porosities associated with larger log transmissivities). Results from the uncertainty analysis of ground-water travel time using the Monte Carlo approach indicate that the mean travel time is smaller for the model with uniform effective porosity (Cases 2 and 6). However, the uncertainty that was based on the coefficients of variation of travel time appears to be very similar for the two models of effective porosity.

Cases 3 and 7 were included to investigate the influence on ground-water travel time uncertainty when both the effective porosity and the log transmissivity are treated as random parameters. The largest uncertainty in ground-water travel time was obtained for Case 3, where effective porosity was assumed to be uniform over the flow domain, as indicated by the largest coefficient of variation. Although the spatially varying effective porosities were assumed to be random for Case 7, the uncertainty in travel time was smaller than the uncertainty calculated for Case 6 in which deterministic effective porosities were used. This decrease in travel time uncertainty can be explained by the assumed one-to-one correlation between the effective porosity and log transmissivity. Therefore, for this data set and modeling assumptions, considering correlation between effective porosity and log transmissivity produced lower uncertainty in ground-water travel time.

The sensitivity studies for Cases 2 and 3 in the saturated zone indicated that the region with the smallest mean transmissivity produced the largest influence on the calculated ground-water travel time. When random effective porosity was considered (Case 3), the effective porosity produced the largest influence on the calculated ground-water travel time, with the smallest value of transmissivity having the next largest influence. The sensitivity studies

for Cases 6 and 7 indicated that the zones with smaller transmissivity produced the largest influence on travel time, with the higher values of effective porosity having the next largest influence. The results of the sensitivity studies are not unexpected because both the smaller values of transmissivity and the higher effective porosities yield longer ground-water travel times [see Equation (12)]; therefore, ground-water travel times in the areas with these parameters are the longest and represent most of the total travel time.

In addition to estimating uncertainty in ground-water travel time through the saturated zone, the first-order approach was used to indicate which hydrologic parameters contribute most to the uncertainty in travel time. Over 70 percent of the uncertainty (i.e., variance) in travel time for Cases 2, 6, and 7 was due to the smallest mean log transmissivity value. For Case 3, over 66 percent of the uncertainty in ground-water travel time can be attributed to the uniform random effective porosity. Thus, for these cases, the most important hydrologic parameters as indicated by the normalized sensitivity coefficients are also the parameters that contribute most to the uncertainty in ground-water travel time. Therefore, a reduction in the uncertainty in these parameters will have a large effect on the travel time uncertainty.

Comparison of the Monte Carlo and first-order estimates of mean ground-water travel time and travel time uncertainty in the saturated zone showed that the first-order approach underestimated both the mean and variance of travel time for all the cases considered (Cases 2, 3, 6, and 7). This underestimation of the mean value of ground-water travel time and its uncertainty suggests that the Monte Carlo approach should be used to estimate the mean travel time and its variance as well as the probability density distribution of travel time. A rigorous Monte Carlo analysis yields the most accurate estimate of uncertainty in model output because generating realizations of input parameters involves the probability density distribution of the input parameters. These realizations allow more accurate representation of the statistical properties of the input parameters. A first-order analysis uses only the variance (or covariance) of the input parameters and does not consider the probability density distribution of the input parameters. The first-order approach may be

useful to indicate which parameters contribute most to the ground-water travel time uncertainty and thus where the effort must be concentrated to reduce the uncertainty in travel time.

Conclusions from this investigation of uncertainty in the saturated zone must be qualified based on limitations of available data, preliminary development of the conceptual and numerical model, and limited statistical information about the parameters. However, the results suggest that for calculating ground-water travel time and its associated uncertainty, consistent data must be used to obtain values that are representative for the ground-water flow system. The Monte Carlo approach is useful to calculate the uncertainty in travel time, whereas a sensitivity study together with a first-order approach for uncertainty may indicate which parameters produce the largest influence on ground-water travel time and its uncertainty. Inasmuch as both the Monte Carlo and first-order approaches to uncertainty analysis yield beneficial information about uncertainty in travel time through the saturated zone, we recommend that both techniques be considered in future uncertainty studies in the unsaturated zone as well as in the saturated zone. Where information is available, the spatial variability of the hydrologic parameters must be considered, in addition to their statistical properties such as mean values, variances, probability density distributions, and correlation structures.

By comparing the uncertainty analyses for the unsaturated and saturated zones at Yucca Mountain, we can assess the relative impact of uncertainty in water travel time through each zone. The uncertainty in water travel time through the unsaturated zone caused by the uncertainty in recharge was 50 to 100 percent of the mean value, depending on the estimate of the variance in recharge. Whereas, for the saturated zone, the uncertainty in ground-water travel time varied from 31 to 50 percent of the mean value, depending on the statistical assumptions about the hydrologic parameters. In summary, the mean travel time for water through the unsaturated zone is two orders of magnitude larger than ground-water travel time through the saturated zone. However, the larger uncertainty in unsaturated zone travel time produces a greater impact on uncertainty of travel time through the combined system than does the uncertainty in saturated zone travel time.

REFERENCES

- Bear, J. 1979. Hydraulics of Groundwater. McGraw-Hill, Inc., New York.
- Benjamin, J. R., and C. A. Cornell. 1970. Probability Statistics and Decision for Civil Engineers. McGraw-Hill, Inc., New York.
- Bentley, C. B. 1984. Geohydrologic Data for Test Well USW G-4 Yucca Mountain Area, Nye County, Nevada. USGS Open File Report 84-063, U.S. Geological Survey, Denver, Colorado.
- Brace, W. F., M. D. Voegele and H. R. Pratt. 1982. Porosity and Permeability, and Their Relationship in Granite, Basalt, and Tuff. ONWI/82/E512-02900/TR-10, Office of Nuclear Waste Isolation, Columbus, Ohio.
- Burington, R. S. 1973. Handbook of Mathematical Tables and Formulas, 5th Ed., McGraw Hill, Inc., New York.
- Clifton, P. M., R. G. Baca and R. C. Arnett. 1983. Stochastic Analysis of Groundwater Traveltimes for Long-Term Repository Performance Assessment. RHO-BW-SA-323P, Rockwell Hanford Operations, Richland, Washington.
- Clifton, P. M., and S. P. Newman. 1982. "Effects of Kriging and Inverse Modeling on Conditional Simulation of the Avra Valley Aquifer in Southern Arizona." Water Resour. Res. 18(4):1215-1234.
- Davis, S. N. 1969. "Porosity and Permeability of Natural Materials." In Flow Through Porous Media, ed. R. J. M. De Wiest, Academic Press, New York.
- Dettinger, M. D., and J. L. Wilson. 1981. "First Order Analysis of Uncertainty in Numerical Models of Groundwater Flow. Part 1. Mathematical Development." Water Resour. Res. 17(1):149-161.
- DOE. 1984. "U.S. Department of Energy, 10 CFR 960, Final General Guidelines for the Recommendation of Sites for Nuclear Waste Repositories."
- Fernandez, J. A., and M. D. Freshley. 1984. Repository Sealing Concepts for the Nevada Nuclear Waste Storage Investigations. SAND83-1778, Sandia National Laboratories, Albuquerque, New Mexico.
- Freeze, R. A. 1975. "A Stochastic-Conceptual Analysis of One-Dimensional Groundwater Flow in Nonuniform Homogeneous Media." Water Resour. Res. 11(5):725-741.
- Freeze, R. A., and J. A. Cherry. 1979. Groundwater. Prentice Hall, Inc., Englewood Cliffs, New Jersey.

- Gardner, W. R. 1958. "Some Steady-State Solutions of the Unsaturated Moisture Flow Equation with Application to Evaporation from a Water Table." Soil Sci. Soc. Am. Proc. 85:228-232.
- Lahoud, R. G., D. H. Lobbmeyer and M. S. Whitfield, Jr. 1984. Geohydrology of Volcanic Tuff Penetrated by Test Well UE-25b #1, Yucca Mountain, Nye County, Nevada. USGS Water-Resources Investigations Report 84-4253, U.S. Geological Survey, Denver, Colorado.
- Leonhart, L. S., R. L. Jackson, D. L. Graham, G. M. Thompson and L. W. Gelhar. 1983. Groundwater Flow and Transport Characteristics of Flood Basalts as Determined from Tracer Experiments. RHO-BW-SA-220P, Rockwell Hanford Operations, Richland, Washington.
- Lobbmeyer, D. H., M. S. Whitfield, Jr. and R. R. Lahoud. 1983. Geohydrologic Data for Test Well UE-25b #1 Nevada Test Site, Nye County, Nevada. USGS Open-File Report 83-855, U.S. Geological Survey, Denver, Colorado.
- McKeon, T. J., S. W. Tyler, D. W. Mayer and A. E. Reisenauer. 1983. TRUSTII Utility Package: Partially Saturated Soil Characterization, Grid Generation, and Advective Transport Analysis. NUREG/CR-3443, U.S. Nuclear Regulatory Commission, Washington, D.C.
- Mualem, Y. 1976. "A New Model for Predicting the Hydraulic Conductivity of Unsaturated Porous Media." Water Resour. Res. 12(3):513-522.
- Neuman, S. P. 1980. "Statistical Characterization of Aquifer Heterogeneities: An Overview." In Recent Trends in Hydrogeology, ed. T. N. Narasimhan, Geol. Soc. Am. Special Paper 189.
- Peters, R., E. Klavetter, I. Hall, S. C. Blair, P. R. Heller and G. W. Gee. 1984. Fracture and Matrix Hydrologic Characteristics of Tuffaceous Materials from Yucca Mountain, Nye County, Nevada. SAND84-1471, Sandia National Laboratories, Albuquerque, New Mexico.
- Reisenauer, A. E. 1979. Variable Thickness Transient Groundwater Flow Model (3 Volumes), PNL-3160, Pacific Northwest Laboratory, Richland, Washington.
- Rice, W. A. 1984. Preliminary Two-Dimensional Regional Hydrologic Model of the Nevada Test Site and Vicinity. SAND83-7466, Sandia National Laboratories, Albuquerque, New Mexico.
- Richards, L. A. 1931. "Capillary Conduction of Liquids in Porous Mediums." Physics 1:318-333.
- Roseboom, E. H. Jr. 1983. Disposal of High-Level Nuclear Waste Above the Water Table in and Regions. USGS Circular 903, U.S. Geological Survey, Alexandria, Virginia.

- Rush, F. E., W. Thordarson and L. Bruckheimer. 1983. Geohydrologic and Drill-Hole Data Test Well USW H-1, Adjacent to Nevada Test Site, Nye County, Nevada. USGS Open-File Report 83-141, U.S. Geological Survey, Denver, Colorado.
- Sammis, T. W., D. D. Evans and A. W. Warrick. 1982. "Comparison of Methods to Estimate Deep Percolation Rates." Water Resour. Bull. 18(3):465-470.
- Sinnock, S., Y. T. Lin and J. P. Brannen. 1984. Preliminary Bounds on the Expected, Postclosure Performance of the Yucca Mountain Repository Site, Southern Nevada. SAND84-1492, Sandia National Laboratories, Albuquerque, New Mexico.
- Thompson, F. L., F. H. Dove and K. M. Krupka. 1984. Preliminary Consequence Analysis for a Waste Repository at Yucca Mountain, Nevada. SAND83-7475, Sandia National Laboratories, Albuquerque, New Mexico.
- Waddell, R. K. 1982. Two-Dimensional, Steady-State Model of Ground-Water Flow, Nevada Test Site and Vicinity, Nevada-California. USGS Water Resources Investigations 81-4085, U.S. Geological Survey, Denver, Colorado.
- Winograd, I. J., and W. Thordarson. 1975. Hydrogeologic and Hydrochemical Framework South-Central Great Basin, Nevada-California, with Special Reference to the Nevada Test Site. U.S. Geological Survey Prof. Paper 712-C.

APPENDIX A

ONE-DIMENSIONAL ANALYTIC SOLUTION FOR PRESSURE HEAD IN THE UNSATURATED ZONE

In deriving the one-dimensional, steady-state, analytic solution for unsaturated flow, the following assumptions were made:

- water flow is steady state
- the hydraulic gradient is vertically downward
- water table conditions exist at the lower boundary
- the upper boundary condition is constant flux.

Darcy's law in three dimensions is as follows:

$$\underline{q} = \underline{K} \nabla h \quad (\text{A.1})$$

where \underline{q} is the vector of specific discharge with dimensions [L/t], \underline{K} is the hydraulic conductivity tensor [L/t], and ∇h is the hydraulic head gradient [L/L]. Hydraulic head h is the sum of pressure head ψ and elevation head z ; $h = \psi + z$. In the unsaturated zone, ψ is less than zero and $K = K(\psi)$.

Let \underline{x}_3 be the unit normal vector, which is positive in the upward direction. Then

$$q_{\underline{x}_3} = -K(\psi) \frac{\partial h}{\partial z} \underline{x}_3 \quad (\text{A.2})$$

Rewriting the equation such that $q_{\underline{x}_3}$ is downward into the profile and dropping vector notation gives

$$q = -K(\psi) \left(\frac{d\psi}{dz} + 1 \right) \quad (\text{A.3})$$

which, when rearranged becomes

$$-qdz = -K(\psi)d\psi - K(\psi)dz \quad (\text{A.4})$$

$$(K(\psi) - q)dz = -K(\psi)d\psi$$

$$dz = \frac{K(\psi)}{q - K(\psi)} d\psi$$

$$dz = \frac{d\psi}{q/K(\psi) - 1}$$

The integral of the above expression between depths in the profile is

$$\int_{z_{i-1}}^{z_i} dz = \int_{\psi_{i-1}}^{\psi_i} \frac{d\psi}{q/K(\psi) - 1} \quad (\text{A.5})$$

$$\text{Let } \Delta z_i = \int_{z_{i-1}}^{z_i} dz = z_i - z_{i-1}$$

If Δz_i is small and ψ_{i-1} does not vary much from ψ_i , then $K_i(\psi)$ is relatively constant and the integral may be written as

$$\Delta z_i = \int_{\psi_{i-1}}^{\psi_i} \frac{d\psi}{q/K_i - 1} \quad (\text{A.6})$$

Solving the expression for ψ_i gives

$$\Delta z_i = \left[\frac{\psi}{q/K_i - 1} \right] \Big|_{\psi_{i-1}}^{\psi_i}$$

$$\Delta z_i = \frac{1}{q/K_i - 1} [\psi_i - \psi_{i-1}]$$

$$\Delta z_i (q/K_i - 1) = \psi_i - \psi_{i-1}$$

$$\psi_i = \psi_{i-1} + \Delta z_i (q/K_i - 1) \quad (\text{A.7})$$

Because the profile is most likely to be layered horizontally, a harmonic mean hydraulic conductivity is used for K. The harmonic mean (K^*) is derived by considering the equation of continuity.

$$q_i = q_{i-1} = q_T = q \quad (\text{A.8})$$

The values of flux are predicted by Darcy's law

$$q_i = -K_i \frac{\delta h_i}{\delta z_i} \quad (\text{A.9})$$

$$q_{i-1} = -K_{i-1} \frac{\delta h_{i-1}}{\delta z_{i-1}}$$

where the variables in the equations are defined in Figure A.1.

We also have

$$q_T = -K^* \frac{\Delta h_i}{\Delta z_i} \quad (\text{A.10})$$

where $\Delta h_i = \delta h_i + \delta h_{i-1}$ and $\Delta z_i = \delta z_i + \delta z_{i-1}$. Then,

$$q_T = -K^* \left[\frac{\delta h_i + \delta h_{i-1}}{\delta z_i + \delta z_{i-1}} \right] \quad (\text{A.11})$$

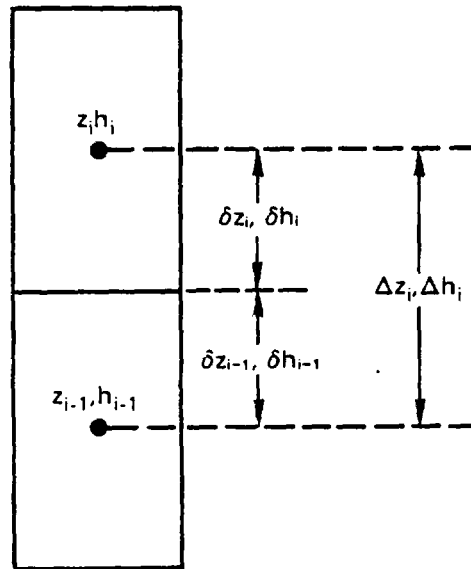


FIGURE A.1. Discretization Between Grid Points

$$q_T = -K^* \left[\frac{-\frac{q_i \delta z_i}{K_i} - \frac{q_{i-1} \delta z_{i-1}}{K_{i-1}}}{\delta z_i + \delta z_{i-1}} \right]$$

and with $q_T = q_i = q_{i-1}$

$$1 = K^* \left[\frac{\delta z_i / K_i + \delta z_{i-1} / K_{i-1}}{\delta z_i + \delta z_{i-1}} \right]$$

The harmonic mean hydraulic conductivity K^* is

$$K^* = \frac{\Delta z_i}{\delta z_i / K_i + \delta z_{i-1} / K_{i-1}} \quad (\text{A.12})$$

The analytic solution then becomes

$$\psi_i = \psi_{i-1} + \Delta z_i (q/K^* - 1) \quad (\text{A.13})$$

This expression is evaluated numerically over a one-dimensional grid, beginning at a lower water table boundary and working up. At each step, ψ_{i-1} and K_{i-1} are known; ψ_i , K_i and K^* are solved iteratively.

$$\psi_i^m = \psi_{i-1} + \Delta z_i (q/K^{*m} - 1) \quad (\text{A.14})$$

where m denotes the level of iteration.

The solution is analytic except for iterating to obtain K_i and K^* . Empirical functions are used for the moisture-retention characteristics $\theta(\psi)$ and unsaturated hydraulic conductivity $K(\psi)$. Volumetric moisture content θ is saturation multiplied by porosity. The functions are statistically fit to measured moisture-retention and generated hydraulic conductivity data to obtain expressions that can be used in modeling.

The formula for moisture-retention characteristics developed by Haverkamp and described by McKeon et al. (1983) is

$$\theta = \frac{\alpha(\theta_s - \theta_r)}{\alpha + |\psi|^\beta} + \theta_r \quad (\text{A.15})$$

where θ_s is the moisture content at saturation, θ_r is the residual moisture content, and α , β are empirical constants derived from fitting the data.

Haverkamp's formula for unsaturated hydraulic conductivity is (McKeon et al. 1983)

$$K(\psi) = K_s \frac{A}{A + |\psi|^B} \quad (\text{A.16})$$

where K_s is the saturated hydraulic conductivity and A, B are empirical parameters used to fit the unsaturated hydraulic conductivities.

Solution for Travel Time

Darcy's law in the vertical direction is (in magnitude without vector notation)

$$q = K(\psi) \frac{dh}{dz} \quad (\text{A.17})$$

The average linear pore velocity \bar{v} is (Bresler et al. 1982)

$$\bar{v} = q/\theta_e \quad (\text{A.18})$$

where θ_e is the effective volumetric moisture content through which flow can occur. Effective moisture content is defined as $\theta_e = S n_e$ where S is saturation and n_e is effective porosity. Combining Equations (A.17) and (A.18) gives

$$\bar{v} \theta_e = K \frac{dh}{dz} \quad (\text{A.19})$$

where $K = K(\psi)$. Because \bar{v} is a velocity, we can also define \bar{v} as

$$\bar{v} = \Delta z / \Delta t \quad (\text{A.20})$$

where t denotes time. We can write dh/dz as $\Delta h / \Delta z$ so that

$$\frac{\Delta z}{\Delta t} \theta_e = K \frac{\Delta h}{\Delta z} \quad (\text{A.21})$$

Rearranging the equation gives:

$$\Delta t = \frac{(\Delta z)^2 \theta_e}{K \Delta h} \quad (\text{A.22})$$

Between points of the profile, the travel time is

$$\Delta t_i = \frac{(\Delta z_i)^2 \theta_i^*}{K_i^* \Delta h_i} \quad (\text{A.23})$$

where the variables are described as in Figure A.1 and θ_i^* is the harmonic mean of the effective moisture content. The total travel time T_r over the profile is

$$T_r = \sum_{i=1}^n \Delta t_i = \sum_{i=1}^n \frac{(\Delta z_i)^2 \theta_i^*}{K_i^* \Delta h_i} \quad (\text{A.24})$$

where n is the number of discretized node points.

Verification of Numerical Evaluation of the Analytic Solution Against a Fully Analytic Solution

To verify whether numerical evaluation of the analytic solution for infiltration is correct, we compared results to those predicted by a fully-analytic solution. The equation

$$\int_{z_{i-1}}^{z_i} dz = \int_{\psi_{i-1}}^{\psi_i} \frac{d\psi}{q/K(\psi)-1} \quad (\text{A.25})$$

can be integrated directly for simple forms of $K(\psi)$ where

$$K(\psi) = K_s \frac{A}{A + |\psi|^B}$$

as before. Specifically, the integral can be evaluated for $B=1, 3/2, 2$, etc. We assumed $B=2$ to verify numerical evaluation of the analytic solution.

The integrand on the right-hand side of the infiltration equation is

$$\begin{aligned} \frac{1}{q/K(\psi)-1} &= \frac{1}{q\left(\frac{|\psi|^2 + A}{K_s A}\right) - 1} \\ &= \frac{K_s A}{q(|\psi|^2 + A) - K_s A} \\ &= \frac{K_s A}{q|\psi|^2 + (q - K_s) A} \\ &= \frac{\frac{K_s}{q - K_s}}{\frac{q}{(q - K_s)A} |\psi|^2 + 1} \\ &= \left[\frac{K_s}{q - K_s} \right] \left[\frac{1}{a|\psi|^2 + c} \right] \end{aligned} \tag{A.26}$$

where $a = \frac{q}{(q - K_s) A}$ and $c = 1$. In the unsaturated zone, $K_s > q$ so that a is always negative.^s The solution of this indefinite integral is (Burington 1973).

$$\int \frac{dx}{ax^2 + c} = \frac{1}{2\sqrt{-ac}} \ln \frac{\sqrt{c} + x\sqrt{a}}{\sqrt{c} - x\sqrt{a}} \tag{A.27}$$

where \ln denotes the natural logarithm and $x = |\psi|$. Then the infiltration equation becomes

$$\Delta z_i = \left[\frac{K_s}{q - K_s} \frac{1}{2\sqrt{-ac}} \right] \ln \left[\frac{\sqrt{c} + x\sqrt{a}}{\sqrt{c} - x\sqrt{a}} \right], \quad \left| \begin{array}{l} x_i \\ x_{i-1} \end{array} \right.$$

or

$$\Delta z_i = \left[\frac{K_s}{q - K_s} \frac{1}{2\sqrt{-a}} \right] \ln \left[\frac{1 + x\sqrt{-a}}{1 - x\sqrt{-a}} \right], \quad \left| \begin{array}{l} x_i \\ x_{i-1} \end{array} \right. \quad (\text{A.28})$$

where a , c , and x are defined as before and $\Delta z = z_i - z_{i-1}$.

$$2\sqrt{-a} \Delta z_i \left(\frac{q - K_s}{K_s} \right) = \ln \left[\frac{1 + x\sqrt{-a}}{1 - x\sqrt{-a}} \right], \quad \left| \begin{array}{l} x_i \\ x_{i-1} \end{array} \right. \quad (\text{A.29})$$

Let $B = 1\sqrt{-a} (\Delta z_i) \left(\frac{q - K_s}{K_s} \right)$. Then,

$$B = \ln \frac{1 + x_i \sqrt{-a}}{1 - x_i \sqrt{-a}} - \ln \frac{1 + x_{i-1} \sqrt{-a}}{1 - x_{i-1} \sqrt{-a}} \quad (\text{A.30})$$

$$B = \ln \frac{(1 + x_i \sqrt{-a})(1 - x_{i-1} \sqrt{-a})}{(1 - x_i \sqrt{-a})(1 + x_{i-1} \sqrt{-a})}$$

$$e^B = \frac{1 + x_i \sqrt{-a} - x_{i-1} \sqrt{-a} + x_i(x_{i-1})(a)}{1 - x_i \sqrt{-a} + x_{i-1} \sqrt{-a} + x_i(x_{i-1})(a)}$$

$$(1 - x_i \sqrt{-a} + x_{i-1} \sqrt{-a} + x_i(x_{i-1})a)e^B = 1 + x_i \sqrt{-a} - x_{i-1} \sqrt{-a} + x_i(x_{i-1})a$$

$$-x_i \sqrt{-a} e^B + x_i(x_{i-1})ae^B - x_i \sqrt{-a} - x_i(x_{i-1})a = 1 - x_{i-1} \sqrt{-a} - e^B - x_{i-1} \sqrt{-a} e^B$$

$$x_i (-\sqrt{-a} e^B + x_{i-1} ae^B - \sqrt{-a} - x_{i-1} a) = 1 - x_{i-1} \sqrt{-a} - e^B - x_{i-1} \sqrt{-a} e^B$$

Solving for x_i

$$x_i = \frac{1 + x_{i-1} \sqrt{-a} - e^B - x_{i-1} \sqrt{-a} e^B}{-\sqrt{-a} e^B + x_{i-1} ae^B - \sqrt{-a} - x_{i-1} a} \quad (\text{A.31})$$

where $x_i = |\phi|$, $a = \frac{q}{(q - K_s) A}$ and $B = 2\sqrt{-a} (\Delta z_i) \left(\frac{q - K_s}{K_s} \right)$

Results of travel time based on numerical evaluation of the analytic solution and the fully analytic solution were compared over a 100-m profile. For an input flux of 0.02 cm/yr, the total travel times for the numerical and fully-analytic solutions were within 0.17 percent of each other. At an input flux of 0.20 cm/yr, only an 0.02 percent difference occurred between total travel times. These differences are well within an acceptable range of error.

The travel time estimated from numerical evaluation of the analytic solution was also compared to the travel time used by Thompson et al. (1984) in the consequence analysis for Nevada Nuclear Waste Storage Investigations Performance Assessment. The travel time estimated for the consequence analysis was approximately 10 percent greater than that estimated by the analytic solution.

REFERENCES

- Bresler, E., B. L. McNeal and D. L. Carter. 1982. Saline and Sodic Soils; Principles-Dynamics-Modeling. Springer-Verlag, Berlin, West Germany.
- Burington, R. S. 1973. Handbook of Mathematical Tables and Formulas, 5th Ed., McGraw Hill, Inc., New York.
- McKeon, T. J., S. W. Tyler, D. W. Mayer and A. E. Reisenauer. 1983. TRUSTII Utility Package: Partially Saturated Soil Characterization, Grid Generation, and Advective Transport Analysis. NUREG/CR-3443, U.S. Nuclear Regulatory Commission, Washington, D.C.
- Thompson, F. L., F. H. Dove and K. M. Krupka. 1984. Preliminary Consequence Analysis for a Waste Repository at Yucca Mountain, Nevada. SAND83-7475, Sandia National Laboratories, Albuquerque, New Mexico.

APPENDIX B

DERIVATION OF EQUATIONS FOR THE FIRST-ORDER UNCERTAINTY ANALYSIS

The first-order uncertainty analysis consists of sensitivity coefficients combined with parameter uncertainty. Sensitivity coefficients and the equations for first-order uncertainty are explained and derived in this appendix.

DETERMINATION OF SENSITIVITY

Sensitivity coefficients can be combined with parameter uncertainty to perform an uncertainty analysis for a model of a particular system. Sensitivity coefficients express the rate of change of one variable caused by the rate of change of another variable. With respect to modeling, sensitivity coefficients describe change in model output caused by change in model input.

The mathematical meaning of sensitivity can be described by considering an arbitrary function

$$F = f(p_1, p_2, \dots, p_n) \quad (\text{B.1})$$

where the function F depends on parameters p_1, p_2, \dots, p_n (McCuen 1973). The change in F resulting from a change in a single parameter Δp_i is given by the Taylor Series expansion

$$f(p_i + \Delta p_i) = F + \frac{\partial F}{\partial p_i} \Delta p_i + \frac{1}{2!} \frac{\partial^2 F}{\partial p_i^2} (\Delta p_i)^2 + \dots \quad (\text{B.2})$$

If the nonlinear terms of the Taylor Series expansion can be ignored, the general definition of a sensitivity coefficient is given by

$$S_i = \frac{\partial F}{\partial p_i} = \lim_{\Delta p_i \rightarrow 0} [f(p_i + \Delta p_i) - f(p_i)] / \Delta p_i \quad (\text{B.3})$$

where S_i is the sensitivity coefficient with respect to the parameter p_i . Coleman and DeCoursey (1976) suggest a finite-difference approximation to the partial derivative

$$S_i = \frac{F_2 - F_1}{p_{i2} - p_{i1}} = \frac{\Delta F}{\Delta p_i} \quad (\text{B.4})$$

where subscripts 1 and 2, respectively, correspond to the state of the system at negative and positive variations of p_i .

The sensitivity coefficients of a system can be calculated by a number of different methods including the following: simple differentiation, perturbation analysis, the adjoint approach, and a Monte Carlo (Latin Hypercube) method. The adjoint technique is discussed by Oblow (1978) and Harper (1983); the Latin Hypercube method was developed primarily at Sandia National Laboratories and is discussed by Iman et al. (1978). The perturbation approach to sensitivity is being used for investigation of flow through Yucca Mountain.

The perturbation method for determining sensitivity coefficients consists of repeated simulations with a model, while varying the input parameters. Sensitivity coefficients are then calculated with respect to the varied input parameters.

First-Order Uncertainty

Benjamin and Cornell (1970) discuss three distinct types of uncertainty. The first is the fundamental uncertainty of the parameter itself caused by natural variation. The second type of uncertainty is statistical and is caused by errors in estimating model parameters. Benjamin and Cornell (1970) describe the third type of uncertainty as model uncertainty, associated with the form of the actual model. This last type of uncertainty, that of the model, is not addressed by the first-order uncertainty analysis. The first two types of uncertainty are combined by considering parameter uncertainty.

To derive the equation for the first-order uncertainty analysis, we assume the expected value of a parameter, p , is (Dettinger and Wilson 1982):

$$E(p) = p_0 \quad (\text{B.5})$$

where p_0 is the mean infiltration rate and $E(p)$ denotes the expectation of p .

If the function F is travel time Tr , the Taylor series expansion for travel time about p_0 is:

$$Tr = Tr(p_0) + \frac{\partial Tr}{\partial p} (p - p_0) + \frac{1}{2} \frac{\partial^2 Tr}{\partial p^2} (p - p_0)^2 + \dots \quad (\text{B.6})$$

The expected value (mean) of Tr is

$$\begin{aligned} E[Tr] &= E[Tr(p_0)] + \frac{\partial Tr}{\partial p} E[p - p_0] + \frac{1}{2} \frac{\partial^2 Tr}{\partial p^2} E[(p - p_0)^2] + \dots \\ &= Tr(p_0) + 0 + \frac{1}{2} \frac{\partial^2 Tr}{\partial p^2} \text{Var}(p) + \dots \end{aligned} \quad (\text{B.7})$$

where $E[p - p_0] = E[p] - E[p_0] = p_0 - p_0 = 0$, $E[(p - p_0)^2] = \text{Var}(p)$, and Var denotes variance. If we assume the second-order derivative defining curvature of travel time versus the parameter p is small, then

$$E[Tr] = Tr(p_0) \quad (\text{B.8})$$

The variance of Tr is arrived at by rearranging the Taylor Series expansion of Tr

$$Tr - Tr(p_0) = \frac{\partial Tr}{\partial p} (p - p_0) + \frac{1}{2} \frac{\partial^2 Tr}{\partial p^2} (p - p_0)^2 + \dots \quad (B.9)$$

The square of this is

$$\begin{aligned} (Tr - Tr(p_0))^2 &= \left(\frac{\partial Tr}{\partial p}\right)^2 (p - p_0)^2 + \frac{1}{2} \frac{\partial Tr}{\partial p} \frac{\partial^2 Tr}{\partial p^2} (p - p_0)^3 \\ &+ \frac{1}{4} \left(\frac{\partial^2 Tr}{\partial p^2}\right)^2 (p - p_0)^4 + \dots \end{aligned} \quad (B.10)$$

and taking the expectation, we arrive at

$$\begin{aligned} E[(Tr - Tr(p_0))^2] &= \left(\frac{\partial Tr}{\partial p}\right)^2 E[(p - p_0)^2] + \frac{1}{2} \frac{\partial Tr}{\partial p} \frac{\partial^2 Tr}{\partial p^2} E[(p - p_0)^3] \\ &+ \frac{1}{4} \left(\frac{\partial^2 Tr}{\partial p^2}\right)^2 E[(p - p_0)^4] + \dots \end{aligned} \quad (B.11)$$

If we again neglect second and higher order derivatives, we obtain

$$\text{Var}(Tr) = \left(\frac{\partial Tr}{\partial p}\right)^2 \text{Var}(p) \quad (B.12)$$

which relates variance in the input parameter p to variance in travel time.

REFERENCES

- Benjamin, J. R., and C. A. Cornell. 1970. Probability Statistics and Decision for Civil Engineers. McGraw-Hill, Inc., New York.
- Coleman, G. and D. G. DeCoursey. 1976. "Sensitivity and Model Variance Analysis Applied to Some Evaporation and Evapotranspiration Models." Water Resour. Res. 12(5):873-879.
- Dettinger, M. D., and J. L. Wilson. 1981. "First Order Analysis of Uncertainty in Numerical Models of Groundwater Flow. Part 1. Mathematical Development." Water Resour. Res. 17(1):149-161.
- Harper, W. V. 1983. Sensitivity/Uncertainty Analysis Techniques for Nonstochastic Computer Codes. ONWI-444, Office of Nuclear Waste Isolation, Battelle Memorial Institute, Columbus, Ohio.
- Iman, R. L., J. C. Helton and J. C. Campbell. 1978. Risk Methodology for Geologic Disposal of Radioactive Waste: Sensitivity Analysis Techniques. NUREG/CR-0394, U.S. Nuclear Regulatory Commission, Washington D.C.
- McCuen, R. H. 1973. "The Role of Sensitivity Analysis Hydrologic Modeling." J. Hydrol. 18:37-53.
- Oblow, E. M. 1978. "Sensitivity Analyses for General Nonlinear Algebraic Equations with Constraints." Nucl. Sci. and Eng. Tech. Note 65:187-191.

DISTRIBUTION LIST

B. C. Rusche (RW-1)
Director
Office of Civilian Radioactive
Waste Management
U.S. Department of Energy
Forrestal Building
Washington, DC 20585

Ralph Stein (RW-23)
Office of Geologic Repositories
U.S. Department of Energy
Forrestal Building
Washington, DC 20585

J. J. Fiore, (RW-22)
Program Management Division
Office of Geologic Repositories
U.S. Department of Energy
Forrestal Building
Washington, DC 20585

M. W. Frei (RW-23)
Engineering & Licensing Division
Office of Geologic Repositories
U.S. Department of Energy
Forrestal Building
Washington, DC 20585

E. S. Burton (RW-25)
Siting Division
Office of Geologic Repositories
U.S. Department of Energy
Forrestal Building
Washington, D.C. 20585

C. R. Cooley (RW-24)
Geosciences & Technology Division
Office of Geologic Repositories
U.S. Department of Energy
Forrestal Building
Washington, DC 20585

V. J. Cassella (RW-22)
Office of Geologic Repositories
U.S. Department of Energy
Forrestal Building
Washington, DC 20585

T. P. Longo (RW-25)
Program Management Division
Office of Geologic Repositories
U.S. Department of Energy
Forrestal Building
Washington, DC 20585

Cy Klingsberg (RW-24)
Geosciences and Technology Division
Office of Geologic Repositories
U. S. Department of Energy
Forrestal Building
Washington, DC 20585

B. G. Gale (RW-25)
Siting Division
Office of Geologic Repositories
U.S. Department of Energy
Forrestal Building
Washington, D.C. 20585

R. J. Blaney (RW-22)
Program Management Division
Office of Geologic Repositories
U.S. Department of Energy
Forrestal Building
Washington, DC 20585

R. W. Gale (RW-40)
Office of Policy, Integration, and
Outreach
U.S. Department of Energy
Forrestal Building
Washington, D.C. 20585

J. E. Shaheen (RW-44)
Outreach Programs
Office of Policy, Integration and
Outreach
U.S. Department of Energy
Forrestal Building
Washington, DC 20585

J. O. Neff, Manager
Salt Repository Project Office
U.S. Department of Energy
505 King Avenue
Columbus, OH 43201

D. C. Newton (RW-23)
Engineering & Licensing Division
Office of Geologic Repositories
U.S. Department of Energy
Forrestal Building
Washington, DC 20585

S. A. Mann, Manager
Crystalline Rock Project Office
U.S. Department of Energy
9800 South Cass Avenue
Argonne, IL 60439

O. L. Olson, Manager
Basalt Waste Isolation Project Office
U.S. Department of Energy
Richland Operations Office
Post Office Box 550
Richland, WA 99352

K. Street, Jr.
Lawrence Livermore National
Laboratory
Post Office Box 808
Mail Stop L-209
Livermore, CA 94550

D. L. Vieth, Director (4)
Waste Management Project Office
U.S. Department of Energy
Post Office Box 14100
Las Vegas, NV 89114

L. D. Ramspott (3)
Technical Project Officer for NNWSI
Lawrence Livermore National
Laboratory
P.O. Box 808
Mail Stop L-204
Livermore, CA 94550

D. F. Miller, Director
Office of Public Affairs
U.S. Department of Energy
Post Office Box 14100
Las Vegas, NV 89114

W. J. Purcell (RW-20)
Office of Geologic Repositories
U.S. Department of Energy
Forrestal Building
Washington, DC 20585

D. A. Nowack (12)
Office of Public Affairs
U.S. Department of Energy
Post Office Box 14100
Las Vegas, NV 89114

D. T. Oakley (4)
Technical Project Officer for NNWSI
Los Alamos National Laboratory
P.O. Box 1663
Mail Stop F-619
Los Alamos, NM 87545

B. W. Church, Director
Health Physics Division
U.S. Department of Energy
Post Office Box 14100
Las Vegas, NV 89114

W. W. Dudley, Jr. (3)
Technical Project Officer for NNWSI
U.S. Geological Survey
Post Office Box 25046
418 Federal Center
Denver, CO 80225

Chief, Repository Projects Branch
Division of Waste Management
U.S. Nuclear Regulatory Commission
Washington, D.C. 20555

NTS Section Leader
Repository Project Branch
Division of Waste Management
U.S. Nuclear Regulatory Commission
Washington, D.C. 20555

Document Control Center
Division of Waste Management
U.S. Nuclear Regulatory Commission
Washington, D.C. 20555

V. M. Glanzman
U.S. Geological Survey
Post Office Box 25046
913 Federal Center
Denver, CO 80225

P. T. Prestholt
NRC Site Representative
1050 East Flamingo Road
Suite 319
Las Vegas, NV 89109

M. E. Spaeth
Technical Project Officer for NNWSI
Science Applications
International, Corporation
2769 South Highland Drive
Las Vegas, NV 89109

SAIC-T&MSS Library (2)
Science Applications
International, Corporation
2950 South Highland Drive
Las Vegas, NV 89109

W. S. Twenhofel, Consultant
Science Applications
International, Corp.
820 Estes Street
Lakewood, CO 80215

A. E. Gurrola
General Manager
Energy Support Division
Holmes & Narver, Inc.
Post Office Box 14340
Las Vegas, NV 89114

J. A. Cross, Manager
Las Vegas Branch
Fenix & Scisson, Inc.
Post Office Box 15408
Las Vegas, NV 89114

Neal Duncan (RW-44)
Office of Policy, Integration, and
Outreach
U.S. Department of Energy
Forrestal Building
Washington, DC 20585

John Fordham
Desert Research Institute
Water Resources Center
Post Office Box 60220
Reno, NV 89506

J. B. Wright
Technical Project Officer for NNWSI
Westinghouse Electric Corporation
Waste Technology Services Division
Nevada Operations
Post Office Box 708
Mail Stop 703
Mercury, NV 89023

ONWI Library
Battelle Columbus Laboratory
Office of Nuclear Waste Isolation
505 King Avenue
Columbus, OH 43201

W. M. Hewitt, Program Manager
Roy F. Weston, Inc.
2301 Research Blvd., 3rd Floor
Rockville, MD 20850

H. D. Cunningham
General Manager
Reynolds Electrical &
Engineering Co., Inc.
Post Office Box 14400
Mail Stop 555
Las Vegas, NV 89114

T. Hay, Executive Assistant
Office of the Governor
State of Nevada
Capitol Complex
Carson City, NV 89710

R. R. Loux, Jr., Director (3)
Nuclear Waste Project Office
State of Nevada
Capitol Complex
Carson City, NV 89710

C. H. Johnson, Technical
Program Manager
Nuclear Waste Project Office
State of Nevada
Capitol Complex
Carson City, NV 89710

Dr. Martin Mifflin
Desert Research Institute
Water Resources Center
Suite 1
2505 Chandler Avenue
Las Vegas, NV 89120

Department of Comprehensive
Planning
Clark County
225 Bridger Avenue, 7th Floor
Las Vegas, NV 89155

Lincoln County Commission
Lincoln County
Post Office Box 90
Pioche, NV 89043

Community Planning and
Development
City of North Las Vegas
Post Office Box 4086
North Las Vegas, NV 89030

City Manager
City of Henderson
Henderson, NV 89015

N. A. Norman
Project Manager
Bechtel National Inc.
P. O. Box 3965
San Francisco, CA 94119

Flo Butler
Los Alamos Technical Associates
1650 Trinity Drive
Los Alamos, New Mexico 87544

Timothy G. Barbour
Science Applications
International Corporation
1626 Cole Boulevard, Suite 270
Golden, CO 80401

6300 R. W. Lynch
6310 T. O. Hunter
6310 NNWSICF
6311 L. W. Scully
6311 L. Perrine
6312 F. W. Bingham
6312 R. W. Prindle
6312 M. S. Tierney (3)
6313 T. E. Blejwas
6314 J. R. Tillerson
6315 S. Sinnock
6332 WMT Library (20)
6430 N. R. Ortiz
3141 C. M. Ostrander (5)
3151 W. L. Garner (3)
8024 M. A. Pound
DOE/TIC (28)
(3154-3, C. H. Dalin)

Planning Department
Nye County
Post Office Box 153
Tonopah, NV 89049

Economic Development
Department
City of Las Vegas
400 East Stewart Avenue
Las Vegas, NV 89101

Director of Community
Planning
City of Boulder City
Post Office Box 367
Boulder City, NV 89005

Commission of the
European Communities
200 Rue de la Loi
B-1049 Brussels
BELGIUM

Technical Information Center
Roy F. Weston, Inc.
2301 Research Boulevard,
Third Floor
Rockville, MD 20850

R. Harig
Parsons Brinkerhoff Quade &
Douglas, Inc.
1625 Van Ness Ave.
San Francisco, CA 94109-3678

Dr. Madan M. Singh, President
Engineers International, Inc.
98 East Naperville Road
Westmont, IL 60559-1595

Battelle Memorial Institute (25)
Pacific Northwest Laboratory
P.O. Box 999
Richland, WA 99352
Attn: F. H. Dove (4)
D. W. Dragnich
M. D. Freshley (4)
P. D. Hays
M. R. Kreiter
E. A. Jacobson (5)
J. A. Stottlemire
L. L. Wendell
Publishing Coordination (2)
Technical Information
Library (5)